

# **EFFICIENT LOCALIZATION METHODS FOR A POINT SOURCE AND RIGID BODY**

---

A Dissertation presented to  
the Faculty of the Graduate School  
at the University of Missouri

---

In Partial Fulfillment  
of the Requirements for the Degree  
Doctor of Philosophy


---

by  
Shanjie Chen  
Dr. Dominic K. C. Ho, Dissertation Supervisor  
DECEMBER 2015

The undersigned, appointed by the Dean of the Graduate School, have examined the dissertation entitled:

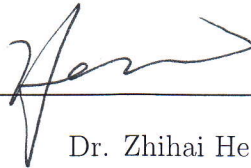
EFFICIENT LOCALIZATION METHODS  
FOR A POINT SOURCE AND RIGID BODY

presented by Shanjie Chen,  
a candidate for the degree of Doctor of Philosophy and hereby certify that, in their opinion, it is worthy of acceptance.



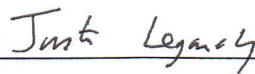
---

Dr. Dominic K. C. Ho



---

Dr. Zhihai He



---

Dr. Justin Legarsky



---

Dr. Yunxin Zhao

## ACKNOWLEDGMENTS

I would like to take this opportunity to gratefully acknowledge everyone who made this dissertation possible. First I want to express my sincere appreciation to my supervisor, Dr. Dominic K. C. Ho, for his support, inspiration, and invaluable guidance in my academic research. I would also like to express my sincere gratitude to the committee members Dr. Zhihai He, Dr. Justin Legarsky, and Dr. Yunxin Zhao for spending their valuable time and giving important suggestions that improved the quality of this dissertation.

I would like to express my appreciation to my labmates, Zhenhua Ma, Liyang Rui, Yue Wang, Bo-Yu Su, Yun Liu, and Jinzhou Li for their assistance and wonderful friendship. I would like to thank Le Yang for the academic discussion. I sincerely thank my friends Miao Sun, Xiaobo Ren, Changzhe Jiao, and Chao Chen for the friendship and the help. And the special thanks are given to my language partners Trevor Eischen, Mallory Williams, Adam Johnson, Jack Stallone, and Shannon Zaloz for sharing American culture and improving my English skill.

Last but not least, I would like to thank my parents and my girlfriend Ding Xiao for continuous support in many aspects of life.

## TABLE OF CONTENTS

<b>ACKNOWLEDGMENTS</b>	<b>ii</b>
<b>LIST OF FIGURES</b>	<b>viii</b>
<b>ABSTRACT</b>	<b>xiii</b>
<b>CHAPTER</b>	
<b>1 Introduction</b>	<b>1</b>
1.1 Background and Motivation	1
1.1.1 Point Source Localization	1
1.1.2 Rigid Body Localization – Position and Orientation Estimation	3
1.2 Basics for Point Source Localization	6
1.3 Basics for Rigid Body Localization – Position and Orientation Estimation	8
1.4 Contributions of the Research	10
1.5 Content Organization	13
<b>2 Range Weighting for Squared Measurements Based Least Squares</b>	<b>14</b>
2.1 Range Based Localization	15
2.1.1 Localization Scenario	15
2.1.2 CRLB	17
2.2 Weighted Squared Range Localization	18
2.2.1 Cost Function and Solution	18
2.2.2 Analysis and Comparison with CRLB	20

2.2.3	Special Geometries . . . . .	26
2.3	Weighted Squared Range Difference Localization . . . . .	27
2.3.1	Cost Function and Solution . . . . .	27
2.3.2	Analysis and Comparison with CRLB . . . . .	29
2.3.3	Special Geometries . . . . .	34
2.4	Simulations . . . . .	38
2.4.1	Comparison of SR-LS and SR-WLS . . . . .	39
2.4.2	Comparison of SRD-LS and SRD-WLS . . . . .	44
2.5	Conclusion . . . . .	52
<b>3</b>	<b>Weighting Technique in the Presence of Sensor Position Errors . . . . .</b>	<b>54</b>
3.1	Localization Scenario and CRLB . . . . .	55
3.1.1	Localization Scenario . . . . .	55
3.1.2	CRLB . . . . .	56
3.2	Squared Range Cost Function and Analysis . . . . .	57
3.2.1	New SR-WLS Cost Function . . . . .	57
3.2.2	MSE Analysis . . . . .	59
3.3	Squared Range Difference Cost Function and Analysis . . . . .	61
3.3.1	New SRD-WLS Cost Function . . . . .	61
3.3.2	MSE Analysis . . . . .	62
3.4	Simulations . . . . .	63
3.5	Conclusion . . . . .	66
<b>4</b>	<b>Estimation of Rigid Body Position and Orientation . . . . .</b>	<b>68</b>

4.1	Scenario . . . . .	69
4.2	Stationary Rigid Body Localization . . . . .	72
4.2.1	Step-1: Preliminary Solution . . . . .	72
4.2.2	Step-2: Refinement . . . . .	74
4.3	2D Case . . . . .	78
4.3.1	Step-1 . . . . .	79
4.3.2	Step-2 . . . . .	82
4.4	Moving Rigid Body Localization . . . . .	83
4.4.1	Step-1 . . . . .	85
4.4.2	Step-2 . . . . .	86
4.5	Performance . . . . .	88
4.5.1	Accuracy . . . . .	88
4.5.2	Computational Complexity . . . . .	90
4.6	Simulations . . . . .	91
4.6.1	Stationary Rigid Body . . . . .	93
4.6.2	Moving Rigid Body . . . . .	100
4.7	Alternative Method for Moving Rigid Body in 2D Case . . . . .	104
4.7.1	New Method . . . . .	104
4.7.2	Simulations . . . . .	109
4.8	Conclusion . . . . .	112
<b>5</b>	<b>Estimation of Position and Orientation Using AOA Measurements</b>	<b>115</b>
5.1	Scenario . . . . .	116

5.2	Single Sensor in 3D . . . . .	117
5.3	Multiple Sensors . . . . .	119
5.3.1	3D Case . . . . .	120
5.3.2	2D Case . . . . .	122
5.4	Simulations . . . . .	122
5.4.1	3D Single Sensor . . . . .	123
5.4.2	Multiple Sensors . . . . .	124
5.5	Conclusion . . . . .	125
<b>6</b>	<b>Future Work . . . . .</b>	<b>127</b>
<b>APPENDIX</b>		
<b>A</b>	<b>Appendix for Chapter 2 . . . . .</b>	<b>129</b>
A.1	Bias of SR-LS . . . . .	129
A.2	Bias of SR-WLS . . . . .	130
A.3	Bias of SRD-LS . . . . .	131
A.4	Bias of SRD-WLS . . . . .	132
<b>B</b>	<b>Appendix for Chapter 4 . . . . .</b>	<b>134</b>
B.1	CRLB for 2D Stationary Rigid Body Localization: Parameterization of Rotation Matrix $\mathbf{R}$ by Rotation Angle $\theta$ . . . . .	134
B.2	CRLB for Moving Rigid Body Localization . . . . .	135
B.2.1	2D Case . . . . .	135
B.2.2	3D Case . . . . .	136
B.3	Definition of $\gamma$ and $\mathbf{L}$ for Multiplicative Corrective Rotation Matrix .	137

B.4 The Two-Stage Method for Localization Using TOA and Doppler Measurements . . . . .	138
B.5 Implementation Details for SCLS and CLS . . . . .	140
<b>BIBLIOGRAPHY . . . . .</b>	<b>141</b>
<b>VITA . . . . .</b>	<b>154</b>



## LIST OF FIGURES

Figure		Page
2.1	Special geometries for comparison of SRD-LS and SRD-WLS. (a) Case 1. (b) Case 2. (c) Case 3. . . . .	34
2.2	Average MSE for SR-LS and SR-WLS in the first scenario, $M = 5$ . . .	40
2.3	Average bias for SR-LS and SR-WLS in the first scenario, $M = 5$ . . .	40
2.4	Empirical probability density functions of bias ratio between SR-LS and SR-WLS with different sensor numbers $M$ in the first scenario. . .	41
2.5	Average of MSE ratio $\Delta$ between SR-LS and SR-WLS with different sensor numbers $M$ and noise correlation factors $a$ in the first scenario. . .	43
2.6	Average of bias ratio $\delta$ between SR-LS and SR-WLS with different sensor numbers $M$ and noise correlation factors $a$ in the first scenario. . .	43
2.7	MSE and bias comparison of SR-LS and SR-WLS under Special Case 4 in [19] with $p = 20$ . . . . .	44
2.8	Average MSE for SRD-LS and SRD-WLS in the first scenario, $M = 5$ . . .	45
2.9	Average bias for SRD-LS and SRD-WLS in the first scenario, $M = 5$ . . .	46
2.10	Average MSE for SRD-LS and SRD-WLS in the second scenario, $M = 5$ . . .	46
2.11	Average bias for SRD-LS and SRD-WLS in the second scenario, $M = 5$ . . .	47

2.12	Empirical probability density functions of MSE ratio between SRD-LS and SRD-WLS with different sensor numbers $M$ in the first scenario.	48
2.13	Empirical probability density functions of bias ratio between SRD-LS and SRD-WLS with different sensor numbers $M$ in the first scenario.	49
2.14	Average of MSE ratio $\Delta$ between SRD-LS and SRD-WLS with different sensor numbers $M$ and noise correlation factors $a$ in the first scenario.	49
2.15	Average of bias ratio $\delta$ between SRD-LS and SRD-WLS with different sensor numbers $M$ and noise correlation factors $a$ in the first scenario.	50
2.16	MSE and bias comparison of SRD-LS and SRD-WLS under Case 3 with correlated noise, $p = 20$ ; where dashed line and $\square$ represent theoretical and simulated bias of SRD-LS, and dotted line and $\times$ represent theoretical and simulated bias of SRD-WLS. . . . .	51
3.1	Localization scenario. Open circles are the true sensor positions and closed circles are the available sensor positions. . . . .	56
3.2	Range (TOA) localization performance of SR-WLS considering sensor position errors, under the specific geometry in Table 1. . . . .	65
3.3	Range (TOA) localization performance of SR-WLS considering sensor position errors, under the 200 random geometries. . . . .	65
3.4	Range difference (TDOA) localization performance of SRD-WLS considering sensor position errors, under the specific geometry in Table 1. . . . .	66
3.5	Range difference (TDOA) localization performance of SRD-WLS considering sensor position errors, under the 200 random geometries. . .	67

4.1	An illustration for rigid body localization, shown in 2D for ease of illustration. (a) The known sensor position $\mathbf{c}_i$ in the local reference frame $\mathcal{B}$ ; (b) The unknown sensor position $\mathbf{s}_i$ in the inertial reference frame $\mathcal{I}$ that is related to $\mathbf{c}_i$ by (4.2) through the rotation and translation between the two reference frames. . . . .	70
4.2	Performance for rotation matrix $\mathbf{R}$ estimation in the 3D case, averaged over 200 realizations of anchor positions. . . . .	94
4.3	Performance for position $\mathbf{t}$ estimation in the 3D case, averaged over 200 realizations of anchor positions. . . . .	95
4.4	Bias for rotation matrix $\mathbf{R}$ estimation in the 3D case, averaged over 200 realizations of anchor positions. . . . .	96
4.5	Bias for position $\mathbf{t}$ estimation in the 3D case, averaged over 200 realizations of anchor positions. . . . .	96
4.6	Computation time (millisecond) in each Monte-Carlo run in the 3D case, averaged over 200 realizations of anchor positions. . . . .	97
4.7	Performance for orientation $\theta$ (deg) estimation in the 2D case, averaged over 200 realizations of anchor positions. . . . .	98
4.8	Performance for position $\mathbf{t}$ estimation in the 2D case, averaged over 200 realizations of anchor positions. . . . .	99
4.9	Bias for orientation $\theta$ (deg) estimation in the 2D case, averaged over 200 realizations of anchor positions. . . . .	99
4.10	Bias for position $\mathbf{t}$ estimation in the 2D case, averaged over 200 realizations of anchor positions. . . . .	100

4.11	Computation time (millisecond) in each Monte-Carlo run in the 2D case, averaged over 200 realizations of anchor positions. . . . .	101
4.12	RMSE and bias performance of the rotation matrix $\mathbf{R}$ estimation for a moving rigid body in the 3D case, averaged over 200 realizations of anchor positions. . . . .	102
4.13	RMSE and bias performance of the position $\mathbf{t}$ estimation for a moving rigid body in the 3D case, averaged over 200 realizations of anchor positions. . . . .	102
4.14	RMSE and bias performance of angular velocity $\boldsymbol{\omega}$ estimation for a moving rigid body in the 3D case, averaged over 200 realizations of anchor positions. . . . .	103
4.15	RMSE and bias performance of translational velocity $\dot{\mathbf{t}}$ estimation for a moving rigid body in the 3D case, averaged over 200 realizations of anchor positions. . . . .	103
4.16	Performance for orientation $\theta$ (deg, upper curves) and angular velocity $\omega$ (lower curves) estimations. . . . .	110
4.17	Performance for position $\mathbf{t}$ (upper curves) and translational velocity $\dot{\mathbf{t}}$ (lower curves) estimations. . . . .	111
4.18	Performance for sensor positions (upper curves) and velocities (lower curves) estimations. . . . .	112
4.19	Computational times vs anchor number $M$ . . . . .	113
5.1	3D single sensor case, performance for position (upper curves) and orientation (lower curves) estimations. . . . .	123

5.2	3D multiple sensors case, performance for position (upper curves) and orientation (lower curves) estimations. . . . .	124
5.3	2D multiple sensors case, performance for position (upper curves) and orientation (lower curves, in deg) estimations. . . . .	125

## ABSTRACT

Localization has been a very important and fundamental research topic in GPS, radar, sonar, and especially in mobile communications and sensor networks over the past few years. Localization of a signal source is often accomplished by using a number of sensors that measure the radiated signal from the source, here we consider the range based measurements, including time of arrival (TOA) and time difference of arrival (TDOA). In such study, the object is far away or only the position information is needed, and we refer this as point source localization. For some applications, e.g., robotics, spacecraft, and gaming, orientation information in addition to position is also needed. Although an inertial measurement unit (IMU) can perform such task once the initial state is available, it suffers from long-term performance deviation and requires accurate calibration using additional devices. Here we consider joint position and orientation estimation using the distance or AOA measurements between the fixed sensors on the object and the anchors at fixed locations, and it is called rigid body localization.

Our research has two manifolds:

First, for the point source localization, the original squared range least squares (SR-LS) admits global and computationally efficient solution using generalized trust region subproblems (GTRS) technique but with non-optimal accuracy, therefore we add proper range weighting (SR-WLS) into it and investigate the resulting performances of mean squared error (MSE) and bias. Its asymptotic efficiency is proven theoretically and validated by simulations. The effects of range weighting on the localization performance under different sensor number, noise correlation, and local-

ization geometry are examined. We also conduct similar range weighting for squared range difference least squares (SRD-LS and SRD-WLS) under TDOA measurements. In addition, the weighting technique is extended to the scenario where the sensor positions are not exactly known. The resultant cost function has the same structure as that without sensor position errors, thereby existing algebraic or exact solutions to the squared measurements can still be used without requiring new optimization method.

Second, for the rigid body localization, under distance measurements, the existing method cancels the quadratic term of the sensor position in the squared distance measurement equations, which may cause serious degradation. Our proposed estimators are non-iterative and have two steps: preliminary and refinement. The preliminary step provides a coarse estimate and the refinement step improves the first step estimate to yield an accurate solution. When the rigid body is stationary, we are able to locate the rigid body with accuracy higher than the solutions of comparable complexity found in the literature. When the rigid body is moving, we introduce additional Doppler shift measurements and develop an estimator that contains the additional unknowns of angular and translational velocities. Simulations show that the proposed estimators, in both stationary and moving cases, can approach the Cramer-Rao lower bound (CRLB) performance under Gaussian noise over the small error region.

Under AOA measurements, we solve the 3D scenario that is seldom considered before, through estimating its distances to landmarks and contrasting the landmark positions in object local frame and the global frame. Furthermore, we extend it to the scenario where there is more than one AOA sensor on-board, which either increases the robustness and accuracy or decreases the minimum requirement on

number of landmarks. And the methods for 2D and 3D are designed respectively. The simulations confirm the effectiveness of proposed methods.



# Chapter 1

## Introduction

### 1.1 Background and Motivation

#### 1.1.1 Point Source Localization

Localization has been a very important and fundamental research topic in GPS, radar, sonar, and especially in mobile communications and sensor networks over the past few years [1, 2, 3, 4, 5, 6, 7, 8, 9, 10]. When the object is far away or only the position information is needed, we can consider the object as a point source and refer this positioning task as point source localization in this dissertation. Localization of a signal source is often accomplished by using a number of sensors that measure the radiated signal from the source. The positioning parameters such as time of arrival (TOA) or time difference of arrival (TDOA) are obtained from the received signals. The relationship between the source location and the positioning parameters is exploited next to determine where the source is.

Nearly all algebraic solutions use the approach of squaring the measurements first, then introduce an auxiliary variable and define a constraint relating the extra variable and the source position to obtain a location estimate. For example, [12] and [13] derive closed-form solutions through subtracting the squared measurements to eliminate the auxiliary variable. [14], on the other hand, ignores the constraint and solves the squared measurement equation using linear least squares (LLS). [15] and [16] express the source location in terms of the auxiliary variable and solution finding reduces to determining the auxiliary variable that minimizes the corresponding cost function. Although simple and computationally attractive, these solutions do not reach the CRLB accuracy.

Recently, [17] utilizes the squared range least squares (SR-LS) cost function and imposes the constraint explicitly during the minimization process to obtain a global minimum solution through the generalized trust region subproblems (GTRS) technique [18]. Good localization accuracy, sometimes reaching the CRLB for uncorrelated Gaussian noise, has been reported over other competing methods. However, [19] has shown that even for the fundamental case of uncorrelated Gaussian noise, the approach of squaring the range (TOA) measurements to solve the localization problem will not be able to yield the same performance as using the measurements directly, e.g. from MLE, unless under some special and restricted localization geometries. Indeed, the asymptotic localization error from SR-LS relative to the CRLB could be unbounded for some configurations.

To compensate this degradation while remaining the computational advantage from squared range cost function, we introduce range weighting into it. Fundamental investigation of its resulting MSE is conducted and compared with CRLB, the bias

is also studied.

Similar study extends to the TDOA localization. We investigate the possible performance loss by squaring the range difference measurements when solving for the source location using least squares. The analysis shows that squared range difference least squares (SRD-LS) is not able to reach the CRLB performance in general, and the performance could be very worse in some cases. We would also introduce the range weighting and verify its theoretical performance.

Until now, the weighting technique considered assumes the exact sensor positions are known. In practice, the sensor positions are not known exactly, such as in a sensor network in which the node positions are estimated by anchors. Sensor position errors degrade the localization performance considerably [39], and its effect is not negligible even if the number of sensors is large [40], therefore their statistics should be taken into consideration in order to reach better performance [41, 42]. We would derive the new weightings for the squared TOA and TDOA measurements when sensor position errors are present.

### **1.1.2 Rigid Body Localization – Position and Orientation Estimation**

In addition to position, many applications including robotics, spacecraft and gaming [48, 49, 50, 51] requires both position and orientation information, and we refer this positioning task as rigid body localization in this dissertation. This is also called pose estimation in robotics community. An inertial measurement unit (IMU), such as accelerometer and gyroscope, can provide the position and orientation information when properly initialized, but it may suffer from long-term performance deviation

and requires accurate calibration using additional devices [52]. Using GPS for the positioning task could be costly and involve complicated receivers and processings [53], and it is limited to outdoor environments.

An alternative approach is to place a few sensors on the rigid body and use distance or angle of arrival (AOA) measurements [53, 54, 55] with respect to a few landmarks (simply called anchors) to determine the position and orientation. This is a constrained nonlinear estimation problem, due to the rotation matrix belonging to the special orthogonal ( $SO$ ) group [62] and the measurement equation highly nonlinear with the unknowns, making it very challenging to solve.

### **Under Distance Measurements**

Different from the traditional sensor node localization using anchors [57], the relative locations of the sensors are known. A direct solution but rather complicated to implement is the maximum likelihood estimator (MLE) that is obtained through an iterative geometric descent approach, where the optimization is performed in the Riemannian manifolds [54] to satisfy the  $SO$  group constraint. The estimator requires good initial guesses for convergence to the correct solution. Under the noise free assumption, [55] derives a solution by constructing a dynamic system that evolves on the special Euclidean group  $SE(3)$  where local asymptotic stability can be maintained. This method requires many numerical integrations to determine the evolving state of the system and its performance under noisy measurements is not guaranteed. [53] addresses the nonlinear estimation problem using the range-based localization technique. It converts the measurement equation to a linear form by taking the squares and eliminating the quadratic unknown terms. Two main solutions were developed,

one is the constrained least squares (CLS) which is iterative and the other is the simplified constrained least squares (SCLS) that is non-iterative. However, they are not asymptotically efficient in general. One may consider using CLS or SCLS to initialize an iterative implementation of the MLE to reach a better solution. The MLE is rather difficult to realize [54] since the  $SO$  group constraint must be imposed in each iteration. We conduct this study and propose closed-form estimator to approach the CRLB performance.

The scenario considered above assumes stationary object, while most rigid bodies of interests are often not standstill, and obvious examples are UAVs and robots. Indeed, many engineering applications [52, 63, 64, 65] are related to the localization and tracking of a moving object. A moving rigid body has the additional parameters of angular and translational velocities. If they are known, [66] has proposed a tracking solution. They are, however, often not known without using IMU and we have not come across any solution from the literature. The need to develop a localization method for a moving rigid body with unknown velocities is evident. We propose the use of additional Doppler measurements to obtain the motion parameter information, and extend our method for stationary rigid body to this new problem.

### **Under AOA Measurements**

The pose estimation using the AOA measurements with respect to known landmarks has been studied much more extensively than that using distance measurements. [80] makes use of representation of landmarks by complex numbers; [81] transforms the measurement into linear system with constraint that can be solved by singular value decomposition; [82, 83] use different pseudolinear equations and propose different bias

compensation.

However, these studies only handle 2D scenario. Some examples in 3D scenario are the flying aircraft and the robot on uneven ground. In 3D, the rotational degrees of freedom increase to 3 and corresponding rotation matrix belongs to special orthogonal group  $SO(3)$ . To our best knowledge, few works provide the solution to this under non-tracking scenario. [84] assumes the roll and pitch angles are coarsely known or close to zero, which limits its applicability. And the simultaneous localization and mapping (SLAM) using bearing only [85, 86, 87] normally handles it in tracking scenario, and the initialization is needed for the operation of filter, e.g. extended Kalman filter or particle filter. In our work, we consider the general 3D scenario and propose the method that does not need initialization.

With single sensor on-board, the AOA measurement with respect to certain landmark may be unavailable due to the blockage in the line of sight (LOS) path, and the number of landmarks may be not enough to uniquely recover the pose of the object in changing environment. Therefore, we extend the study to the scenario where there are multiple sensors on-board, which either increases the robustness and accuracy of localization system or decreases the minimum requirement on number of landmarks.

## 1.2 Basics for Point Source Localization

The localization accuracy is related to the received waveforms, signal and noise bandwidths, signal-noise ratio (SNR) and observation time [34, 44, 45, 46, 47], and also the localization approach. One approach is to directly estimate the position from the received signal, which is called direct positioning [8]; it can have better performance

when SNR is quite small, but is very time consuming since it often relies on grid search. The alternative approach is to obtain positioning parameter first, such as the TOA, TDOA, received signal strength (RSS), and AOA, and then perform localization based on this positioning parameter. Such indirect positioning, or two-step positioning, is much more popular in research. The performance of location estimator can be evaluated in terms of computational efficiency, estimation accuracy and robustness under different localization geometries.

Obtaining the source location from the range-based measurements is not an easy task, since the measurement equation is nonlinear with respect to the unknowns. Solving the source position directly from the measurements which contains the root square operation of source position, such as by the MLE [89], requires an iterative solution whose performance depends highly on initialization.

Most of researches square the measurements first, then introduce an auxiliary variable and define a constraint relating the extra variable and the source position to obtain a location estimate. For example, the well known two-stage estimator for TDOA localization [2] contains usual unconstrained least squares in the first stage and then correct the solution by considering the constraint in the second stage, and it reaches CRLB performance when noise is sufficiently small; however, its thresholding effect appears earlier compared to the MLE.

[17] utilizes existing GTRS technique to globally solve the SR-LS cost function which can be formulated as quadratic minimization under one quadratic equality constraint. The Lagrange multiplier method needs to solve all the roots in the equality constraint and obtain corresponding solutions, and then pick up the solution resulting in the minimum, while GTRS guarantees that the optimal solution corresponds to

the largest real root whose lower bound is also specified. [17] also provides global solution for SRD-LS cost function.

When the sensor positions have uncertainties, the sensor positions become nuisance variables and they need to be solved jointly with the source position. The number of unknowns becomes large and it presents challenges to an iterative solution in reaching the global optimum and in maintaining the computational efficiency. For example, [41] addressed the sensor position uncertainty by jointly estimating the source and sensor positions through an iterative implementation of MLE. [42] handled the situation by joint estimation as well using semidefinite programming (SDP). This motivates the development of closed-form solutions for the localization problem and it has been an active research area.

### **1.3 Basics for Rigid Body Localization – Position and Orientation Estimation**

The position and orientation of object reveal the translation and rotation between body-fixed reference frame in object and global reference frame. The rotation matrix and translation vector are nonlinearly related to the measurements and they are strongly coupled. In addition, the rotation matrix must belong to the special orthogonal ( $SO$ ) group [62], meaning that its elements must satisfy certain quadratic constraints in 2D and cubic constraints in 3D. Alternatively, rotation can be described by different parameterizations [62], such as Euler angle, axis-angle representation, Gibbs vector, modified Rodrigues parameters, and unit quaternion.

Inertial measurement unit is the most common device for joint position and ori-



entation estimation. It obtains linear acceleration measurement from accelerometers and angular velocity measurement from gyroscopes, and then performs the integration based on known initial states. Therefore, the drift problem exists. In some applications, we are interested in the pose of the object with respect to local environment, the IMU cannot be used since its measurement is always with respect to the inertial reference frame.

Distance measurement can be also exploited for pose estimation [53, 54, 55]. Since the distance measurement is independent of reference frame, multiple sensors on-board are needed to disclose the orientation information of local frame. And the sensor positions in this local reference frame should be known *a priori*. The difficulty in estimation is that even we square the distance measurement, it contains quadratic cross term of rotation matrix and translation while constraint on rotation matrix should be guaranteed.

The pose estimation using AOA measurements is significantly different from that using distance measurements. First, the AOA measurement is always conducted with respect to certain reference frame, even only one sensor on-board is sufficient to disclose the orientation information of the object. Second, the distance measurement requires either time synchronization between sensors and landmarks (anchors) or round trip signal transmission while AOA measurement does not have such requirement. If the object position is known, this problem becomes attitude determination using vector observation, which is directly related to orthogonal Procrustes problem (OPP) [90, 91, 92].

## 1.4 Contributions of the Research

This dissertation conducts the study of weighting technique for localization based on squared measurement in the absence or presence of sensor position errors, and of the algorithm for pose estimation using distance measurements (additional Doppler measurements for moving object) or AOA measurements.

In **Chapter 2**, we show the approach of squaring the range measurements for localization is able to provide the CRLB performance asymptotically regardless of the geometry (except the source is very close to a sensor), when suitable range weightings are introduced to the squared measurements before solving for the solution. The efficiency of new SR-WLS solution is shown analytically through small noise analysis. The asymptotic bias of the source location estimate from SR-WLS is found to be larger than that of SR-LS. However, the bias is relatively insignificant compared to variance.

Another advance in our study is that by introducing suitable weightings to the squared range difference measurements before least squares minimization, denoted as squared range difference weighted least squares (SRD-WLS), the performance loss will be compensated for and the CRLB performance can be reached. This is again shown analytically and supported by simulations. Different from the range measurement case, the proposed SRD-WLS has smaller bias than SRD-LS when the number of sensors is not near critical.

In **Chapter 3**, in the presence of sensor position errors, we derive the optimal weighting for the SR-WLS and SRD-WLS cost functions. The benefits for this extension are threefold. First, a typical algorithm such as the MLE needs to jointly estimate the source and sensor positions, while the proposed new cost function estimates

the source position only. Obviously, the dimension reduction in optimization can significantly reduce the computational complexity. Second, the new cost functions have the same structure as those in [17], thereby existing algebraic or exact solutions to the squared measurements can still be used without requiring new optimization method. Third, the solutions of the new cost functions achieve asymptotically the CRLB performance under Gaussian noise.

In **Chapter 4**, we propose closed-form solutions to the rigid body localization problem where the rigid body can be stationary or moving. The aim is to achieve better performance than the previous computationally attractive methods such as SCLS and CLS while maintaining similar complexity. The proposed solutions use a two-step approach. The first step obtains a preliminary solution by using the divide and conquer (DAC) technique [67] that solves the individual sensor positions first and then the rotation and translation parameters with the rotation matrix structure imposed. The preliminary solution is reasonably accurate as supported by the theory of the DAC approach, but not able to reach the optimum performance due to some simplifications taken in arriving at a closed-form solution. The second step reformulates the estimation problem in terms of the correction to the preliminary solution for obtaining a better result. In the special case of 2D scenario, we can take the advantage of the simpler rotation matrix structure so that both processing steps can be reformulated as two separate GTRS [18, 17] optimizations in which computationally efficient closed-form solutions exist.

Finally, we proceed to solve the localization of a moving rigid body that includes the additional unknowns of angular and translational velocities. In addition to distance measurements, we also make use of the Doppler measurements. A sequential

estimation is proposed, and the initial velocities are estimated based on available estimation of position and orientations. For special 2D case, we first obtain from the measurements the sensor positions and velocities pretending no knowledge among them and then exploit their relative positions to directly estimate the unknown parameters. We focus on the second step here and develop a closed-form solution through nuisance variables and nonlinear transformations.

In **Chapter 5**, we study the pose estimation using AOA measurements instead. For 3D case under one sensor that is seldom considered before, we can obtain the anchor positions in local frame and compare with their positions in global frame to obtain the pose, but it is quite difficult to directly obtain the anchor positions. Although converting the AOA equations into the linear form of anchor position simplifies the relationship, it causes the presence of two possible anchor positions, which prevents solving certain optimization using semidefinite relaxation. Furthermore, even we can obtain two optimal solutions simultaneously, we still need to pick up the best solutions according to the original AOA measurements, e.g. through the residual comparison. Our idea for determining the anchor position in local frame is to obtain its distances to landmarks and then combine them with the measured unit vectors pointing from sensor to anchors. And such distances can be obtained by exploiting the law of cosine for the triangle consisting one sensor and two anchors.

For multiple sensors case, we directly solve the pose through proper parameterization of rotation matrix based on the abovementioned transformed linear equation of anchor position. In 3D case, we use the unit quaternion parameterization and therefore the rotation matrix and constraints are quadratic in quaternion variables, which facilitates the use of semidefinite relaxation technique [57]; in 2D case, we use

the rotation angle and propose the closed-form solution based on GTRS technique [17, 18].

## **1.5 Content Organization**

The rest chapters are organized as follows. Chapter 2 presents the investigation of range weighting in squared measurements cost function and its resulting MSE and bias. Chapter 3 extends the weighting study when there are sensor position errors. Chapter 4 develops closed-form pose estimator for stationary and moving rigid body. Chapter 5 develops estimator for rigid body pose under AOA measurements. Chapter 6 discusses the future work.

## Chapter 2

# Range Weighting for Squared Measurements Based Least Squares

The existing SR-LS cost function solved by GTRS admits global solution but with suboptimum performance; to maintain its computational advantage and improve the accuracy, we propose to add range weighting and study its resultant MSE and bias. And we are interested in the effects of range weighting on the localization performance under different sensor number, noise correlation, and localization geometry. The range weighting study will also be extended to the SRD-LS cost function under TDOA measurements.

In the following, we shall first describe the localization scenario, the TOA and TDOA measurements and the corresponding CRLBs. Section 2.2 introduces the proposed range weighting version cost function SR-WLS, derives the MSE matrix and bias of its location estimate, and shows that SR-WLS achieves asymptotically

the CRLB performance. Section 2.3 conducts the same study for range weighting version cost function SRD-WLS under TDOA measurements. Section 2.4 presents the simulation results to compare the performance between SR-LS and SR-WLS, and between SRD-LS and SRD-WLS, and Section 2.5 concludes this chapter.

## 2.1 Range Based Localization

### 2.1.1 Localization Scenario

The purpose of localization is to determine the source position using measurements from a number of sensors. We shall consider two types of measurements, TOA and TDOA, that are based on the ranges between the source and the sensors. We shall use TOA and range, and TDOA and range difference interchangeably because they differ from each other by a constant scaling factor only. The source position is  $\mathbf{u}^o$  and the  $i$ -th sensor position is  $\mathbf{s}_i$ ,  $i = 1, 2, \dots, M$ , where  $M$  is the number of sensors.  $\mathbf{u}^o$  and  $\mathbf{s}_i$  are  $N \times 1$  vectors of Cartesian coordinates where  $N = 2$  for 2D and  $N = 3$  for 3D localization. The true distance between the source  $\mathbf{u}^o$  and the  $i$ -th sensor is  $r_i^o = \|\mathbf{u}^o - \mathbf{s}_i\|$ , and  $\|\cdot\|$  is the Euclidean norm.

For TOA localization, the true distance  $r_i^o$  is corrupted by additive noise  $n_i$  and the measurements are

$$r_i = r_i^o + n_i, \quad i = 1, 2, \dots, M. \quad (2.1)$$

In compact form,

$$\mathbf{r} = \mathbf{r}^o + \mathbf{n} \quad (2.2)$$

where  $\mathbf{r} = [r_1 \ r_2 \ \dots \ r_M]^T$  and  $\mathbf{r}^o = [r_1^o \ r_2^o \ \dots \ r_M^o]^T$ . The noise vector  $\mathbf{n} = [n_1 \ n_2 \ \dots \ n_M]^T$

is zero-mean Gaussian with covariance matrix  $\mathbf{Q}$ . The average measurement noise power is  $\sigma^2 = \text{tr}(\mathbf{Q})/M$ . We are interested in estimating  $\mathbf{u}^o$  from  $\mathbf{r}$ .

For TDOA localization, the true range difference of the source to the  $i$ -th and the 1st sensor is

$$r_{i1}^o = \|\mathbf{u}^o - \mathbf{s}_i\| - \|\mathbf{u}^o - \mathbf{s}_1\|, \quad i = 2, 3, \dots, M, \quad (2.3)$$

whose noisy version from measurement is

$$r_{i1} = r_{i1}^o + n_{i1}. \quad (2.4)$$

The 1st sensor is the reference to obtain the range difference. The vector form is

$$\mathbf{r}_d = \mathbf{r}_d^o + \mathbf{n}_d \quad (2.5)$$

where  $\mathbf{r}_d = [r_{21} \ r_{31} \ \dots \ r_{M1}]^T$  and  $\mathbf{r}_d^o = [r_{21}^o \ r_{31}^o \ \dots \ r_{M1}^o]^T$ . The noise vector  $\mathbf{n}_d = [n_{21} \ n_{31} \ \dots \ n_{M1}]^T$  is zero-mean Gaussian with covariance matrix  $\mathbf{Q}_d$ . The average measurement noise power is  $\sigma_d^2 = \text{tr}(\mathbf{Q}_d)/(M - 1)$ . TDOA localization uses  $\mathbf{r}_d$  to obtain the source position.



For convenient purpose in later sections, we shall define some notations as follows:

$$\begin{aligned}
\boldsymbol{\rho}_i &= \frac{\mathbf{u}^o - \mathbf{s}_i}{\|\mathbf{u}^o - \mathbf{s}_i\|}, \quad i = 1, 2, \dots, M, \\
\boldsymbol{\Gamma} &= [\boldsymbol{\rho}_1 \quad \boldsymbol{\rho}_2 \quad \cdots \quad \boldsymbol{\rho}_M], \\
\boldsymbol{\rho}_{i1} &= \boldsymbol{\rho}_i - \boldsymbol{\rho}_1, \quad i = 2, 3, \dots, M, \\
\boldsymbol{\Gamma}_d &= [\boldsymbol{\rho}_{21} \quad \boldsymbol{\rho}_{31} \quad \cdots \quad \boldsymbol{\rho}_{M1}], \\
\mathbf{B} &= \text{diag}(\mathbf{r}^o), \\
\mathbf{B}_d &= \text{diag}(\mathbf{r}_d^o) + r_1^o \mathbf{I}.
\end{aligned} \tag{2.6}$$

$\boldsymbol{\rho}_i$  is the unit vector pointing from the  $i$ -th sensor to the source  $\mathbf{u}^o$  and  $\boldsymbol{\rho}_{i1}$  is the difference between  $\boldsymbol{\rho}_i$  and  $\boldsymbol{\rho}_1$ .  $\mathbf{B}$  and  $\mathbf{B}_d$  are diagonal matrices containing the ranges of the source to different sensors. Furthermore,  $\mathbf{1}$  is used to denote a vector of unity and  $\mathbf{I}$  is an identity matrix.  $\text{diag}(\mathbf{a})$  is a diagonal matrix formed by the elements in  $\mathbf{a}$  and the operator  $\odot$  is element-by-element multiplication.

### 2.1.2 CRLB

We shall use the CRLB [20] as a benchmark to examine the performance of a location estimator. The CRLB is for unbiased estimator and the localization problem is non-linear that could yield a biased solution. Hence we shall use the CRLB over small error region only where the bias is negligible compared to variance. The CRLB of a source location estimate for TOA positioning is [21]

$$\text{CRLB} = \text{FIM}(\mathbf{u}^o)^{-1} = (\boldsymbol{\Gamma} \mathbf{Q}^{-1} \boldsymbol{\Gamma}^T)^{-1}. \tag{2.7}$$

The CRLB for TDOA positioning is [22]

$$\text{CRLB} = \text{FIM}(\mathbf{u}^o)^{-1} = (\mathbf{\Gamma}_d \mathbf{Q}_d^{-1} \mathbf{\Gamma}_d^T)^{-1}. \quad (2.8)$$

## 2.2 Weighted Squared Range Localization

### 2.2.1 Cost Function and Solution

The range least squares (R-LS) method finds  $\mathbf{u}^o$  by minimizing the cost function

$$f_{\text{R-LS}}(\mathbf{u}) = \sum_{i=1}^M (r_i - \|\mathbf{u} - \mathbf{s}_i\|)^2. \quad (2.9)$$

Under Gaussian noise with  $\mathbf{Q} = \sigma^2 \mathbf{I}$ , R-LS gives the maximum likelihood estimate and achieves the CRLB performance. The cost function  $f_{\text{R-LS}}(\mathbf{u})$  is difficult to solve due to the square root operation in the Euclidean distance. One has to rely on grid search, or iterative numerical solution where performance could be highly dependent on initializations.

As an alternative to simplify the solution finding, many closed-form efficient solutions can be obtained by minimizing the SR-LS cost function

$$f_{\text{SR-LS}}(\mathbf{u}) = \sum_{i=1}^M (r_i^2 - \|\mathbf{u} - \mathbf{s}_i\|^2)^2. \quad (2.10)$$

In particular, [17] shows that the global minimum of this cost function can be efficiently solved through the utilization of the GTRS technique [18].

However, the large-sample analysis performed in [19] finds that SR-LS has worse

asymptotic localization accuracy than R-LS in general and there are localization geometries for which the performance difference between them is unbounded.

We propose a new cost function  $f_{\text{SR-WLS}}(\mathbf{u})$  based on  $f_{\text{SR-LS}}(\mathbf{u})$  by introducing the weighting factors  $1/r_i^2$

$$f_{\text{SR-WLS}}(\mathbf{u}) = \sum_{i=1}^M \frac{1}{r_i^2} (r_i^2 - \|\mathbf{u} - \mathbf{s}_i\|^2)^2. \quad (2.11)$$

The rationale behind this new cost function is that when the noise relative to the source range is small and  $\mathbf{u}$  is close to  $\mathbf{u}^o$  such that  $r_i = r_i^o \left(1 + \frac{n_i}{r_i^o}\right) \approx r_i^o \approx \|\mathbf{u} - \mathbf{s}_i\|$ , we have

$$\begin{aligned} f_{\text{SR-WLS}}(\mathbf{u}) &= \sum_{i=1}^M \left( r_i - \frac{\|\mathbf{u} - \mathbf{s}_i\|^2}{r_i} \right)^2 \\ &\approx \sum_{i=1}^M (r_i - \|\mathbf{u} - \mathbf{s}_i\|)^2 \end{aligned} \quad (2.12)$$

which is the  $f_{\text{R-LS}}(\mathbf{u})$  given in (2.9). Hence it is expected that the new squared range weighted least squares (SR-WLS) cost function has similar performance as R-LS when we are near the solution. SR-WLS will remain to enjoy the computational efficiency as in SR-LS because no square root appears in the cost function.

Another reason for introducing the weights  $1/r_i^2$  in the proposed cost function (2.11) is that squaring the ranges will emphasize the TOA measurements from the sensors that are farther away from the source. The SR-LS cost function (2.10) will therefore yield a solution that puts more emphasis to the measurements from the far than from the near sensors. To compensate this undesirable effect, we use the weights inversely proportional to the square of the distances. The net effect is that it

equalizes the contributions of measurements from far and near sensors when obtaining the solution.

The aforementioned cost functions correspond to uncorrelated noise covariance matrix  $\mathbf{Q} = \sigma^2 \mathbf{I}$ . It is natural to extend our investigation to the general case for Gaussian noise with arbitrary non-singular covariance matrix  $\mathbf{Q} = [Q_{ij}]$ . Let's represent its inverse as  $\mathbf{Q}^{-1} = [\bar{Q}_{ij}]$ , then we have

$$f_{\text{R-LS}}(\mathbf{u}) = \sum_{i,j=1}^M \bar{Q}_{ij} (r_i - \|\mathbf{u} - \mathbf{s}_i\|) (r_j - \|\mathbf{u} - \mathbf{s}_j\|), \quad (2.13)$$

$$f_{\text{SR-LS}}(\mathbf{u}) = \sum_{i,j=1}^M \bar{Q}_{ij} (r_i^2 - \|\mathbf{u} - \mathbf{s}_i\|^2) (r_j^2 - \|\mathbf{u} - \mathbf{s}_j\|^2), \quad (2.14)$$

and

$$f_{\text{SR-WLS}}(\mathbf{u}) = \sum_{i,j=1}^M \frac{\bar{Q}_{ij}}{r_i r_j} (r_i^2 - \|\mathbf{u} - \mathbf{s}_i\|^2) (r_j^2 - \|\mathbf{u} - \mathbf{s}_j\|^2), \quad (2.15)$$

where (2.13) is the maximum likelihood cost function.

The analysis on the MSE and bias will be based on (2.14) and (2.15). We shall show that SR-WLS can asymptotically achieve the CRLB performance, while SR-LS cannot.

### 2.2.2 Analysis and Comparison with CRLB

We shall perform the small noise analysis of the solutions obtained from the SR-LS and SR-WLS cost functions. The analysis is up to second order noise terms, and it gives asymptotic performance when the SNR of the signal measurements to obtain

TOA is high or the signal observation period is long.

Let  $\hat{\mathbf{u}}$  be the global minimum of  $f$ . Also, let us assume  $f$  is smooth around  $\hat{\mathbf{u}}$  such that the derivatives of  $f$  at  $\hat{\mathbf{u}}$  exist up to third order. Obviously, the gradient of  $f$  at  $\hat{\mathbf{u}}$  is zero. Using the Taylor series expansion around the true value  $\mathbf{u}^o$ ,

$$\mathbf{0} = \left. \frac{\partial f(\mathbf{u})}{\partial \mathbf{u}} \right|_{\mathbf{u}=\hat{\mathbf{u}}} \approx \mathbf{f}' + \mathbf{F}''(\hat{\mathbf{u}} - \mathbf{u}^o) + \frac{1}{2} \begin{bmatrix} \text{tr}(\mathbf{F}_1''' \mathbf{M}) \\ \vdots \\ \text{tr}(\mathbf{F}_N''' \mathbf{M}) \end{bmatrix}$$

where

$$\mathbf{f}' = \left. \frac{\partial f(\mathbf{u})}{\partial \mathbf{u}} \right|_{\mathbf{u}=\mathbf{u}^o}, \quad \mathbf{F}'' = \left. \frac{\partial^2 f(\mathbf{u})}{\partial \mathbf{u} \partial \mathbf{u}^T} \right|_{\mathbf{u}=\mathbf{u}^o}, \quad \mathbf{F}_l''' = \left. \frac{\partial}{\partial u_l} \frac{\partial^2 f(\mathbf{u})}{\partial \mathbf{u} \partial \mathbf{u}^T} \right|_{\mathbf{u}=\mathbf{u}^o}, \quad l = 1, 2, \dots, N,$$

$u_l$  is the  $l$ -th element of  $\mathbf{u}$ ,  $N$  is length of  $\mathbf{u}$  and  $\mathbf{M} = (\hat{\mathbf{u}} - \mathbf{u}^o)(\hat{\mathbf{u}} - \mathbf{u}^o)^T$ . The approximation comes from truncating the expansion up to the second order term. Note that  $\mathbf{F}''$  is symmetric. Rearranging gives

$$\hat{\mathbf{u}} - \mathbf{u}^o \approx -\mathbf{F}''^{-1} \mathbf{f}' - \frac{1}{2} \mathbf{F}''^{-1} \begin{bmatrix} \text{tr}(\mathbf{F}_1''' \mathbf{M}) \\ \vdots \\ \text{tr}(\mathbf{F}_N''' \mathbf{M}) \end{bmatrix}. \quad (2.16)$$

To examine the MSE, we multiply (2.16) by its transpose and take expectation, giving

$$E [(\hat{\mathbf{u}} - \mathbf{u}^o)(\hat{\mathbf{u}} - \mathbf{u}^o)^T] \approx E [\mathbf{F}''^{-1} \mathbf{f}' \mathbf{f}'^T \mathbf{F}''^{-1}] \quad (2.17)$$

where the second term in (2.16) has been ignored. This is because the last term in

(2.16) will contribute to the  $\sigma^4$  component in the MSE which is negligible for small noise analysis. Since  $\mathbf{f}'$  contains only noise, retaining up to  $\sigma^2$  term reduces (2.17) to

$$E[(\hat{\mathbf{u}} - \mathbf{u}^o)(\hat{\mathbf{u}} - \mathbf{u}^o)^T] \approx \bar{\mathbf{F}}''^{-1} E[\mathbf{f}'\mathbf{f}'^T] \bar{\mathbf{F}}''^{-1} \quad (2.18)$$

where  $\bar{\mathbf{F}}'' = \lim_{\sigma^2 \rightarrow 0} \mathbf{F}''$ . (2.18) is indeed the formula given in [23] to obtain the asymptotic MSE as  $\sigma^2 \rightarrow 0$ . It is also the formula [19] used to perform large-sample analysis of SR-LS.

The bias can be obtained by taking the expectation of (2.16),

$$E[\hat{\mathbf{u}} - \mathbf{u}^o] \approx -E[\mathbf{F}''^{-1}\mathbf{f}'] - \frac{1}{2}\bar{\mathbf{F}}''^{-1} \begin{bmatrix} \text{tr}(\bar{\mathbf{F}}_1''' E[\mathbf{M}]) \\ \vdots \\ \text{tr}(\bar{\mathbf{F}}_N''' E[\mathbf{M}]) \end{bmatrix} \quad (2.19)$$

where  $\bar{\mathbf{F}}_l''' = \lim_{\sigma^2 \rightarrow 0} \mathbf{F}_l'''$  and we have made approximation in the last term to keep up to second order noise components only. Note that  $E[\mathbf{M}]$  is the MSE matrix.

The MSE and bias formulae (2.18) and (2.19) are accurate up to second order noise terms and the approximations come from ignoring some higher order terms. For simplicity two formulae are considered exact in the following analysis.

We shall evaluate the terms in (2.18) and (2.19) to obtain the MSE and bias. In general,  $\mathbf{f}'$  contains the 1st order, 2nd order, and higher order noise components.  $\mathbf{F}''$  contains a fixed term independent of noise, as well as 1st order, 2nd order, and higher order noise terms. Evaluating (2.18) only needs the linear noise component of  $\mathbf{f}'$ . However, obtaining the first term of (2.19) requires up to 2nd order noise portion of  $\mathbf{f}'$  and up to 1st order noise portion of  $\mathbf{F}''$ . Hence we retain only up to 2nd order

noise terms of  $\mathbf{f}'$  and up to 1st order noise terms of  $\mathbf{F}''$ .

We shall use small-o notation to provide more precise order of approximation in the followings. In our representation,  $a(x) = o(b(x))$  means  $\lim_{x \rightarrow 0} a(x)/b(x) = 0$ .

The analysis below concentrates on the MSE. The bias study is a little tedious and the details are provided in Appendix A.

### Asymptotic Performance of SR-LS

The first derivative of  $f_{\text{SR-LS}}(\mathbf{u})$  in (2.14) is

$$\frac{\partial f_{\text{SR-LS}}(\mathbf{u})}{\partial \mathbf{u}} = -4 \sum_{i,j=1}^M \bar{Q}_{ij} (r_i^2 - \|\mathbf{u} - \mathbf{s}_i\|^2) (\mathbf{u} - \mathbf{s}_j) \quad (2.20)$$

where we have used the symmetric property that  $\bar{Q}_{ij} = \bar{Q}_{ji}$ . Then

$$\mathbf{f}'_{\text{SR-LS}} = -4 \sum_{i,j=1}^M \bar{Q}_{ij} (2r_i^o n_i + n_i^2) r_j^o \boldsymbol{\rho}_j = -4[2\mathbf{K}\mathbf{B}\mathbf{n} + \mathbf{K}(\mathbf{n} \odot \mathbf{n})] \quad (2.21)$$

where

$$\mathbf{K} = [\mathbf{k}_1 \ \mathbf{k}_2 \ \cdots \ \mathbf{k}_M] = \mathbf{\Gamma}\mathbf{B}\mathbf{Q}^{-1}, \quad \mathbf{k}_i = \sum_{j=1}^M \bar{Q}_{ij} r_j^o \boldsymbol{\rho}_j. \quad (2.22)$$

Therefore,

$$E[\mathbf{f}'_{\text{SR-LS}} \mathbf{f}_{\text{SR-LS}}^T] = 64\mathbf{K}\mathbf{B}\mathbf{Q}\mathbf{B}\mathbf{K}^T + o(\sigma^2)\mathbf{1}\mathbf{1}^T. \quad (2.23)$$

We continue by calculating the second derivative of  $f_{\text{SR-LS}}(\mathbf{u})$  from (2.20),

$$\frac{\partial^2 f_{\text{SR-LS}}(\mathbf{u})}{\partial \mathbf{u} \partial \mathbf{u}^T} = -4 \sum_{i,j=1}^M \bar{Q}_{ij} [-2(\mathbf{u} - \mathbf{s}_i)(\mathbf{u} - \mathbf{s}_j)^T + (r_i^2 - \|\mathbf{u} - \mathbf{s}_i\|^2)\mathbf{I}]. \quad (2.24)$$

Hence

$$\begin{aligned}\mathbf{F}_{\text{SR-LS}}'' &= -4 \sum_{i,j=1}^M \bar{Q}_{ij} [-2(\mathbf{u}^o - \mathbf{s}_i)(\mathbf{u}^o - \mathbf{s}_j)^T + (2r_i^o n_i + n_i^2)\mathbf{I}] \\ &= 8 [\mathbf{K}\mathbf{B}\mathbf{\Gamma}^T - (\mathbf{n}^T \mathbf{B}\mathbf{Q}^{-1} \mathbf{1})\mathbf{I}] + o(\|\mathbf{n}\|)\mathbf{I},\end{aligned}\tag{2.25}$$

whose asymptotic value as  $\sigma^2 \rightarrow 0$  is

$$\bar{\mathbf{F}}_{\text{SR-LS}}'' = 8\mathbf{K}\mathbf{B}\mathbf{\Gamma}^T.\tag{2.26}$$

Consequently, we obtain from (2.18) the asymptotic MSE matrix of SR-LS as

$$\mathbf{Q}_{\text{SR-LS}} = (\mathbf{K}\mathbf{B}\mathbf{\Gamma}^T)^{-1} \mathbf{K}\mathbf{B}\mathbf{Q}\mathbf{B}\mathbf{K}^T (\mathbf{K}\mathbf{B}\mathbf{\Gamma}^T)^{-1}.\tag{2.27}$$

In general, (2.27) is not equal to the CRLB unless for a few special cases. One such a case is when all  $r_i^o$ 's are equal such that  $\mathbf{B} = b\mathbf{I}$ , where  $b$  is positive constant.  $\mathbf{K}$  in (2.22) becomes  $\mathbf{K} = b\mathbf{\Gamma}\mathbf{Q}^{-1}$  and (2.27) reduces to  $\mathbf{Q}_{\text{SR-LS}} = (\mathbf{\Gamma}\mathbf{Q}^{-1}\mathbf{\Gamma}^T)^{-1}$ , which is the CRLB in (2.7).

The bias of the SR-LS solution is evaluated using (2.26), (2.27), (A.2) and (A.3) into (2.19).

### Asymptotic Performance of SR-WLS

The first derivative of  $f_{\text{SR-WLS}}(\mathbf{u})$  is

$$\frac{\partial f_{\text{SR-WLS}}(\mathbf{u})}{\partial \mathbf{u}} = -4 \sum_{i,j=1}^M \frac{\bar{Q}_{ij}}{r_i r_j} (r_i^2 - \|\mathbf{u} - \mathbf{s}_i\|^2) (\mathbf{u} - \mathbf{s}_j).\tag{2.28}$$



From series expansion,

$$\frac{1}{r_i} = \frac{1}{r_i^o \left(1 + \frac{n_i}{r_i^o}\right)} = \frac{1}{r_i^o} \left(1 - \frac{n_i}{r_i^o}\right) + o\left(\frac{n_i}{r_i^o}\right). \quad (2.29)$$

Using (2.29) in (2.28) gives

$$\begin{aligned} \mathbf{f}'_{\text{SR-WLS}} &= -4 \sum_{i,j=1}^M \frac{\bar{Q}_{ij}}{r_i^o} \left(1 - \frac{n_i}{r_i^o} - \frac{n_j}{r_j^o}\right) (2r_i^o n_i + n_i^2) \boldsymbol{\rho}_j + o(\|\mathbf{n}\|^2) \mathbf{1} \\ &= -4 \left[ 2\boldsymbol{\Gamma} \mathbf{Q}^{-1} \mathbf{n} - \boldsymbol{\Gamma} \mathbf{Q}^{-1} \mathbf{B}^{-1} (\mathbf{n} \odot \mathbf{n}) - 2\boldsymbol{\Gamma} \text{diag}(\mathbf{n}) \mathbf{B}^{-1} \mathbf{Q}^{-1} \mathbf{n} \right] + o(\|\mathbf{n}\|^2) \mathbf{1}. \end{aligned} \quad (2.30)$$

Hence

$$E[\mathbf{f}'_{\text{SR-WLS}} \mathbf{f}_{\text{SR-WLS}}^T] = 64\boldsymbol{\Gamma} \mathbf{Q}^{-1} \boldsymbol{\Gamma}^T + o(\sigma^2) \mathbf{1} \mathbf{1}^T. \quad (2.31)$$

The second derivative of  $f_{\text{SR-WLS}}(\mathbf{u})$  from (2.28) is

$$\frac{\partial^2 f_{\text{SR-WLS}}(\mathbf{u})}{\partial \mathbf{u} \partial \mathbf{u}^T} = -4 \sum_{i,j=1}^M \frac{\bar{Q}_{ij}}{r_i r_j} \left[ -2(\mathbf{u} - \mathbf{s}_i)(\mathbf{u} - \mathbf{s}_j)^T + (r_i^2 - \|\mathbf{u} - \mathbf{s}_i\|^2) \mathbf{I} \right] \quad (2.32)$$

and therefore

$$\begin{aligned}
& \mathbf{F}_{\text{SR-WLS}}'' \\
&= -4 \sum_{i,j=1}^M \frac{\overline{Q}_{ij}}{r_i^o r_j^o} \left( 1 - \frac{n_i}{r_i^o} - \frac{n_j}{r_j^o} + o(\|\mathbf{n}\|) \right) [-2r_i^o r_j^o \boldsymbol{\rho}_i \boldsymbol{\rho}_j^T + (2r_i^o n_i + n_i^2) \mathbf{I}] \\
&= 8 [\boldsymbol{\Gamma} \mathbf{Q}^{-1} \boldsymbol{\Gamma}^T - (\mathbf{n}^T \mathbf{Q}^{-1} \mathbf{B}^{-1} \mathbf{1}) \mathbf{I} - \boldsymbol{\Gamma} \mathbf{B}^{-1} \text{diag}(\mathbf{n}) \mathbf{Q}^{-1} \boldsymbol{\Gamma}^T - \boldsymbol{\Gamma} \mathbf{Q}^{-1} \text{diag}(\mathbf{n}) \mathbf{B}^{-1} \boldsymbol{\Gamma}^T] \\
&\quad + o(\|\mathbf{n}\|) \mathbf{1} \mathbf{1}^T.
\end{aligned} \tag{2.33}$$

Its asymptotic value as  $\sigma^2 \rightarrow 0$  is

$$\overline{\mathbf{F}}_{\text{SR-WLS}}'' = 8 \boldsymbol{\Gamma} \mathbf{Q}^{-1} \boldsymbol{\Gamma}^T. \tag{2.34}$$

As a result, putting (2.31) and (2.34) into (2.18) gives the asymptotic MSE matrix of SR-WLS as

$$\mathbf{Q}_{\text{SR-WLS}} = (\boldsymbol{\Gamma} \mathbf{Q}^{-1} \boldsymbol{\Gamma}^T)^{-1}. \tag{2.35}$$

$\mathbf{Q}_{\text{SR-WLS}}$  is exactly equal to the CRLB (2.7) for TOA localization and the solution of the SR-WLS cost function is asymptotically efficient.

The bias of the SR-WLS solution is obtained by applying (2.34), (2.35), (A.5) and (A.6) to (2.19).

### 2.2.3 Special Geometries

Under independent and identically distributed (i.i.d.) measurement noise such that  $\mathbf{Q} = \sigma^2 \mathbf{I}$ , [19] lists four classes of special geometries to demonstrate that SR-LS is

worse than R-LS in general. [19] also generates random geometries to illustrate the distribution of the MSE ratio between the solutions from SR-LS and R-LS. Since the proposed SR-WLS has the same asymptotic accuracy as R-LS up to the second order noise term, we can essentially draw the same conclusion when comparing SR-LS with SR-WLS.

In the situation where the source signal is not available or when there is an unknown but constant time offset in the signals acquired, TOA cannot be used to locate the source and TDOA will need to be applied instead. TDOA does not require the source signal to be known since it can be obtained through cross-correlation. Furthermore, the constant time offset is irrelevant because TDOA measures the time differences. In fact, the performance of TDOA localization is the same as TOA positioning with an unknown common clock bias (time offset) [24]. We shall next examine the localization performance using the squared range differences.

## 2.3 Weighted Squared Range Difference Localization

### 2.3.1 Cost Function and Solution

For measurement noise with arbitrary non-singular covariance matrix  $\mathbf{Q}_d$ , the cost function for range difference least squares (RD-LS) is

$$f_{\text{RD-LS}}(\mathbf{u}) = \sum_{i,j=2}^M \overline{Q}_{dij} (r_{i1} + \|\mathbf{u} - \mathbf{s}_1\| - \|\mathbf{u} - \mathbf{s}_i\|) (r_{j1} + \|\mathbf{u} - \mathbf{s}_1\| - \|\mathbf{u} - \mathbf{s}_j\|), \quad (2.36)$$

where  $\overline{Q}_{dij}$  is the element in the  $(i-1)$ -th row and  $(j-1)$ -th column of  $\mathbf{Q}_d^{-1}$ ,  $i, j = 2, 3, \dots, M$ . The RD-LS solution corresponds to the MLE and has the CRLB performance when the noise is Gaussian. (2.36) is difficult to solve and quite often the squared range difference least squares (SRD-LS) cost function is used instead,

$$f_{\text{SRD-LS}}(\mathbf{u}) = \sum_{i,j=2}^M \overline{Q}_{dij} p_i p_j, \quad (2.37)$$

where

$$p_i = (r_{i1} + \|\mathbf{u} - \mathbf{s}_1\|)^2 - \|\mathbf{u} - \mathbf{s}_i\|^2.$$

$f_{\text{SRD-LS}}(\mathbf{u})$  can be obtained from  $f_{\text{SR-LS}}(\mathbf{u})$  in (2.10) by replacing  $r_i$  with  $r_{i1} + \|\mathbf{u} - \mathbf{s}_1\|$ . The SRD-LS cost function used in [17] is a special case of (2.37) when the noise is i.i.d. Generally speaking, the solution of SRD-LS is worse than that of RD-LS.

Motivated by the result that SR-WLS can asymptotically achieve the CRLB accuracy, we propose to add weighting factor  $1/(r_i r_j)$  to the SRD-LS and generate the squared range difference weighted least squares (SRD-WLS) cost function

$$f_{\text{SRD-WLS}}(\mathbf{u}) = \sum_{i,j=2}^M \frac{\overline{Q}_{dij}}{r_i r_j} p_i p_j. \quad (2.38)$$

The rationale for using the weighting  $1/(r_i r_j)$  is the same as for SR-WLS. In particular, the weights are used to compensate for the artificial effect of emphasizing more the TDOA measurements from the far sensors than from the near sensors caused by squaring the measurements. The  $r_i$  in the weighting factor is approximated by

$$r_i \approx r_{i1} + \|\tilde{\mathbf{u}} - \mathbf{s}_1\| \quad (2.39)$$

where  $\tilde{\mathbf{u}}$  is from some initial source position estimate which will be elaborated later.

### 2.3.2 Analysis and Comparison with CRLB

We shall perform the small noise analysis of the solutions obtained from SRD-LS and the proposed SRD-WLS.

#### Asymptotic Performance of SRD-LS

The first derivative of  $f_{\text{SRD-LS}}$  is

$$\frac{\partial f_{\text{SRD-LS}}(\mathbf{u})}{\partial \mathbf{u}} = 4 \sum_{i,j=2}^M \bar{Q}_{dij} p_i \left( \mathbf{s}_j - \mathbf{s}_1 + r_{j1} \frac{\mathbf{u} - \mathbf{s}_1}{\|\mathbf{u} - \mathbf{s}_1\|} \right). \quad (2.40)$$

Evaluating at the true source location gives

$$\begin{aligned} \mathbf{f}'_{\text{SRD-LS}} &= 4 \sum_{i,j=2}^M \bar{Q}_{dij} (2r_i^o n_{i1} + n_{i1}^2) (-r_j^o \boldsymbol{\rho}_{j1} + \boldsymbol{\rho}_1 n_{j1}) \\ &= 4 \left[ -2\mathbf{K}_d \mathbf{B}_d \mathbf{n}_d + 2\boldsymbol{\rho}_1 (\mathbf{n}_d^T \mathbf{B}_d \mathbf{Q}_d^{-1} \mathbf{n}_d) - \mathbf{K}_d (\mathbf{n}_d \odot \mathbf{n}_d) \right] + o(\|\mathbf{n}_d\|^2) \mathbf{1} \end{aligned} \quad (2.41)$$

where

$$\mathbf{K}_d = [\mathbf{k}_{d2} \ \mathbf{k}_{d3} \ \cdots \ \mathbf{k}_{dM}] = \boldsymbol{\Gamma}_d \mathbf{B}_d \mathbf{Q}_d^{-1}, \quad \mathbf{k}_{di} = \sum_{j=2}^M \bar{Q}_{dij} r_j^o \boldsymbol{\rho}_{j1}. \quad (2.42)$$

Thus

$$E[\mathbf{f}'_{\text{SRD-LS}} \mathbf{f}_{\text{SRD-LS}}'^T] = 64 \mathbf{K}_d \mathbf{B}_d \mathbf{Q}_d \mathbf{B}_d \mathbf{K}_d^T + o(\sigma_d^2) \mathbf{1} \mathbf{1}^T. \quad (2.43)$$

We continue by calculating second derivative of  $f_{\text{SRD-LS}}(\mathbf{u})$  from (2.40),

$$\begin{aligned} & \frac{\partial^2 f_{\text{SRD-LS}}(\mathbf{u})}{\partial \mathbf{u} \partial \mathbf{u}^T} \\ &= 4 \sum_{i,j=2}^M \bar{Q}_{dij} \left[ 2 \left( \mathbf{s}_i - \mathbf{s}_1 + r_{i1} \frac{\mathbf{u} - \mathbf{s}_1}{\|\mathbf{u} - \mathbf{s}_1\|} \right) \left( \mathbf{s}_j - \mathbf{s}_1 + r_{j1} \frac{\mathbf{u} - \mathbf{s}_1}{\|\mathbf{u} - \mathbf{s}_1\|} \right)^T + p_i r_{j1} \mathbf{X} \right] \end{aligned} \quad (2.44)$$

where  $\mathbf{X} = \frac{\partial}{\partial \mathbf{u}} \left( \frac{\mathbf{u} - \mathbf{s}_1}{\|\mathbf{u} - \mathbf{s}_1\|} \right)^T$ . Retaining up to linear error terms gives

$$\begin{aligned} & \mathbf{F}_{\text{SRD-LS}}'' \\ &= 4 \sum_{i,j=2}^M \bar{Q}_{dij} \left[ 2(-r_i^o \boldsymbol{\rho}_{i1} + \boldsymbol{\rho}_1 n_{i1})(-r_j^o \boldsymbol{\rho}_{j1} + \boldsymbol{\rho}_1 n_{j1})^T + (2r_i^o n_{i1} + n_{i1}^2)(r_{j1}^o + n_{j1}) \mathbf{X}^o \right] \\ &= 8 \left\{ \mathbf{K}_d \mathbf{B}_d \boldsymbol{\Gamma}_d^T - [\mathbf{K}_d \mathbf{n}_d \boldsymbol{\rho}_1^T + \boldsymbol{\rho}_1 (\mathbf{K}_d \mathbf{n}_d)^T - (\mathbf{n}_d^T \mathbf{B}_d \mathbf{Q}_d^{-1} \mathbf{r}_d^o) \mathbf{X}^o] \right\} + o(\|\mathbf{n}_d\|) \mathbf{1} \mathbf{1}^T, \end{aligned} \quad (2.45)$$

where  $\mathbf{X}^o = \mathbf{X}|_{\mathbf{u}=\mathbf{u}^o} = (\mathbf{I} - \boldsymbol{\rho}_1 \boldsymbol{\rho}_1^T)/r_1^o$ . Its asymptotic value as  $\sigma_d^2 \rightarrow 0$  is

$$\bar{\mathbf{F}}_{\text{SRD-LS}}'' = 8 \mathbf{K}_d \mathbf{B}_d \boldsymbol{\Gamma}_d^T. \quad (2.46)$$

Finally, we obtain from (2.18), (2.43) and (2.46) that the asymptotic MSE matrix of SRD-LS is

$$\mathbf{Q}_{\text{SRD-LS}} = (\mathbf{K}_d \mathbf{B}_d \boldsymbol{\Gamma}_d^T)^{-1} \mathbf{K}_d \mathbf{B}_d \mathbf{Q}_d \mathbf{B}_d \mathbf{K}_d^T (\mathbf{K}_d \mathbf{B}_d \boldsymbol{\Gamma}_d^T)^{-1}. \quad (2.47)$$

Generally speaking, (2.47) is larger than the CRLB. One exception is that all  $r_i^o$ 's,  $i = 2, 3, \dots, M$ , are equal. In such a case,  $\mathbf{B}_d$  is proportional to an identity matrix and putting in (2.42), (2.47) becomes the CRLB in (2.8) for TDOA localization. This

special case corresponds to the localization geometry where all sensors, except the first, are lying on a circle and the source is at the center.

The bias of the SRD-LS solution is obtained using (2.46), (2.47), (A.8) and (A.9) in (2.19).

### Asymptotic Performance of SRD-WLS

The first derivative of  $f_{\text{SRD-WLS}}$  is

$$\frac{\partial f_{\text{SRD-WLS}}(\mathbf{u})}{\partial \mathbf{u}} = 4 \sum_{i,j=2}^M \frac{\bar{Q}_{dij}}{r_i r_j} p_i \left( \mathbf{s}_j - \mathbf{s}_1 + r_{j1} \frac{\mathbf{u} - \mathbf{s}_1}{\|\mathbf{u} - \mathbf{s}_1\|} \right) \quad (2.48)$$

and  $r_i$  is obtained from (2.39). Assuming  $\tilde{\mathbf{u}}$  is relatively accurate and has small error  $\Delta \mathbf{u} = \mathbf{A} \mathbf{n}_d$ , where  $\mathbf{A}$  is a matrix determined by the algorithm to obtain  $\tilde{\mathbf{u}}$ , the use of Taylor series expansion gives  $\|\tilde{\mathbf{u}} - \mathbf{s}_1\| = \|\mathbf{u}^o - \mathbf{s}_1 + \mathbf{A} \mathbf{n}_d\| \approx r_1^o + \boldsymbol{\alpha}^T \mathbf{n}_d$ , where  $\boldsymbol{\alpha} = \mathbf{A}^T \boldsymbol{\rho}_1$ . Therefore,  $r_i \approx r_{i1}^o + n_{i1} + r_1^o + \boldsymbol{\alpha}^T \mathbf{n}_d = r_i^o + n_{i1} + \boldsymbol{\alpha}^T \mathbf{n}_d$  and the error in  $r_i$  is  $n_{i1} + \boldsymbol{\alpha}^T \mathbf{n}_d$ . Approximating  $1/r_i$  as  $(1 - (n_{i1} + \boldsymbol{\alpha}^T \mathbf{n}_d)/r_i^o) / r_i^o$  gives

$$\begin{aligned} & \mathbf{f}'_{\text{SRD-WLS}} \\ &= 4 \sum_{i,j=2}^M \frac{\bar{Q}_{dij}}{r_i^o r_j^o} \left( 1 - \frac{n_{i1} + \boldsymbol{\alpha}^T \mathbf{n}_d}{r_i^o} - \frac{n_{j1} + \boldsymbol{\alpha}^T \mathbf{n}_d}{r_j^o} + o(\|\mathbf{n}_d\|) \right) (2r_i^o n_{i1} + n_{i1}^2) (-r_j^o \boldsymbol{\rho}_{j1} + \boldsymbol{\rho}_1 n_{j1}) \\ &= 4 \sum_{i,j=2}^M \bar{Q}_{dij} \left[ -2\boldsymbol{\rho}_{j1} n_{i1} + \frac{1}{r_i^o} \boldsymbol{\rho}_{j1} n_{i1}^2 + \frac{2}{r_j^o} \boldsymbol{\rho}_j n_{i1} n_{j1} + 2 \left( \frac{1}{r_i^o} + \frac{1}{r_j^o} \right) \boldsymbol{\rho}_{j1} n_{i1} \boldsymbol{\alpha}^T \mathbf{n}_d \right] + o(\|\mathbf{n}_d\|^2) \mathbf{1} \\ &= 4 \left[ -2\boldsymbol{\Gamma}_d \mathbf{Q}_d^{-1} \mathbf{n}_d + \boldsymbol{\Gamma}_d \mathbf{Q}_d^{-1} \mathbf{B}_d^{-1} (\mathbf{n}_d \odot \mathbf{n}_d) + 2(\boldsymbol{\Gamma}_d + \boldsymbol{\rho}_1 \mathbf{1}^T) \text{diag}(\mathbf{n}_d) \mathbf{B}_d^{-1} \mathbf{Q}_d^{-1} \mathbf{n}_d \right. \\ & \quad \left. + 2\boldsymbol{\Gamma}_d (\mathbf{Q}_d^{-1} \mathbf{B}_d^{-1} + \mathbf{B}_d^{-1} \mathbf{Q}_d^{-1}) \mathbf{n}_d \boldsymbol{\alpha}^T \mathbf{n}_d \right] + o(\|\mathbf{n}_d\|^2) \mathbf{1}. \end{aligned} \quad (2.49)$$

Hence

$$E[\mathbf{f}'_{\text{SRD-WLS}} \mathbf{f}_{\text{SRD-WLS}}^T] = 64\mathbf{\Gamma}_d \mathbf{Q}_d^{-1} \mathbf{\Gamma}_d^T + o(\sigma_d^2) \mathbf{1}\mathbf{1}^T. \quad (2.50)$$

The second derivative of  $f_{\text{SRD-WLS}}(\mathbf{u})$  from (2.48) is

$$\begin{aligned} & \frac{\partial^2 f_{\text{SRD-WLS}}(\mathbf{u})}{\partial \mathbf{u} \partial \mathbf{u}^T} \\ &= 4 \sum_{i,j=2}^M \frac{\overline{Q}_{dij}}{r_i r_j} \left[ 2 \left( \mathbf{s}_i - \mathbf{s}_1 + r_{i1} \frac{\mathbf{u} - \mathbf{s}_1}{\|\mathbf{u} - \mathbf{s}_1\|} \right) \left( \mathbf{s}_j - \mathbf{s}_1 + r_{j1} \frac{\mathbf{u} - \mathbf{s}_1}{\|\mathbf{u} - \mathbf{s}_1\|} \right)^T + p_i r_{j1} \mathbf{X} \right] \end{aligned} \quad (2.51)$$

and

$$\begin{aligned} & \mathbf{F}_{\text{SRD-WLS}}'' \\ &= 4 \sum_{i,j=2}^M \frac{\overline{Q}_{dij}}{r_i^o r_j^o} \left[ 1 - \frac{n_{i1}}{r_i^o} - \frac{n_{j1}}{r_j^o} - \boldsymbol{\alpha}^T \mathbf{n}_d \left( \frac{1}{r_i^o} + \frac{1}{r_j^o} \right) + o(\|\mathbf{n}_d\|) \right] \times \\ & \quad \left[ 2(-r_i^o \boldsymbol{\rho}_{i1} + \boldsymbol{\rho}_1 n_{i1})(-r_j^o \boldsymbol{\rho}_{j1} + \boldsymbol{\rho}_1 n_{j1})^T + (2r_i^o n_{i1} + n_{i1}^2)(r_{j1}^o + n_{j1}) \mathbf{X}^o \right] \\ &= 8 \sum_{i,j=2}^M \frac{\overline{Q}_{dij}}{r_i^o r_j^o} \left\{ r_i^o r_j^o \boldsymbol{\rho}_{i1} \boldsymbol{\rho}_{j1}^T - [r_i^o \boldsymbol{\rho}_{i1} n_{j1} \boldsymbol{\rho}_j^T + \boldsymbol{\rho}_i r_j^o \boldsymbol{\rho}_{j1}^T n_{i1} - r_i^o r_{j1}^o n_{i1} \mathbf{X}^o + \boldsymbol{\alpha}^T \mathbf{n}_d (r_i^o + r_j^o) \boldsymbol{\rho}_{i1} \boldsymbol{\rho}_{j1}^T] \right\} \\ & \quad + o(\|\mathbf{n}_d\|) \mathbf{1}\mathbf{1}^T \\ &= 8 \left\{ \mathbf{\Gamma}_d \mathbf{Q}_d^{-1} \mathbf{\Gamma}_d^T - [\mathbf{\Gamma}_d \mathbf{Q}_d^{-1} \mathbf{B}_d^{-1} \text{diag}(\mathbf{n}_d) (\mathbf{\Gamma}_d + \boldsymbol{\rho}_1 \mathbf{1}^T)^T + (\mathbf{\Gamma}_d + \boldsymbol{\rho}_1 \mathbf{1}^T) \text{diag}(\mathbf{n}_d) \mathbf{B}_d^{-1} \mathbf{Q}_d^{-1} \mathbf{\Gamma}_d^T \right. \\ & \quad \left. - (\mathbf{n}_d^T \mathbf{Q}_d^{-1} \mathbf{B}_d^{-1} \mathbf{r}_d^o) \mathbf{X}^o + (\mathbf{\Gamma}_d \mathbf{Q}_d^{-1} (\mathbf{\Gamma}_d \mathbf{B}_d^{-1})^T + \mathbf{\Gamma}_d \mathbf{B}_d^{-1} \mathbf{Q}_d^{-1} \mathbf{\Gamma}_d^T) \boldsymbol{\alpha}^T \mathbf{n}_d \right\} + o(\|\mathbf{n}_d\|) \mathbf{1}\mathbf{1}^T. \end{aligned} \quad (2.52)$$



Its asymptotic value as  $\sigma_d^2 \rightarrow 0$  is

$$\bar{\mathbf{F}}''_{\text{SRD-WLS}} = 8\mathbf{\Gamma}_d \mathbf{Q}_d^{-1} \mathbf{\Gamma}_d^T. \quad (2.53)$$

Consequently, putting (2.50) and (2.53) into (2.18) gives the asymptotic MSE matrix of SRD-WLS as

$$\mathbf{Q}_{\text{SRD-WLS}} = (\mathbf{\Gamma}_d \mathbf{Q}_d^{-1} \mathbf{\Gamma}_d^T)^{-1}. \quad (2.54)$$

$\mathbf{Q}_{\text{SRD-WLS}}$  is exactly identical to the CRLB (2.8) for TDOA localization, meaning that the solution from the SRD-WLS cost function is asymptotically efficient.

The bias of the SRD-WLS solution is evaluated by putting (2.53), (2.54), (A.11) and (A.12) into (2.19).

The MSE performance of the proposed SRD-WLS cost function is independent of the choice of reference sensor over the small noise region. This is because from the relationship  $r_{ij} = r_{i1} - r_{j1}$ , using sensor  $j$  as reference instead of sensor 1 is equivalent to applying a linear transformation to the TDOA data vector  $\mathbf{r}_d$  in (2.5) through the pre-multiplication of an invertible  $(M-1) \times (M-1)$  matrix. The same linear transformation applies to the TDOA covariance matrix  $\mathbf{Q}_d$  and the gradient matrix  $\mathbf{\Gamma}_d$ . Since the transformation is linear and invertible, we will have the same MSE matrix given in (2.54) for the source location estimate. It should be noted though the bias could depend on the choice of the reference sensor because it is caused by the non-linearity in the estimation.

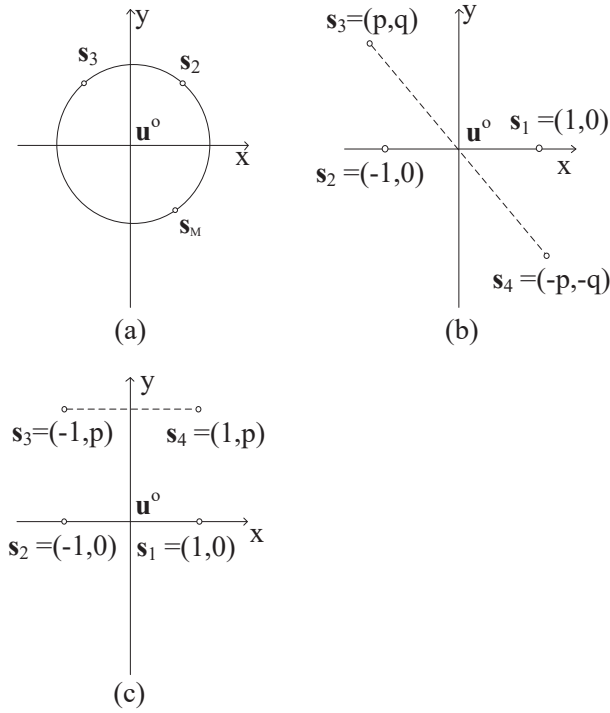


Figure 2.1: Special geometries for comparison of SRD-LS and SRD-WLS. (a) Case 1. (b) Case 2. (c) Case 3.

### 2.3.3 Special Geometries

We have proven SRD-WLS achieves the CRLB accuracy under small noise condition and has better estimation accuracy than SRD-LS. We would like to examine how much performance gain the SRD-WLS can achieve compared to SRD-LS and how the improvement varies with different geometries. For the sake of brevity, we consider 2D localization with sensor number  $M = 4$ . In the following, we construct three classes of special geometries and use the MSE matrices for SRD-LS and SRD-WLS in (2.47) and (2.54) to compare their performance.

The special geometries are shown in Fig. 2.1:

Case 1: All the sensors except the first (reference) are located on a circle with

radius  $R$  and centered at  $\mathbf{u}^o$ , as shown in Fig. 2.1(a).

Case 2: The sensors are at  $\mathbf{s}_1 = [1 \ 0]^T$ ,  $\mathbf{s}_2 = [-1 \ 0]^T$ ,  $\mathbf{s}_3 = [p \ q]^T$ ,  $\mathbf{s}_4 = [-p \ -q]^T$ , and the source  $\mathbf{u}^o$  is at the origin, as depicted in Fig. 2.1(b).

Case 3: The sensors are at  $\mathbf{s}_1 = [1 \ 0]^T$ ,  $\mathbf{s}_2 = [-1 \ 0]^T$ ,  $\mathbf{s}_3 = [-1 \ p]^T$ ,  $\mathbf{s}_4 = [1 \ p]^T$ , and the source  $\mathbf{u}^o$  is at the origin, as illustrated in Fig. 2.1(c). The sensor (anchor) arrangement in this form is quite common in sensor networks.

We shall look at the SRD-WLS performance relative to SRD-LS for uncorrelated and correlated noise, using the ratio  $\Delta = \text{tr}(\mathbf{Q}_{\text{SRD-LS}})/\text{tr}(\mathbf{Q}_{\text{SRD-WLS}})$ .

### Uncorrelated Noise $\mathbf{Q}_d = \sigma_d^2 \mathbf{I}$

The TDOA noise can be uncorrelated when the TDOAs are estimated one by one at different times.

Case 1: In this case,

$$\text{tr}(\mathbf{Q}_{\text{SRD-LS}}) = \text{tr}(\mathbf{Q}_{\text{SRD-WLS}}) = \sigma_d^2 \text{tr}((\mathbf{\Gamma}_d \mathbf{\Gamma}_d^T)^{-1}) \quad (2.55)$$

and both SRD-LS and SRD-WLS achieve the CRLB performance and  $\Delta = 1$ . This result can be explained by the fact that under small noise, the weighting factor  $1/(r_i r_j)$  in the SRD-WLS cost function becomes a constant since  $r_i \approx r_i^o = R$ . Therefore the SRD-WLS cost function differs from the SRD-LS cost function by a constant scaling factor only and hence they have the same performance.

Case 2: For this configuration,

$$\Delta = \frac{\frac{[(p^2+q^2)^2+2(p^2+q^2)+3](p^2+q^2)}{q^2(p^2+q^2+2)^2}}{\frac{2}{3} \frac{p^2+q^2}{q^2}} = \frac{3}{2} \left[ 1 - \frac{2r^2+1}{(r^2+2)^2} \right] \quad (2.56)$$

where  $r = \sqrt{p^2 + q^2}$ . When  $r = 1$ ,  $\Delta$  becomes unity because the geometry is the same as in Case 1. When  $r$  increases, however,  $\Delta$  tends to  $3/2$ . In this special case, SRD-WLS can provide up to 1.76 dB improvement over SRD-LS.

Case 3: In this situation,

$$\Delta = \frac{\frac{p^4 + 8p^2 + 6}{9p^2}}{\frac{2(p^2 + 1)^2}{p^2(2p^2 + 3)}} > \frac{2p^2 + 3}{18}. \quad (2.57)$$

This is a very interesting case because  $\Delta \rightarrow \infty$  as  $p \rightarrow \infty$ . In other word, as  $\mathbf{s}_3$  and  $\mathbf{s}_4$  move away from the source, SRD-WLS provides infinite performance gain over SRD-LS. Note that  $\text{tr}(\mathbf{Q}_{\text{SRD-WLS}})$  is bounded for  $p \geq 1$ ,

$$\text{tr}(\mathbf{Q}_{\text{SRD-WLS}}) = \sigma_d^2 \frac{2(p^2 + 1)^2}{p^2(2p^2 + 3)} < \sigma_d^2 \frac{p^2 + 1}{p^2} \leq 2\sigma_d^2. \quad (2.58)$$

It is because  $\text{tr}(\mathbf{Q}_{\text{SRD-LS}}) \rightarrow \infty$  as  $p \rightarrow \infty$  that makes the performance improvement infinite.

**Correlated Noise**  $\mathbf{Q}_d = \frac{\sigma_d^2}{2} (\mathbf{I} + \mathbf{1}\mathbf{1}^T)$

The TDOA noise is correlated with such a covariance matrix when the TDOAs are estimated jointly and the signals received at the sensors have i.i.d. noise and identical signal-to-noise ratio [2].

Case 1: In this case,

$$\text{tr}(\mathbf{Q}_{\text{SRD-LS}}) = \text{tr}(\mathbf{Q}_{\text{SRD-WLS}}) = \frac{\sigma_d^2}{2} \text{tr} \left( \left[ \mathbf{\Gamma}_d \left( \mathbf{I} - \frac{1}{M} \mathbf{1}\mathbf{1}^T \right) \mathbf{\Gamma}_d^T \right]^{-1} \right). \quad (2.59)$$

The reason that SRD-LS and SRD-WLS have the same performance as CRLB is the

same as before. RD-LS, SRD-LS and SRD-WLS have identical performance under small noise situation.

Case 2: In this scenario with  $p = 0$ ,

$$\Delta = \frac{\frac{q^2(|q|-1)^2}{[(|q|-1)^2+2]^2} + 1}{1}. \quad (2.60)$$

It can be proved that  $1 \leq \Delta \leq 2.23737$  and the maximum 2.23737 is attained at  $|q| = 3 + \sqrt{6}$ . For arbitrary  $p > 0$ , we have not proven the boundedness of  $\Delta$ , but from simulation and over the region  $-1000 \leq p, q \leq 1000$  with a resolution of 1, we find that  $1 \leq \Delta \leq 2.237$ , which is quite similar to the result with  $p = 0$ . The performance improvement is larger than the situation when the noise is uncorrelated.

Case 3: In this configuration,

$$\Delta = \frac{\frac{2p^4 - (p^2+1)^{3/2} - (3+p^2)\sqrt{p^2+1+14p^2+12}}{8p^2}}{\frac{3p^4+7p^2+4}{2p^4+4p^2}} \quad (2.61)$$

which indicates  $\Delta \rightarrow \infty$  as  $p \rightarrow \infty$ . Note that  $\text{tr}(\mathbf{Q}_{\text{SRD-WLS}})$  is bounded for  $p \geq 1$  at the value when  $p = 1$ ,

$$\text{tr}(\mathbf{Q}_{\text{SRD-WLS}}) = \sigma_d^2 \frac{3p^4 + 7p^2 + 4}{2p^4 + 4p^2} \leq \frac{7}{3} \sigma_d^2. \quad (2.62)$$

The infinite performance gain is resulted from  $\text{tr}(\mathbf{Q}_{\text{SRD-LS}}) \rightarrow \infty$  as  $p$  increases.

## 2.4 Simulations

In this section, we shall validate the theoretical study and examine the performance differences in MSE and bias between SR-LS and SR-WLS, and between SRD-LS and SRD-WLS. Since we focus on the solution accuracy of different cost functions and not the methods of solving them, we use the Gauss-Newton method with the true source location  $\mathbf{u}^o$  as the initial guess to obtain the numerical solutions. For SRD-WLS, we use the solution from SRD-LS to do the initialization and to obtain  $r_1 = \|\tilde{\mathbf{u}} - \mathbf{s}_1\|$  in (2.39) for the purpose of generating  $r_i$  for the weighting. The corresponding error in  $r_1$  is  $\boldsymbol{\alpha}^T \mathbf{n}_d \approx \boldsymbol{\rho}_1^T (-\mathbf{F}_{\text{SRD-LS}}''^{-1} \mathbf{f}_{\text{SRD-LS}}') \approx \boldsymbol{\rho}_1^T (\mathbf{K}_d \mathbf{B}_d \boldsymbol{\Gamma}_d^T)^{-1} \mathbf{K}_d \mathbf{B}_d \mathbf{n}_d$ .

We consider two different localization scenarios to examine the influence from the weighting factors. The first scenario fixes the source location and varies the sensor positions to create a number of random geometries. In particular, the source is at the origin and the sensors are randomly placed with uniform distributions in  $x$  and  $y$  coordinates inside the unit circle. The second scenario varies the source location and fixes the sensor positions for creating another set of random geometries. In particular, the source is randomly placed with uniform distributions in  $x$  and  $y$  coordinates inside the circle of radius 0.98 and the  $M$  sensors are allocated uniformly in the unit circle, i.e.,  $\mathbf{s}_i = \left[ \cos \frac{2\pi(i-1)}{M}, \sin \frac{2\pi(i-1)}{M} \right]^T$ .

In the simulation, the number of ensemble runs for each geometry is 1,200; the noise covariance matrix is  $\mathbf{Q}$  (or  $\mathbf{Q}_d$ ) =  $\frac{\sigma^2}{1+a} (\mathbf{I} + a\mathbf{1}\mathbf{1}^T)$  with different nonnegative value  $a$ .

### 2.4.1 Comparison of SR-LS and SR-WLS

We use uncorrelated noise with covariance matrix  $\mathbf{Q} = \sigma^2 \mathbf{I}$  ( $a = 0$ ) for the comparison unless stated otherwise.

#### Average MSE and Bias

Fig. 2.2 shows the average MSE result for  $M = 5$  over 4,000 randomly generated geometries for the first scenario. SR-WLS has 1.14 dB improvement over SR-LS and achieves the CRLB for  $\sigma^2$  less than 0.1. Beyond, the bias in SR-WLS dominates performance, causing the MSE below the CRLB. SR-WLS has larger bias than SR-LS as shown in Fig. 2.3, the difference is 9.20 dB for small noise. The increase in bias may be justified to achieve smaller MSE because the bias is negligible compared to the MSE. If we increase  $M$  to 10, the average MSE improvement of SR-WLS over SR-LS increases to 1.21 dB, and the average bias difference rises to 19.05 dB. Although the average improvement in MSE is not much, the improvement at some common geometries is significant as will be shown in Fig. 2.7.

For the second scenario, the average results with 4,000 random geometries are similar to those in Figs. 2.2 and 2.3. For  $M = 5$ , SR-WLS has 1.22 dB improvement in average MSE at the expense of 21.10 dB increase in average bias. For  $M = 10$ , SR-WLS has 1.28 dB improvement in average MSE and the increase in bias is 8.78 dB.

#### Distribution of MSE Ratio and Bias Ratio

We next examine the distributions of the theoretical MSE ratio and the bias ratio between SR-LS and SR-WLS over different geometries for the first scenario. The

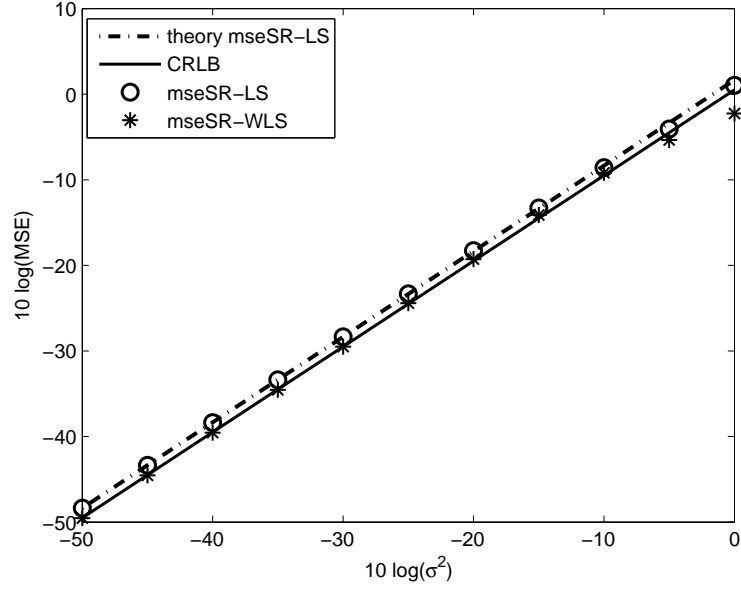


Figure 2.2: Average MSE for SR-LS and SR-WLS in the first scenario,  $M = 5$ .

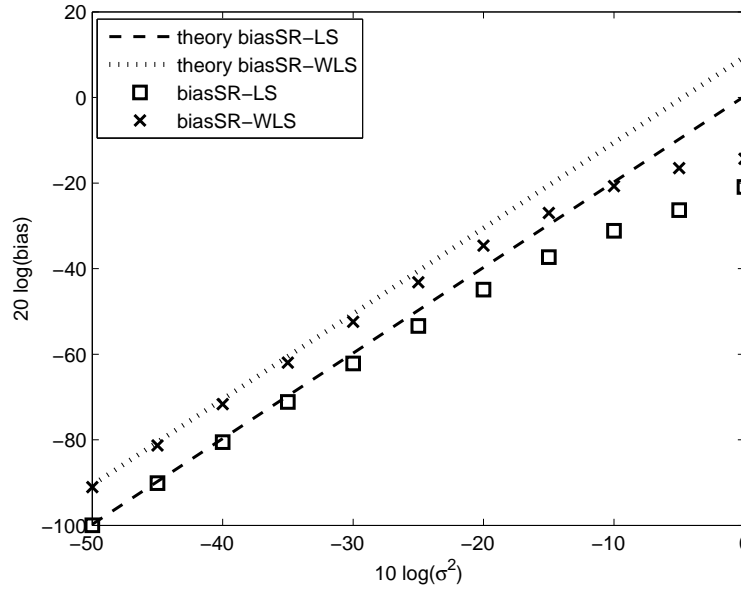


Figure 2.3: Average bias for SR-LS and SR-WLS in the first scenario,  $M = 5$ .



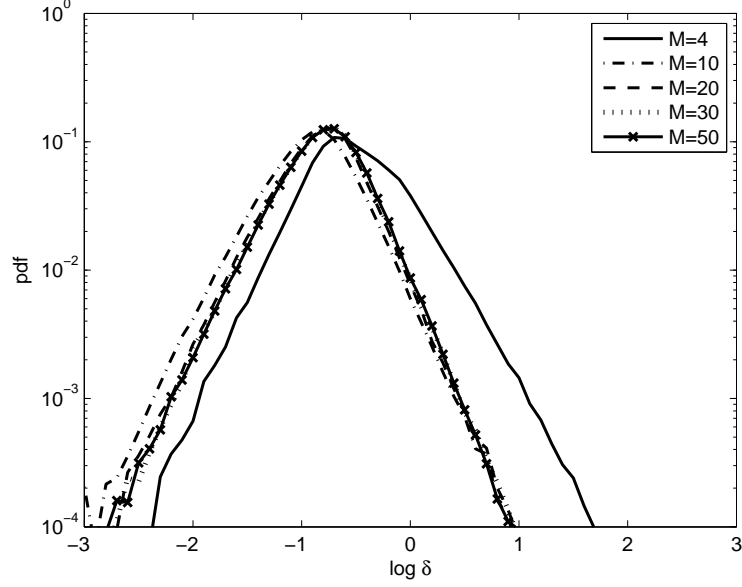


Figure 2.4: Empirical probability density functions of bias ratio between SR-LS and SR-WLS with different sensor numbers  $M$  in the first scenario.

MSE ratio distribution for uncorrelated noise ( $a = 0$ ) has been given in [19] and it tends to concentrate around  $\Delta = 1.3225$  for large enough sensor number. Here we only show the bias ratio distribution obtained from 200,000 random geometries.

Fig. 2.4 shows the empirical probability density functions of the logarithmic bias ratio  $\delta = \text{bias}(\text{SR-LS})/\text{bias}(\text{SR-WLS})$  under 5 different sensor numbers. First, we notice that  $\log \delta$  can be higher than 0, meaning that for some geometries SR-WLS can have smaller bias. Second, the bias ratio tends to concentrate around  $\log \delta = -0.75$ , i.e.,  $\delta = 0.18$  with large enough sensor number  $M$ .

### Comparison under Different Sensor Numbers $M$ and Noise Correlations

We consider the sensor number ranging from 3 to 50 and the noise correlation factor  $a$  varying from integer values of 0 to 5. Fig. 2.5 shows the average of the MSE ratio

$\Delta = \text{tr}(\mathbf{Q}_{\text{SR-LS}})/\text{tr}(\mathbf{Q}_{\text{SR-WLS}})$  over 40,000 random geometries of the first scenario as  $M$  increases. The minimum average ratio  $\Delta$  is 1.26, which occurs when  $M = 3$  and  $a = 0$ . For  $a = 0$  and  $a = 1$ , the average  $\Delta$  keeps increasing before  $M = 10$  and then tends to a constant value with larger sensor number  $M$ . For  $a = 2$ , the average  $\Delta$  varies slightly at the beginning and then stabilizes. When  $a$  further increases, contrary to that in  $a = 0$  and  $a = 1$ , the average  $\Delta$  is much larger for small sensor number  $M$  than the steady value for large  $M$ . It is also noticeable that the MSE improvement from SR-WLS over SR-LS is more significant as the noise becomes more correlated. For  $a = 5$ , the minimum average  $\Delta$  is 1.8.

Fig. 2.6 shows the corresponding results as in Fig. 2.5 for the average of the bias ratio  $\delta = \text{bias}(\text{SR-LS})/\text{bias}(\text{SR-WLS})$ . The average  $\delta$  is smaller than 0.6 in each curve and SR-LS has smaller bias. For uncorrelated noise  $a = 0$ , the average  $\delta$  decreases before  $M = 8$ , increases between  $M = 8$  and  $M = 20$ , and finally converges to 0.24. From  $a = 1$  to  $a = 5$ , each curve decreases with increasing sensor number  $M$ . We also notice that larger  $a$  produces smaller average  $\delta$ .

### Special Case with Large MSE Ratio $\Delta$

Fig. 2.7 shows the simulation result of the geometry from Special Case 4 in [19] with  $p = 20$ , where the source is at  $(0, 0)$  and the sensors are at  $(1, 0)$ ,  $(1, p)$  and  $(-1, p)$ . This geometry is known to be bad for SR-LS. We can see that the MSE of SR-WLS achieves the CRLB, and has more than 18 dB improvement over SR-LS for noise power below  $-20$  dB. In addition, the bias in SR-WLS is about 45 dB smaller than that in SR-LS for noise power below  $-20$  dB.

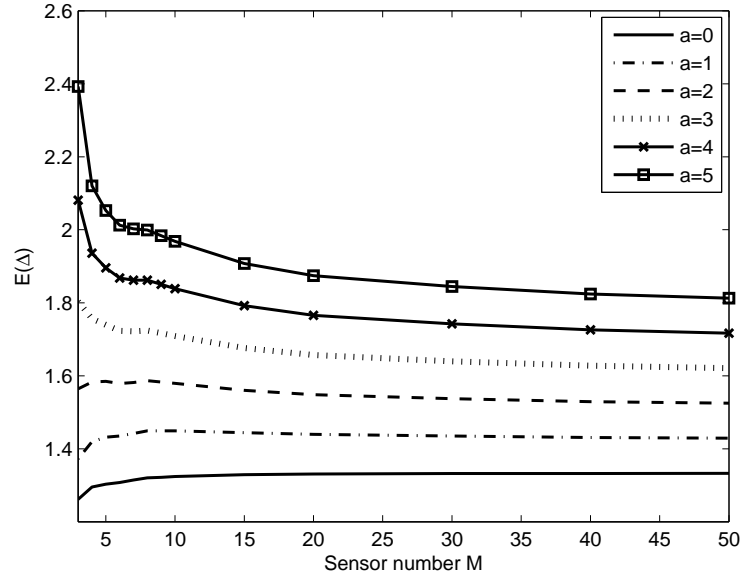


Figure 2.5: Average of MSE ratio  $\Delta$  between SR-LS and SR-WLS with different sensor numbers  $M$  and noise correlation factors  $a$  in the first scenario.

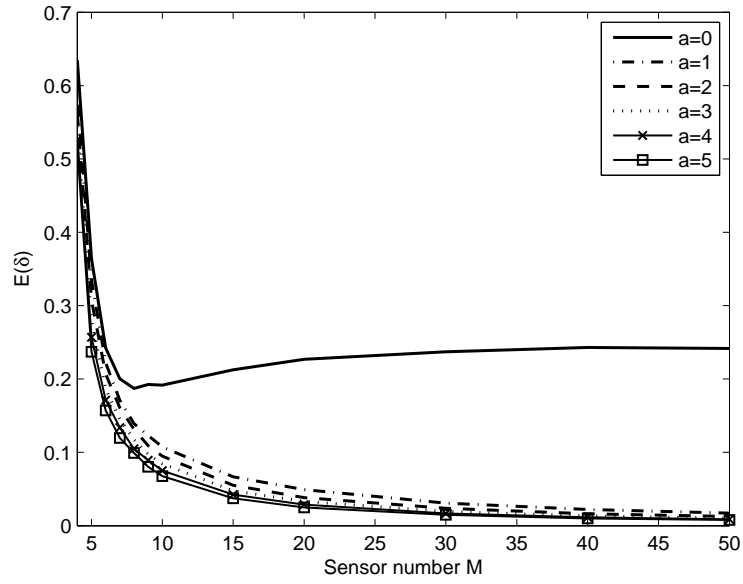


Figure 2.6: Average of bias ratio  $\delta$  between SR-LS and SR-WLS with different sensor numbers  $M$  and noise correlation factors  $a$  in the first scenario.

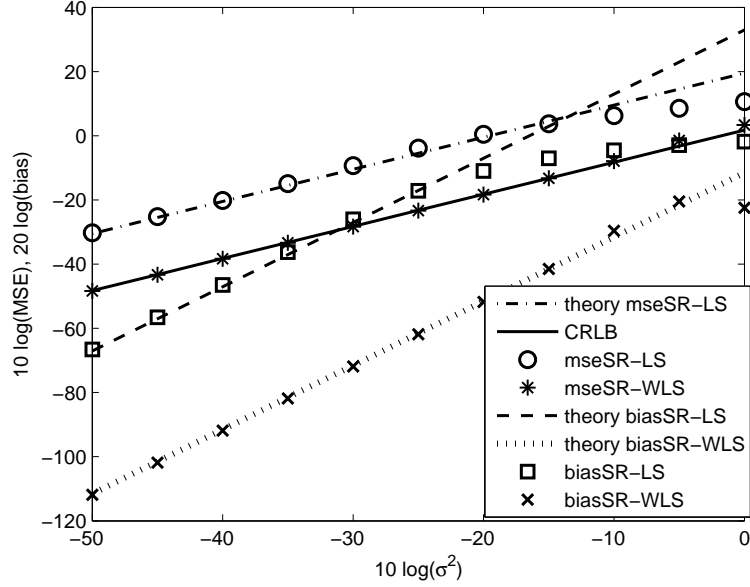


Figure 2.7: MSE and bias comparison of SR-LS and SR-WLS under Special Case 4 in [19] with  $p = 20$ .

### 2.4.2 Comparison of SRD-LS and SRD-WLS

We use the following particular setting unless stated otherwise. The noise covariance matrix is  $\mathbf{Q}_d = \frac{\sigma_d^2}{2}(\mathbf{I} + \mathbf{1}\mathbf{1}^T)$ , corresponding to the noise correlation factor  $a$  equal to 1. For the first scenario, the distances between the sensors and source  $\mathbf{u}^o$  are at least 0.1, i.e., all the sensors are uniformly distributed in the annulus which is inside the unit circle and outside the circle with radius 0.1. The purpose is to avoid the bad geometries where the sensors are too close to the source.

#### Average MSE and Bias

Fig. 2.8 shows the average MSE result for  $M = 5$  over 4,000 random geometries under the first scenario. The average MSE for SRD-WLS is 1.14 dB smaller than

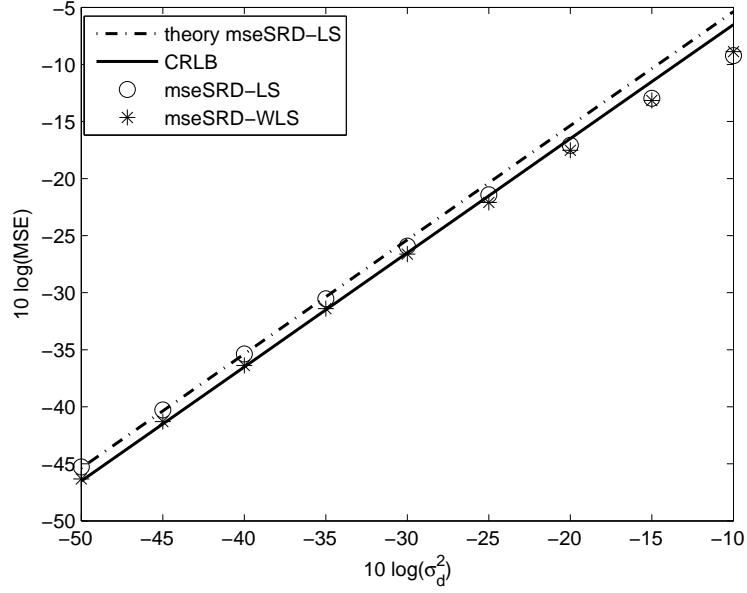


Figure 2.8: Average MSE for SRD-LS and SRD-WLS in the first scenario,  $M = 5$ .

that of SRD-LS and achieves the CRLB accuracy. Unlike SR-WLS, SRD-WLS does not introduce obvious bias compared to SRD-LS as can be seen in Fig. 2.9. If we increase  $M$  to 10, the average improvement is 1.43 dB in MSE and 1.08 dB in bias. The SRD-WLS improvement at some common geometries is significant as will be shown in Fig. 2.16.

The results for the second scenario averaged over 4,000 random geometries are shown in Figs. 2.10–2.11. When  $M = 5$ , SRD-WLS has 3.96 dB improvement in average MSE and 1.79 dB improvement in average bias. For  $M = 10$ , the improvement in MSE and bias increases to 5.93 dB and 6.62 dB.

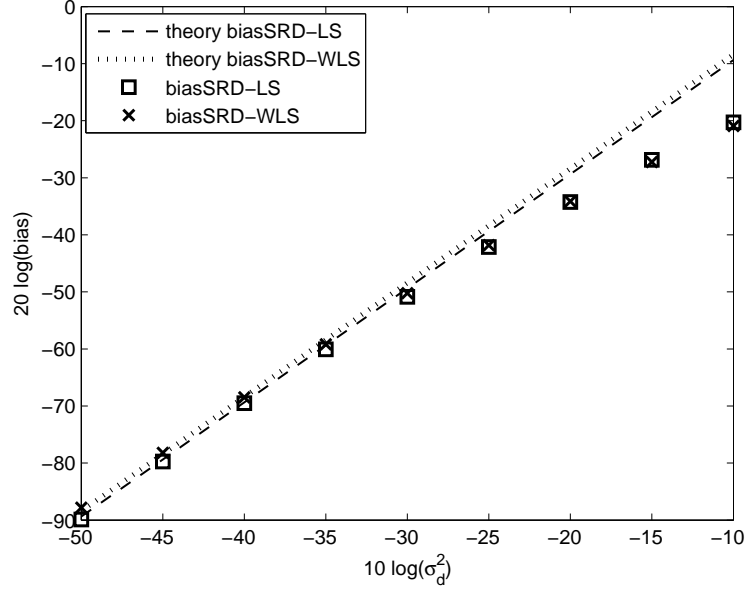


Figure 2.9: Average bias for SRD-LS and SRD-WLS in the first scenario,  $M = 5$ .

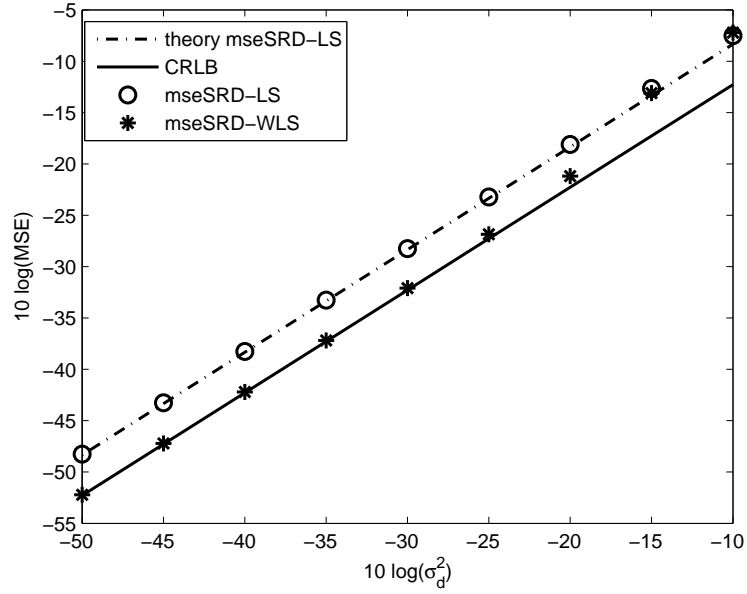


Figure 2.10: Average MSE for SRD-LS and SRD-WLS in the second scenario,  $M = 5$ .

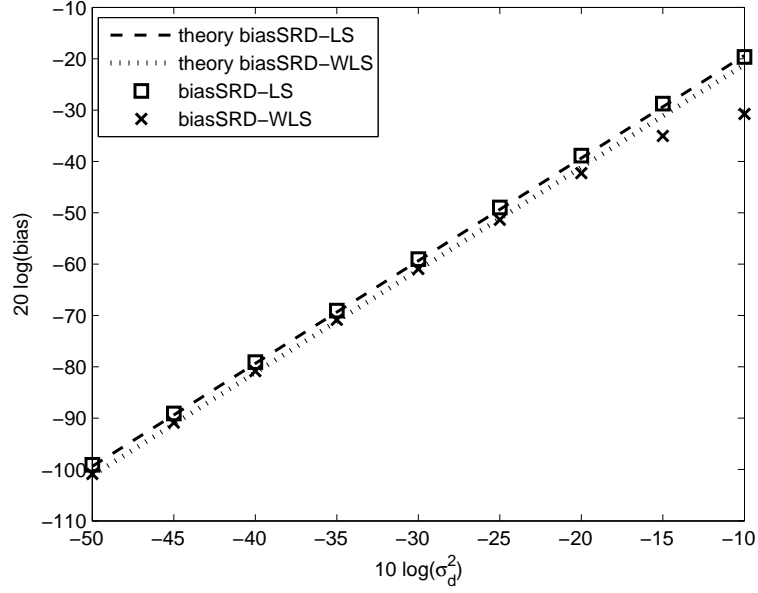


Figure 2.11: Average bias for SRD-LS and SRD-WLS in the second scenario,  $M = 5$ .

### Distribution of MSE Ratio and Bias Ratio

The distributions of the theoretical MSE ratio and the bias ratio are generated from 200,000 random geometries from the first scenario. Fig. 2.12 shows the empirical probability density functions of the MSE ratio  $\Delta = \text{tr}(\mathbf{Q}_{\text{SRD-LS}})/\text{tr}(\mathbf{Q}_{\text{SRD-WLS}})$  under 6 different sensor numbers. From  $M = 4$  to  $M = 30$ , the distribution of  $\Delta$  becomes more concentrated, and the probability that  $\Delta$  is near 1 or larger than 2.6 becomes smaller. At  $M = 30$ , this distribution has mode near  $\Delta = 1.5$  and  $\Delta > 1.5$  has higher probability than  $\Delta < 1.5$ . As  $M$  keeps increasing, the distribution of  $\Delta$  moves toward right hand side. Hence it does not seem to have an upper limit of  $\Delta$  and we can always have larger improvement in  $\Delta$  through increasing sensor number  $M$ .

Fig. 2.13 shows the empirical probability density functions of the logarithmic bias ratio  $\delta = \text{bias}(\text{SRD-LS})/\text{bias}(\text{SRD-WLS})$  under 5 different sensor numbers. For

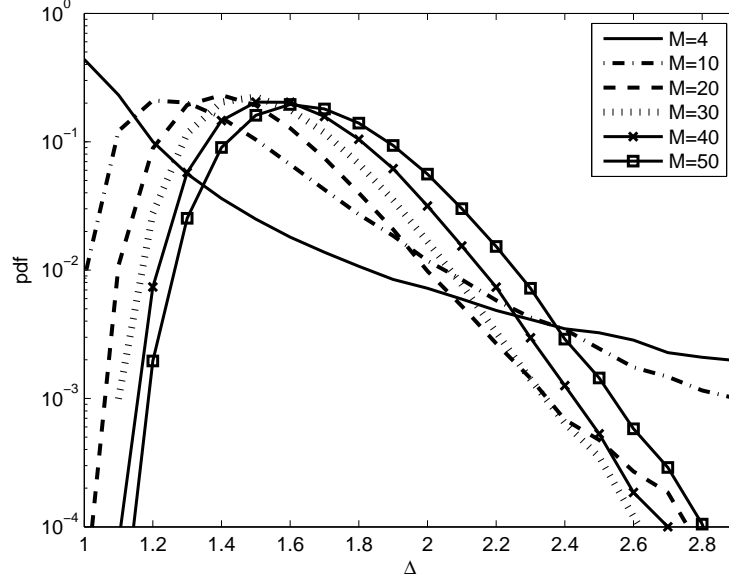


Figure 2.12: Empirical probability density functions of MSE ratio between SRD-LS and SRD-WLS with different sensor numbers  $M$  in the first scenario.

$M = 4$ , SRD-LS has slightly smaller bias. However, as  $M$  increases, the distributions skew to the right and SRD-WLS gives smaller bias.

### Comparison under Different Sensor Numbers $M$ and Noise Correlations

We vary the sensor number  $M$  from 4 to 50 and noise correlation factor from integer values of 0 to 5 in the first scenario and obtain the theoretical results from 4,000 random geometries. In Fig. 2.14, the minimum of the average of  $\Delta$  is 1.2, which occurs when  $M = 4$  and  $a = 0$ . For uncorrelated noise  $a = 0$ , the  $\Delta$  average increases under small  $M$  and settles to 1.32. For the other  $a$  values, after  $M = 8$  it keeps increasing with larger sensor number  $M$ , indicating the MSE improvement of SRD-WLS over SRD-LS can always strengthen as the number of sensors  $M$  increases. Furthermore, larger  $a$  gives larger improvement.



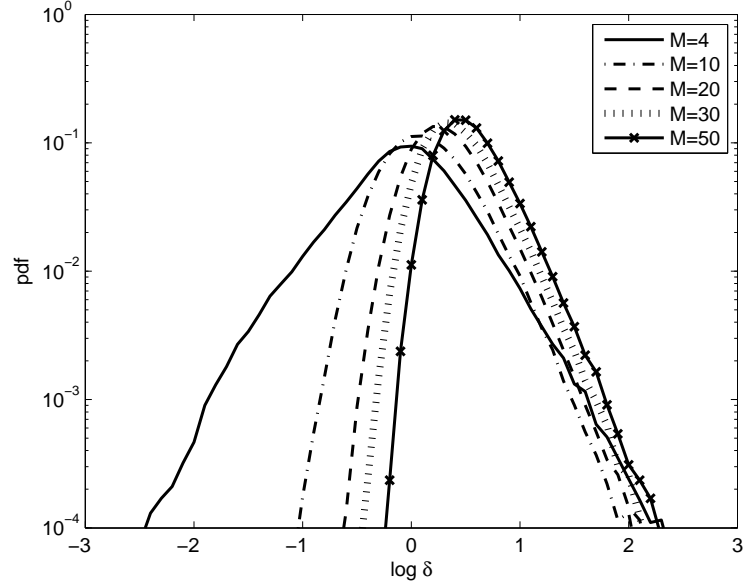


Figure 2.13: Empirical probability density functions of bias ratio between SRD-LS and SRD-WLS with different sensor numbers  $M$  in the first scenario.

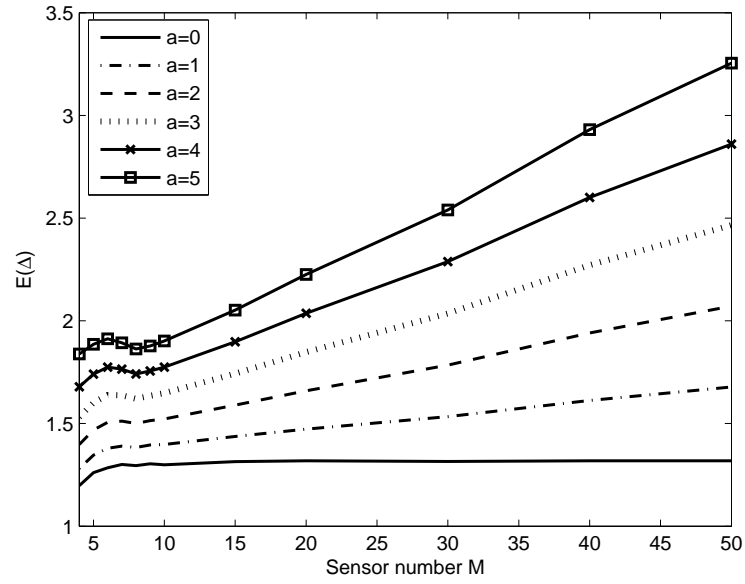


Figure 2.14: Average of MSE ratio  $\Delta$  between SRD-LS and SRD-WLS with different sensor numbers  $M$  and noise correlation factors  $a$  in the first scenario.

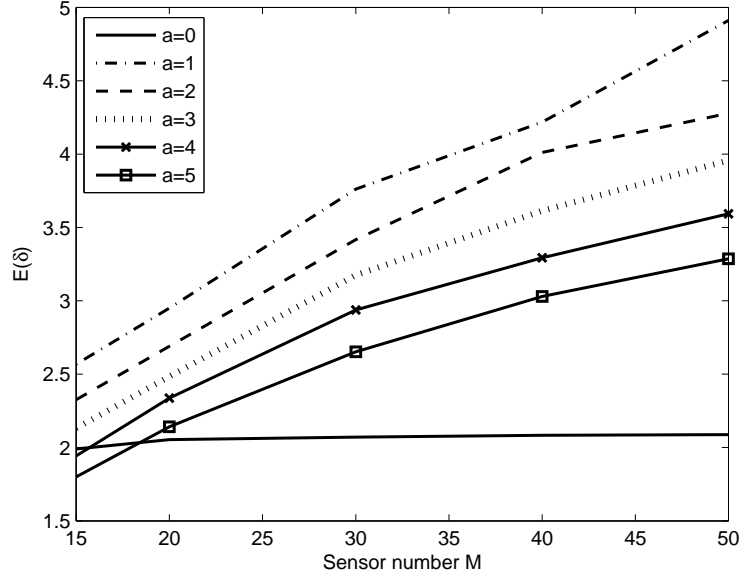


Figure 2.15: Average of bias ratio  $\delta$  between SRD-LS and SRD-WLS with different sensor numbers  $M$  and noise correlation factors  $a$  in the first scenario.

Fig. 2.15 gives the average value of  $\delta$  as the sensor number increases from 15 to 50. We do not give the result for  $M < 15$  because  $\delta$  can be bigger or smaller than 1 with nearly equal chances and its average value may not give proper indication about the relative bias between SRD-LS and SRD-WLS. For uncorrelated noise  $a = 0$ , the average value of  $\delta$  is near 2 for the sensor numbers tested. For  $a$  between 1 and 5, it is larger than 1.8 and tends to increase with larger sensor number.

### Special Case with Large MSE Ratio $\Delta$

Fig. 2.16 shows the simulation result of the Case 3 under correlated noise in Subsection 2.3.3 with  $p = 20$ . When the noise power is below 0.01, SRD-WLS offers 18.07 dB improvement in MSE over SRD-LS and achieves the CRLB performance. The simulation uses the solution from SRD-LS to generate  $r_i$  for the weighting of

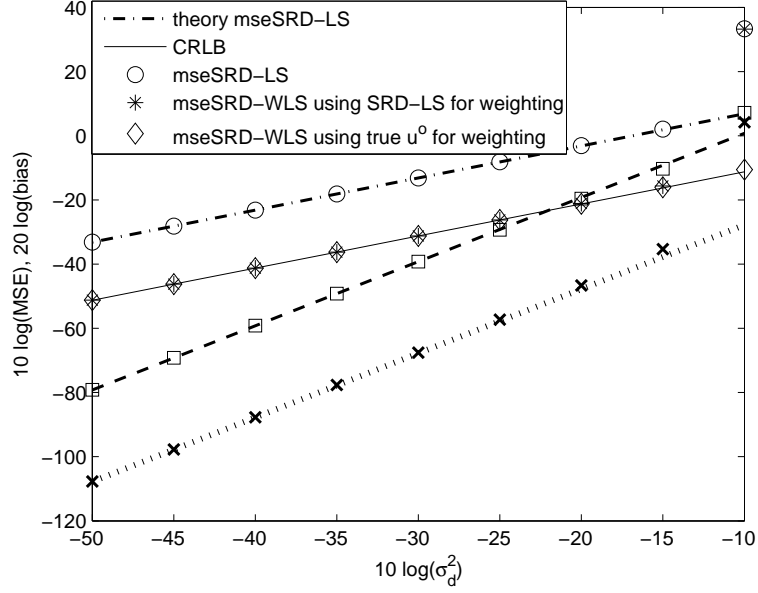


Figure 2.16: MSE and bias comparison of SRD-LS and SRD-WLS under Case 3 with correlated noise,  $p = 20$ ; where dashed line and  $\square$  represent theoretical and simulated bias of SRD-LS, and dotted line and  $\times$  represent theoretical and simulated bias of SRD-WLS.

SRD-WLS. Even though the SRD-LS solution is very inaccurate, SRD-WLS is able to maintain good results when  $\sigma_d^2$  is not larger than 0.01. At  $\sigma_d^2 = 0.1$ , the thresholding effect in the SRD-LS solution occurs, which makes the performance of SRD-WLS deviates quickly from the CRLB. If we use  $\mathbf{u}^o$  instead in SRD-WLS to obtain  $r_i$  for the weighting, we still have good performance at  $\sigma_d^2 = 0.1$ . The bias of SRD-WLS is 28.57 dB smaller than that of SRD-LS when noise level is below  $\sigma_d^2 = 0.01$ .

The average MSE improvements of SR-WLS and SRD-WLS are not obvious as shown in Fig. 2 and Fig. 8 when the sensor number is small. However, under some unfavorable geometries such as the ones used in Fig. 7 and in Fig. 16, significant performance gains are observed. It is expected that SR-WLS and SRD-WLS will be beneficial and offer considerable better results when the localization geometries are

not favorable.

It should be noted that the proposed SR-WLS and SRD-WLS cost functions require the measurement noise covariance matrix to be known, as in the case of typical WLS, in order to reach the optimum CRLB performance.

## 2.5 Conclusion

In this chapter, we propose the introduction of range weighting factors to the SR-LS and SRD-LS cost functions to improve their solution accuracy. The resulting cost functions, called SR-WLS and SRD-WLS, maintain the attractive computational efficiency of SR-LS and SRD-LS to obtain global and closed-form solutions, while overcoming the disadvantage of SR-LS and SRD-LS that have suboptimum performance and yield very large localization errors under some geometries. The location MSE and bias obtained from the solutions of SR-WLS and SRD-WLS are analyzed theoretically and they are contrasted with those from SR-LS and SRD-LS. We also elaborate the performance differences between SR-LS and SR-WLS, and between SRD-LS and SRD-WLS in terms of localization geometry, sensor number and noise correlation. The proposed SR-WLS is shown to yield a solution reaching the CRLB accuracy under Gaussian noise and has better MSE performance than SR-LS. However, SR-WLS has larger bias compared to SR-LS. Nevertheless, the bias is relatively small and negligible compared to the MSE. If needed, the bias can be estimated and subtracted from the location estimate of SR-WLS to reduce the bias. The proposed SRD-WLS is also proved to be able to yield an efficient solution and has lower MSE than SRD-LS. Unlike the case of range measurements, SRD-WLS has smaller solution bias than

SRD-LS as well, when the number of sensors is not critical. In both SR-WLS and SRD-WLS, the improvement over SR-LS and SRD-LS increases as the number of sensors or the amount of noise correlation increases. The study illustrates the advantage of the proposed weighting in improving localization accuracy, especially for range difference based localization.

The performance gain from range weighting factors in SR-WLS or SRD-WLS is quite effective when the source is near or inside the sensors array such as in sensor network applications. If the source is too close to a sensor, the source range could be close to zero and adding a small constant to the range before forming the weight may be needed to avoid numerical instability. The effect of weighting becomes less significant when the source is far away from the sensors, since all the distances between the source and sensors are close and SR-WLS and SRD-WLS will reduce back to SR-LS and SRD-LS.

## Chapter 3

# Weighting Technique in the Presence of Sensor Position Errors

In practice, the sensor positions may not be exactly known, such as in a sensor network in which the node positions are estimated by anchors. Sensor position errors degrade the localization performance considerably [39, 40] and their statistics should be taken into consideration in order to reach better performance [41, 42].

This chapter extends the study of Chapter 2 and derives the weightings when the sensor position uncertainties are present. The resultant cost functions for TOA and TDOA positionings are analyzed and the performance accuracy is shown to attain the CRLB asymptotically under Gaussian noise.

The rest of this chapter is organized as follows. Section 3.1 introduces the scenarios for TOA and TDOA localizations and provides the CRLBs of the source location estimate. Section 3.2 proposes the new cost function for TOA positioning and analyzes its solution accuracy. Section 3.3 is for the new cost function of TDOA position-

ing and its accuracy analysis. Section 3.4 gives the simulation results to verify the performance of the proposed new cost functions and support the theoretical studies. Section 3.5 concludes this chapter.

## 3.1 Localization Scenario and CRLB

### 3.1.1 Localization Scenario

Let us begin the source localization problem in 3D by having  $M$  sensors to collect the range-based measurements from a source as shown in Fig. 3.1. The source position to be estimated is represented by  $\mathbf{u}^o = [x^o y^o z^o]^T$ . The sensor positions during acquisition are  $\mathbf{s}_i^o = [x_i^o y_i^o z_i^o]^T$ ,  $i = 1, 2, \dots, M$ . They are not known to a location estimator and we only have the erroneous positions  $\mathbf{s}_i = \mathbf{s}_i^o + \mathbf{n}_{s_i}$ , where  $\mathbf{n}_{s_i}$  is the position error of sensor  $i$ . We collect the sensor positions in a vector as  $\mathbf{s} = \mathbf{s}^o + \mathbf{n}_s$ , where  $\mathbf{s}^o = [\mathbf{s}_1^{oT} \mathbf{s}_2^{oT} \dots \mathbf{s}_M^{oT}]^T$  and  $\mathbf{n}_s = [\mathbf{n}_{s_1}^T \mathbf{n}_{s_2}^T \dots \mathbf{n}_{s_M}^T]^T$ . In this study, we consider  $\mathbf{n}_s$  is zero-mean Gaussian with known covariance  $\mathbf{Q}_s$ . The localization problem has unknown parameters  $[\mathbf{u}^{oT} \mathbf{s}^{oT}]^T$ .

We assume line-of-sight (LOS) propagation and sufficient SNR such that the acquired TOAs and TDOAs can well be modelled by Gaussian distribution with covariance matrix governed by their CRLBs. The localization accuracy is indirectly related to the received waveforms, signal and noise bandwidths, SNR and observation time through the covariance matrices of the TOAs and TDOAs [34, 44, 45, 46, 47].

The TOA and TDOA measurements are the same as that in Chapter 2, but we need to use  $\mathbf{s}_i^o$  instead to represent the true sensor position. In both range and

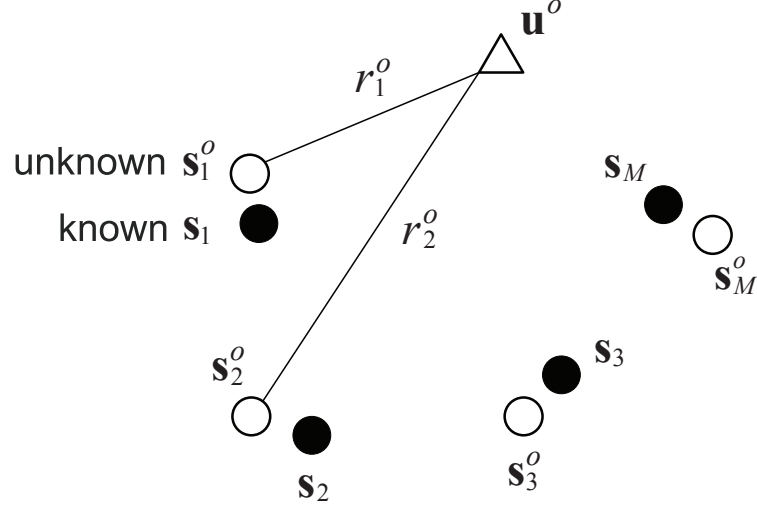


Figure 3.1: Localization scenario. Open circles are the true sensor positions and closed circles are the available sensor positions.

range difference cases, the measurement noise and sensor position noise are assumed independent for ease of illustration. The collection of the measurement and sensor position noise is either  $[\mathbf{n}^T, \mathbf{n}_s^T]^T$  or  $[\mathbf{n}_d^T, \mathbf{n}_s^T]^T$ .

### 3.1.2 CRLB

In the asymptotic region in which the estimation bias is small compared to variance, the localization performance can be characterized by the CRLB. Utilizing the CRLB analysis in [39] and taking further simplification, the CRLB for a source position estimate in range localization is

$$\text{CRLB}(\mathbf{u}^o) = [\mathbf{\Gamma}(\mathbf{Q} + \mathbf{A}^T \mathbf{Q}_s \mathbf{A})^{-1} \mathbf{\Gamma}^T]^{-1}, \quad (3.1)$$



where  $\mathbf{\Gamma} = [\boldsymbol{\rho}_1 \boldsymbol{\rho}_2 \cdots \boldsymbol{\rho}_M]$ ,  $\mathbf{A} = -\text{blkdiag}(\boldsymbol{\rho}_1, \boldsymbol{\rho}_2, \dots, \boldsymbol{\rho}_M)$ , and  $\text{blkdiag}(\star)$  is the block diagonal matrix notation. The vector  $\boldsymbol{\rho}_i = (\mathbf{u}^o - \mathbf{s}_i^o) / \|\mathbf{u}^o - \mathbf{s}_i^o\|$ , which is a unit vector pointing from sensor  $i$  to the source.

For range difference localization, we have

$$\text{CRLB}(\mathbf{u}^o) = [\mathbf{\Gamma}_d(\mathbf{Q}_d + \mathbf{A}_d^T \mathbf{Q}_s \mathbf{A}_d)^{-1} \mathbf{\Gamma}_d^T]^{-1} \quad (3.2)$$

where  $\mathbf{\Gamma}_d = [\boldsymbol{\rho}_{21} \boldsymbol{\rho}_{31} \cdots \boldsymbol{\rho}_{M1}]$ ,  $\boldsymbol{\rho}_{i1} = \boldsymbol{\rho}_i - \boldsymbol{\rho}_1$ ,

$$\mathbf{A}_d = \begin{bmatrix} \boldsymbol{\rho}_1 \mathbf{1}^T \\ -\text{blkdiag}(\boldsymbol{\rho}_2, \boldsymbol{\rho}_3, \dots, \boldsymbol{\rho}_M) \end{bmatrix},$$

and  $\mathbf{1}$  is a length  $(M-1)$  vector of unity.

## 3.2 Squared Range Cost Function and Analysis

### 3.2.1 New SR-WLS Cost Function

We shall define the squared range weighted least-squares (SR-WLS) cost function to obtain the source location estimate as

$$f_{\text{SR-WLS}}(\mathbf{u}) = \sum_{i,j=1}^M \tilde{w}_{ij} (r_i^2 - \|\mathbf{u} - \mathbf{s}_i\|^2)(r_j^2 - \|\mathbf{u} - \mathbf{s}_j\|^2). \quad (3.3)$$

Note that the unknown of the cost function is  $\mathbf{u}$  only and  $\mathbf{s}$  is kept as the noisy sensor positions. The objective is to find the weights  $\tilde{w}_{ij}$  to improve as much accuracy as possible since the cost function is constructed with the noisy sensor positions.

The residual squared range error at the true source location is

$$\begin{aligned}
e_i &= r_i^2 - \|\mathbf{u}^o - \mathbf{s}_i\|^2 \\
&= (r_i^o + n_i)^2 - \|\mathbf{u}^o - \mathbf{s}_i^o - \mathbf{n}_{s_i}\|^2 \\
&\approx 2r_i^o n_i + 2(\mathbf{u}^o - \mathbf{s}_i^o)^T \mathbf{n}_{s_i} \\
&= 2r_i^o (n_i + \boldsymbol{\rho}_i^T \mathbf{n}_{s_i}).
\end{aligned}$$

The approximation comes from ignoring the second order noise terms and we have used  $\boldsymbol{\rho}_i$  to represent  $(\mathbf{u}^o - \mathbf{s}_i^o)/r_i^o$ . According to the WLS estimation theory [20], the weights should be the elements of  $\mathbf{W} = \mathbf{C}^{-1}$ , where  $\mathbf{C}$  is the correlation matrix whose  $(i, j)$ -th element is  $E[e_i e_j]$ . Defining  $\mathbf{B} = 2 \text{diag}(r_1^o, r_2^o, \dots, r_M^o)$ ,

$$\mathbf{W} = [\mathbf{B}(\mathbf{Q} + \mathbf{A}^T \mathbf{Q}_s \mathbf{A})\mathbf{B}]^{-1} \quad (3.4)$$

where  $\mathbf{A}$  is defined below (3.1).  $\mathbf{W}$  is not known since it depends on the true range values and the true source and sensor positions. Let us construct the noisy version of  $\mathbf{B}$  from the measurements as  $\tilde{\mathbf{B}} = 2\text{diag}(r_1, r_2, \dots, r_M)$  and that of  $\mathbf{A}$  as  $\tilde{\mathbf{A}}$  by replacing  $\boldsymbol{\rho}_i$  as  $\tilde{\boldsymbol{\rho}}_i = (\tilde{\mathbf{u}} - \mathbf{s}_i)/r_i$ , where  $\tilde{\mathbf{u}}$  is some estimate of  $\mathbf{u}^o$ . We choose the weights  $\tilde{w}_{ij}$  in (3.3) as the elements of

$$\tilde{\mathbf{W}} = [\tilde{\mathbf{B}}(\mathbf{Q} + \tilde{\mathbf{A}}^T \mathbf{Q}_s \tilde{\mathbf{A}})\tilde{\mathbf{B}}]^{-1}. \quad (3.5)$$

We shall show from the first order analysis that although we use the noisy measurement values to form the weights, the minimum of the cost function (3.3) is able to reach the CRLB accuracy in the asymptotic region.

### 3.2.2 MSE Analysis

We shall evaluate the MSE matrix of the minimum solution of (3.3) using the MSE analysis technique in Chapter 2.

It is reasonable to assume the source location  $\tilde{\mathbf{u}}$  used in forming  $\widetilde{\mathbf{W}}$  is different from the true source location by random noise. Hence the weights in (3.3) can be expressed as  $\tilde{w}_{ij} = w_{ij} + o(1)$ , where  $w_{ij}$  is the  $(i, j)$ -th element of (3.4).

The first derivative from (3.3) is,

$$\frac{\partial f_{\text{SR-WLS}}(\mathbf{u})}{\partial \mathbf{u}} = -4 \sum_{i,j=1}^M \tilde{w}_{ij} (r_i^2 - \|\mathbf{u} - \mathbf{s}_i\|^2) (\mathbf{u} - \mathbf{s}_j). \quad (3.6)$$

Expressing  $\tilde{w}_{ij}$  in terms of  $w_{ij}$  and substituting  $r_i = r_i^o + n_i$  and  $\mathbf{s}_i = \mathbf{s}_i^o + \mathbf{n}_{si}$ , we arrive at after some algebraic manipulations,

$$\begin{aligned} \mathbf{f}'_{\text{SR-WLS}} &= -8 \sum_{i,j=1}^M r_i^o w_{ij} r_j^o (n_i + \boldsymbol{\rho}_i^T \mathbf{n}_{si}) \boldsymbol{\rho}_j + o(\|\mathbf{n}\|) \mathbf{1} \\ &= -2\mathbf{\Gamma} \mathbf{B} \mathbf{W} \mathbf{B} (\mathbf{n} - \mathbf{A}^T \mathbf{n}_s) + o(\|\mathbf{n}\|) \mathbf{1}, \end{aligned} \quad (3.7)$$

where  $\mathbf{1}$  represents a  $3 \times 1$  vector of unity. Hence using (3.4),

$$\begin{aligned} E[\mathbf{f}'_{\text{SR-WLS}} \mathbf{f}'_{\text{SR-WLS}}^T] &\approx 4\mathbf{\Gamma} \mathbf{B} \mathbf{W} \mathbf{B} (\mathbf{Q} + \mathbf{A}^T \mathbf{Q}_s \mathbf{A}) \mathbf{B} \mathbf{W} \mathbf{B}^T \mathbf{\Gamma}^T \\ &= 4\mathbf{\Gamma} (\mathbf{Q} + \mathbf{A}^T \mathbf{Q}_s \mathbf{A})^{-1} \mathbf{\Gamma}^T. \end{aligned} \quad (3.8)$$

For the second derivative,

$$\frac{\partial^2 f_{\text{SR-WLS}}(\mathbf{u})}{\partial \mathbf{u} \partial \mathbf{u}^T} = -4 \sum_{i,j=1}^M \tilde{w}_{ij} [-2(\mathbf{u} - \mathbf{s}_i)(\mathbf{u} - \mathbf{s}_j)^T + (r_i^2 - \|\mathbf{u} - \mathbf{s}_i\|^2) \mathbf{I}] \quad (3.9)$$

where  $\mathbf{I}$  is an identity matrix. Again, expressing the noisy qualities in terms of the true values yields

$$\begin{aligned}\mathbf{F}_{\text{SR-WLS}}'' &= 8 \sum_{i,j=1}^M r_i^o w_{ij} r_j^o \boldsymbol{\rho}_i \boldsymbol{\rho}_j^T + o(1) \mathbf{1} \mathbf{1}^T \\ &= 2\mathbf{\Gamma} \mathbf{B} \mathbf{W} \mathbf{B} \mathbf{\Gamma}^T + o(1) \mathbf{1} \mathbf{1}^T.\end{aligned}\tag{3.10}$$

Its constant component excluding noise is, after using (3.4),

$$\bar{\mathbf{F}}_{\text{SR-WLS}}'' = 2\mathbf{\Gamma}(\mathbf{Q} + \mathbf{A}^T \mathbf{Q}_s \mathbf{A})^{-1} \mathbf{\Gamma}^T.\tag{3.11}$$

Utilizing the MSE formula (2.17) gives immediately

$$\mathbf{Q}_{\text{SR-WLS}} = [\mathbf{\Gamma}(\mathbf{Q} + \mathbf{A}^T \mathbf{Q}_s \mathbf{A})^{-1} \mathbf{\Gamma}^T]^{-1},\tag{3.12}$$

which is exactly the CRLB in (3.1) for range localization in the presence of sensor position errors. Thus the solution of the new SR-WLS cost function is asymptotically efficient.

### 3.3 Squared Range Difference Cost Function and Analysis

#### 3.3.1 New SRD-WLS Cost Function

Let  $p_i = (r_{i1} + \|\mathbf{u} - \mathbf{s}_1\|)^2 - \|\mathbf{u} - \mathbf{s}_i\|^2$ . The new squared range difference weighted least-squares (SRD-WLS) cost function is

$$f_{\text{SRD-WLS}}(\mathbf{u}) = \sum_{i,j=2}^M \tilde{w}_{dij} p_i p_j, \quad (3.13)$$

where the unknown is considered to be  $\mathbf{u}$  only and  $\tilde{w}_{dij}$  is the weights to be found to improve performance.

Since  $\|\mathbf{u}^o - \mathbf{s}_1\| \approx r_1^o - \boldsymbol{\rho}_1^T \mathbf{n}_{s_1}$  by the Taylor series expansion, the residual error at the true source location is

$$(r_{i1} + \|\mathbf{u}^o - \mathbf{s}_1\|)^2 - \|\mathbf{u}^o - \mathbf{s}_i\|^2 \approx 2r_i^o(n_{i1} - \boldsymbol{\rho}_1^T \mathbf{n}_{s_1} + \boldsymbol{\rho}_i^T \mathbf{n}_{s_i}) \quad (3.14)$$

after putting  $r_{i1} = r_{i1}^o + n_{i1}$  and  $\mathbf{s}_i = \mathbf{s}_i^o + \mathbf{n}_{s_i}$ . Using the same argument as for the range case, the ideal weightings are the elements of

$$\mathbf{W}_d = [\mathbf{B}_d(\mathbf{Q}_d + \mathbf{A}_d^T \mathbf{Q}_s \mathbf{A}_d) \mathbf{B}_d]^{-1} \quad (3.15)$$

where  $\mathbf{B}_d = 2\text{diag}(r_2^o, r_3^o, \dots, r_M^o)$  and  $\mathbf{A}_d$  is defined below (3.2). Let  $\tilde{r}_1 = \|\tilde{\mathbf{u}} - \mathbf{s}_1\|$  and  $\tilde{\mathbf{u}}$  is an initial source location estimate. Also, let  $\tilde{r}_i = r_{i1} + \tilde{r}_1$ ,  $i = 2, 3, \dots, M$  and  $\tilde{\boldsymbol{\rho}}_i = (\tilde{\mathbf{u}} - \mathbf{s}_i)/\tilde{r}_i$ . We shall define  $\tilde{\mathbf{B}}_d = 2\text{diag}(\tilde{r}_2, \tilde{r}_3, \dots, \tilde{r}_M)$  and  $\tilde{\mathbf{A}}_d$  as  $\mathbf{A}_d$  by replacing  $\boldsymbol{\rho}_i$  with  $\tilde{\boldsymbol{\rho}}_i$ . The weights  $\tilde{w}_{dij}$  in (2.38) are the elements of

$$\widetilde{\mathbf{W}}_d = [\tilde{\mathbf{B}}_d(\mathbf{Q}_d + \tilde{\mathbf{A}}_d^T \mathbf{Q}_s \tilde{\mathbf{A}}_d) \tilde{\mathbf{B}}_d]^{-1}. \quad (3.16)$$

### 3.3.2 MSE Analysis

Following the same procedure as in the range localization case, we have for the first derivative,

$$\mathbf{f}'_{\text{SRD-WLS}} = -2\Gamma_d \mathbf{B}_d \mathbf{W}_d \mathbf{B}_d (\mathbf{n}_d - \mathbf{A}_d^T \mathbf{n}_s) + o(\|\mathbf{n}\|) \mathbf{1} \quad (3.17)$$

and hence after using (3.15)

$$E[\mathbf{f}'_{\text{SRD-WLS}} \mathbf{f}'_{\text{SRD-WLS}}^T] \approx 4\Gamma_d (\mathbf{Q}_d + \mathbf{A}_d^T \mathbf{Q}_s \mathbf{A}_d)^{-1} \Gamma_d^T. \quad (3.18)$$

For the second derivative,

$$\overline{\mathbf{F}}''_{\text{SRD-WLS}} = 2\Gamma_d (\mathbf{Q}_d + \mathbf{A}_d^T \mathbf{Q}_s \mathbf{A}_d)^{-1} \Gamma_d^T. \quad (3.19)$$

Putting them into (2.17) yields

$$\mathbf{Q}_{\text{SRD-WLS}} = [\Gamma_d (\mathbf{Q}_d + \mathbf{A}_d^T \mathbf{Q}_s \mathbf{A}_d)^{-1} \Gamma_d^T]^{-1}. \quad (3.20)$$

$\mathbf{Q}_{\text{SRD-WLS}}$  is the CRLB expression (3.2) for range difference localization under sensor position errors. As a result, the solution of the new SRD-WLS cost function is also asymptotically efficient.

Generating the new weights  $\tilde{w}_{ij}$  or  $\tilde{w}_{di}$  requires a coarse estimate of the source

location  $\tilde{\mathbf{u}}$ . It can be easily generated by using a localization algorithm, e.g. SR-WLS in Chapter 2, by pretending the sensor position errors are absent.

### 3.4 Simulations

In this section, we shall validate the asymptotic efficient performance of the SR-WLS and SRD-WLS cost functions that address sensor position errors, using one specific geometry and 200 random geometries. The specific localization geometry is taken from [39], where the true locations of the sensors are shown in Table 1 and the source is at  $\mathbf{u}^o = [700, 650, 550]^T$ . The sensor position covariance is  $\mathbf{Q}_s = \sigma_s^2 \text{diag}(1, 2, 10, 40, 20, 3) \otimes \mathbf{I}_3$ ,  $\mathbf{I}_3$  is an identity matrix of size 3 and  $\otimes$  is the Kronecker product. For the random geometries, we use  $M = 10$  sensors. The sensors and the source are placed with independent, identically distributed (IID) uniform distribution in each coordinate within a cube of length 1000. To avoid degenerate geometry that yields poor performance, we maintain a minimum distance of 25 between the source and a sensor. The sensor position covariance is  $\mathbf{Q}_s = \sigma_s^2 \text{diag}(\sigma_1^2, \sigma_2^2, \dots, \sigma_M^2) \otimes \mathbf{I}_3$ , where  $\sigma_i$ 's are created randomly with IID uniform distributions and are normalized so that  $\sum_1^M \sigma_i^2 = 1$ . A new  $\mathbf{Q}_s$  is used for each random geometry.

**Table 1:** The true positions of sensors

sensor no. $i$	1	2	3	4	5	6
$x_i^o$	300	400	300	350	-100	200
$y_i^o$	100	150	500	200	-100	-300
$z_i^o$	150	100	200	100	-100	-200

The GTRS solution [18] is used to solve for the SR-WLS cost function and the exact solution in [17] for the SRD-WLS cost function. For reference purpose, we also provide the results of the MLE that jointly estimates the source and sensor positions. The MLE is implemented by the Gauss-Newton method, where the initialization of each coordinate of the source is the true value added with independent zero-mean Gaussian white noise with variance equal to two times the CRLB, and the initializations of sensor positions are the erroneous sensor positions. We stop the iteration once the parameter change in the current step is larger than that in the previous step.

The range measurement covariance matrix is  $\mathbf{Q} = \sigma^2 \mathbf{I}$ , and that of the range difference measurement is  $\mathbf{Q}_d = \sigma^2(\mathbf{I} + \mathbf{1}\mathbf{1}^T)/2$  [2], where we fix the noise level at  $\sigma^2 = 10^{-3}$ . The performance index is  $\text{mse} = \sum_{l=1}^L \|\mathbf{u}^{(l)} - \mathbf{u}^o\|^2 / L$ , where  $\mathbf{u}^{(l)}$  is the estimate at ensemble  $l$  and  $L = 2000$  is the number of ensemble runs.

Fig. 3.2 shows the results for the specific geometry in range localization. The GTRS solution of the new cost function performs close to the MLE and attains the CRLB accuracy. It provides about 5.5 dB improvement over the previous SR-WLS cost function that does not take the sensor position errors into account when  $\sigma_s^2$  becomes significant. For the random geometry results shown in Fig. 3.3, the observations are consistent and the improvement is about 4 dB.

For range difference localization, the results for the specific geometry are depicted in Fig. 3.4. The new cost function yields the CRLB accuracy and matches the MLE performance. We would like to point out that the MLE experiences the thresholding effect at around  $\sigma_s^2 = 10^{-0.2}$ , which is caused by the sensitivity of initialization and by the large number of unknowns to be found. On the other hand, the solution from the new SRD-WLS cost function is relatively stable and provides about 4 dB



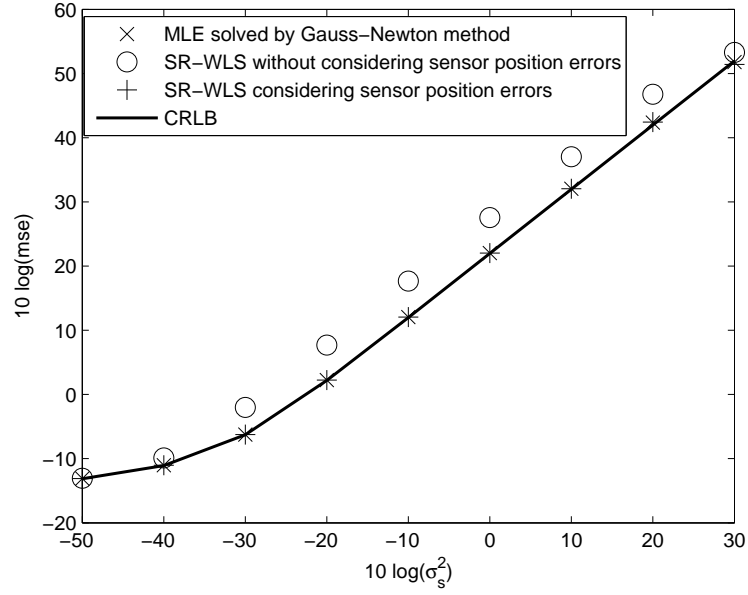


Figure 3.2: Range (TOA) localization performance of SR-WLS considering sensor position errors, under the specific geometry in Table 1.

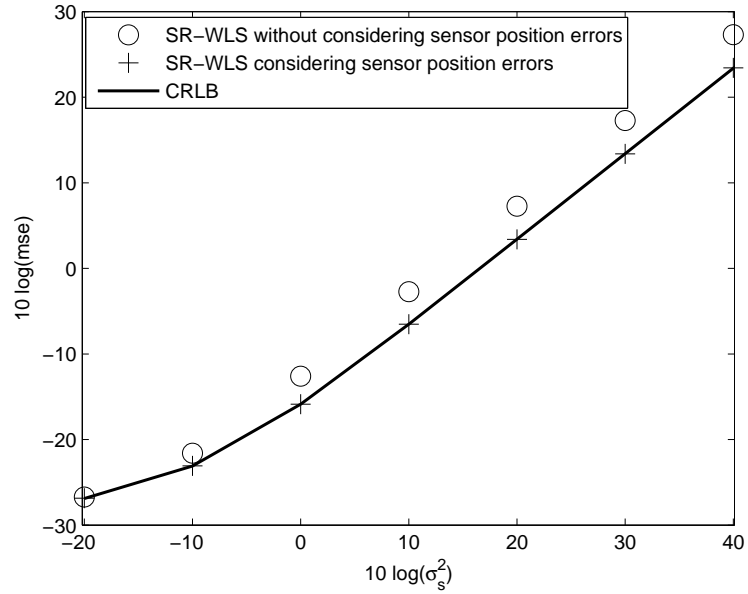


Figure 3.3: Range (TOA) localization performance of SR-WLS considering sensor position errors, under the 200 random geometries.

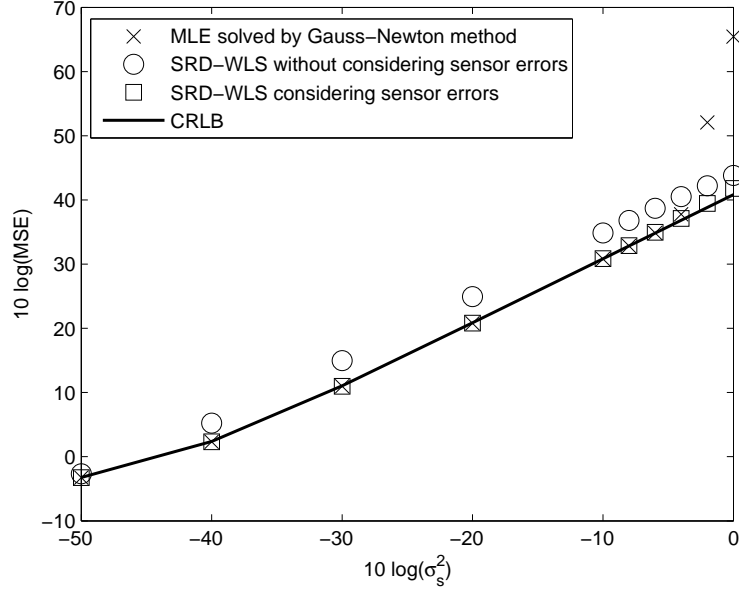


Figure 3.4: Range difference (TDOA) localization performance of SRD-WLS considering sensor position errors, under the specific geometry in Table 1.

improvement over previous SRD-WLS that ignores the sensor position errors. The observations are similar for the random geometry results shown in Fig. 3.5, and the new cost function has about 2.5 dB improvement.

### 3.5 Conclusion

Proper weightings must be used in the squared range and squared range difference cost functions to compensate for the effect of squaring. The weights derived in Chapter 2 is not adequate when the sensor positions contain errors. In this chapter, we generalize the study and develop the new weights that take the sensor position errors into account to improve performance. We show from the first order analysis under Gaussian noise that although the weights are constructed from the measurements that

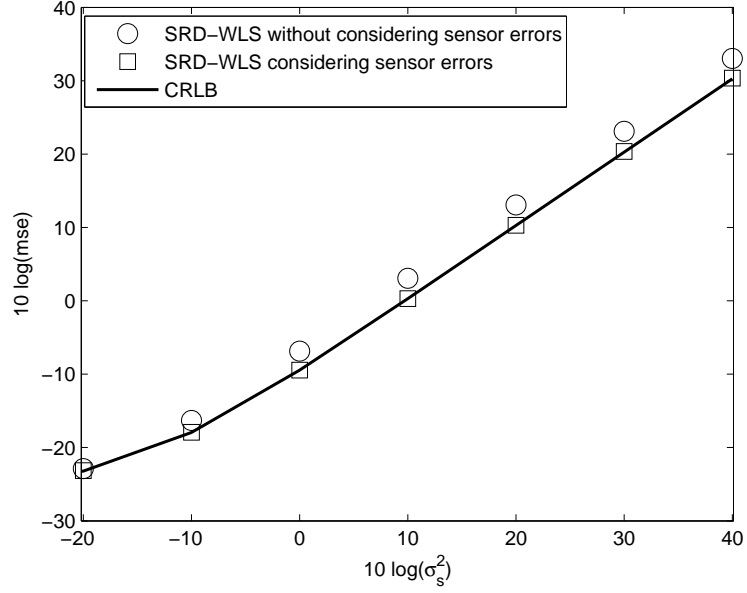


Figure 3.5: Range difference (TDOA) localization performance of SRD-WLS considering sensor position errors, under the 200 random geometries.

are noisy, the performance of the source location solution closely follows the CRLB asymptotically. The new cost functions enable the application and development of algebraic solutions, and improve the computational efficiency relative to the iterative MLE.

## Chapter 4

# Estimation of Rigid Body Position and Orientation

We start to handle the estimation of orientation in addition to position. Obtaining the position and orientation of a rigid body is an important subject for many applications in robotics, automobiles, spacecraft, underwater vehicles, gaming and many others [48, 49, 50, 51]. In this chapter, we discuss the estimation algorithm under distance measurements (additional Doppler measurements for moving rigid body). Similar study under AOA measurements will be discussed in next chapter.

This chapter is organized as follows. Section 4.1 provides the scenario for the rigid body localization problem. Section 4.2 describes the proposed method for locating a stationary rigid body. Section 4.3 presents an additional solution for the localization problem in the 2D space. Section 4.4 focuses on moving rigid body localization. Section 4.5 elaborates on the expected performance of the proposed methods and examines computational complexity. Section 4.6 supports the performance of the

proposed solutions by simulations. Section 4.7 presents alternative method for moving rigid body in 2D case. Section 4.8 concludes the chapter.

In this chapter,  $\text{vec}(\mathbf{A})$  is a column vector by stacking the columns of  $\mathbf{A}$ ,  $\det(\mathbf{A})$  is the determinant. The symbol  $\odot$  represents the Hadamard product and  $\otimes$  the Kronecker product. We have the matrix vectorization formula that [70]

$$\text{vec}(\mathbf{XYZ}) = (\mathbf{Z}^T \otimes \mathbf{X})\text{vec}(\mathbf{Y}). \quad (4.1)$$

## 4.1 Scenario

Fig. 4.1 illustrates the localization scenario. The rigid body we would like to locate has  $N$  sensors mounted whose positions at the local reference frame  $\mathcal{B}$  are  $\mathbf{c}_i \in \mathbb{R}^K$ , where  $i = 1, 2, \dots, N$  and  $K$  is the dimension of localization. The reference frame here refers to a set of oriented orthonormal vectors at a certain position.  $\mathcal{B}$  has the orientation represented by the rotation matrix  $\mathbf{R} \in \mathbb{R}^{K \times K}$  and the origin denoted by the position vector  $\mathbf{t} \in \mathbb{R}^K$  with respect to the inertial reference frame  $\mathcal{I}$ . The rotation matrix must belong to the special orthogonal group  $SO(K) = \{\mathbf{R} \in \mathbb{R}^{K \times K} : \mathbf{R}^T \mathbf{R} = \mathbf{I}, \det(\mathbf{R}) = 1\}$  [62].<sup>1</sup>

In  $\mathcal{I}$  the position of the  $i$ -th sensor is [53]

$$\mathbf{s}_i = \mathbf{R}\mathbf{c}_i + \mathbf{t}. \quad (4.2)$$

We shall determine  $\mathbf{R}$  and  $\mathbf{t}$  using  $M$  anchors whose positions are exactly known

---

<sup>1</sup>Note that the condition  $\mathbf{R}^T \mathbf{R} = \mathbf{I}$  alone is not sufficient since  $\det(\mathbf{R})$  can be +1 or -1, and the case of  $\det(\mathbf{R}) = -1$  yields a reflection matrix that is not able to describe the rigid transformation.

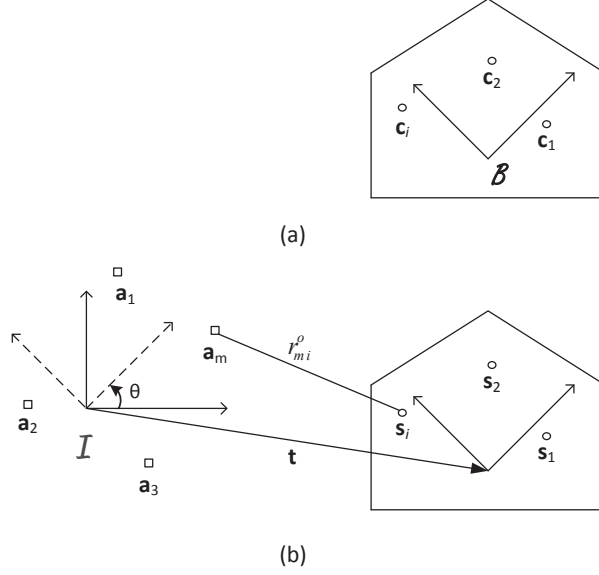


Figure 4.1: An illustration for rigid body localization, shown in 2D for ease of illustration. (a) The known sensor position  $\mathbf{c}_i$  in the local reference frame  $\mathcal{B}$ ; (b) The unknown sensor position  $\mathbf{s}_i$  in the inertial reference frame  $\mathcal{I}$  that is related to  $\mathbf{c}_i$  by (4.2) through the rotation and translation between the two reference frames.

at  $\mathbf{a}_m \in \mathbb{R}^K$  in  $\mathcal{I}$ ,  $m = 1, 2, \dots, M$ . The anchors provide the distance measurements to the sensors which are modelled as [53]

$$r_{mi} = r_{mi}^o + n_{mi} \quad (4.3a)$$

$$= \|\mathbf{a}_m - \mathbf{s}_i\| + n_{mi} \quad (4.3b)$$

$$= \|\mathbf{a}_m - \mathbf{R}\mathbf{c}_i - \mathbf{t}\| + n_{mi} \quad (4.3c)$$

where  $r_{mi}^o = \|\mathbf{a}_m - \mathbf{s}_i\|$  and  $n_{mi}$  is the additive noise. The collection of all measurements together forms the vector  $\mathbf{r} = \mathbf{r}^o + \mathbf{n}$ . The noise vector  $\mathbf{n}$  follows zero-mean Gaussian distribution with covariance matrix  $\mathbf{Q}_n$ .

For a moving rigid body, the velocity of the individual sensor in the inertial frame is  $\dot{\mathbf{s}}_i$ , while the motion of the entire rigid body is characterized by the angular velocity

$\boldsymbol{\omega}$  and translational velocity  $\dot{\mathbf{t}}$ . Applying the time derivative of  $\mathbf{s}_i$  in (4.2) gives the relation

$$\dot{\mathbf{s}}_i = [\boldsymbol{\omega}]^\times \mathbf{R} \mathbf{c}_i + \dot{\mathbf{t}}. \quad (4.4)$$

$[*]^\times$  is the cross product operator matrix [62] that maps the vector  $\boldsymbol{\omega}$  to a skew-symmetric matrix.<sup>2</sup>

The Doppler measurements from the motion of a rigid body are [71]

$$\dot{r}_{mi} = \frac{(\mathbf{s}_i - \mathbf{a}_m)^T}{r_{mi}^o} \dot{\mathbf{s}}_i + \dot{n}_{mi}. \quad (4.5)$$

We use the terms Doppler shift and range rate interchangeably because they differ only by a scaling factor of the propagation speed divided by the carrier frequency. The Doppler measurement vector is  $\dot{\mathbf{r}} = \dot{\mathbf{r}}^o + \dot{\mathbf{n}}$  and the Doppler noise vector  $\dot{\mathbf{n}}$  is zero-mean Gaussian with covariance  $\mathbf{Q}_{\dot{\mathbf{n}}}$ . Together with the distance measurement noise,  $[\mathbf{n}^T, \dot{\mathbf{n}}^T]^T$  follows a zero-mean Gaussian distribution with covariance matrix  $\mathbf{Q}$ .

The problem can be stated as follows. Given the distance measurements  $r_{mi}$  and the relative sensor positions in the local frame  $\mathcal{B}$ , obtain the rotation matrix  $\mathbf{R}$  and the position vector  $\mathbf{t}$  of the rigid body as observed in the inertial reference frame  $\mathcal{I}$ . If the rigid body is moving, estimate the angular and translational velocities as well through the additional Doppler measurements.

---

<sup>2</sup>It is equal to (4.35) in 3D or (4.36) in 2D.

## 4.2 Stationary Rigid Body Localization

The positioning solution for stationary rigid body developed in this section is general and is applicable to both 2D and 3D cases.

### 4.2.1 Step-1: Preliminary Solution

Rather than obtaining  $\mathbf{R}$  and  $\mathbf{t}$  directly from the measurements, we resort to the DAC approach proposed by Abel [67]. The idea is to use the sensor positions in  $\mathcal{I}$  as the intermediate variables to obtain the rotation and translation parameters. Essentially, we first separate the distance measurements to  $N$  non-overlapping sets, each containing the measurements from the anchors to the same sensor. The sensor positions are solved independently from each measurement set. Next, we impose the model (4.2) between  $\mathbf{s}_i$  and  $\mathbf{c}_i$  to determine the rotation matrix and translation vector.

The estimation of a sensor position using distance measurements from a number of anchors is a well known TOA localization problem and the amount of solutions available in the literature is abundant, such as the closed-form two-stage method [2] [39] and the GTRS solution [17]. The two-stage method has a lower noise threshold than the GTRS method but it is much more computationally efficient. Solving the sensor positions individually requires at least  $K + 1$  distance measurements for each sensor to ensure a unique solution. We shall denote the estimated sensor positions as  $\hat{\mathbf{s}}_i$ .

Determining the rotation and translation relationship between two sets of data points at different coordinates,  $\hat{\mathbf{s}}_i$  and  $\mathbf{c}_i$  in our case, is a typical problem in pattern analysis [72, 73] or general Procrustes analysis. It can be formulated as a least squares



minimization problem as

$$\begin{aligned} \min_{\mathbf{R}, \mathbf{t}} \sum_{i=1}^N [\hat{\mathbf{s}}_i - (\mathbf{R}\mathbf{c}_i + \mathbf{t})]^T \mathbf{W}_i [\hat{\mathbf{s}}_i - (\mathbf{R}\mathbf{c}_i + \mathbf{t})] \\ \text{s.t. } \mathbf{R} \in SO(K) \end{aligned} \quad (4.6)$$

where the optimal weighting  $\mathbf{W}_i$  is the inverse of the covariance of  $\hat{\mathbf{s}}_i$ . This optimization in general does not admit a closed-form solution except for the 2D case. Alternatively, we consider the non-negative scalar weighting

$$\begin{aligned} \min_{\mathbf{R}, \mathbf{t}} J = \sum_{i=1}^N w_i \|\hat{\mathbf{s}}_i - (\mathbf{R}\mathbf{c}_i + \mathbf{t})\|^2 \\ \text{s.t. } \mathbf{R} \in SO(K) \end{aligned} \quad (4.7)$$

which corresponds to the weighting matrix of the form  $\mathbf{W}_i = w_i \mathbf{I}$ .

Let us denote the weighted average values

$$\bar{\mathbf{s}} = \sum_{i=1}^N w_i \hat{\mathbf{s}}_i / \sum_{i=1}^N w_i, \quad \bar{\mathbf{c}} = \sum_{i=1}^N w_i \mathbf{c}_i / \sum_{i=1}^N w_i.$$

By setting to zero the derivative of  $J$  with respect to  $\mathbf{t}$ , we obtain the solution of  $\mathbf{t}$  as

$$\mathbf{t} = \bar{\mathbf{s}} - \mathbf{R}\bar{\mathbf{c}}. \quad (4.8)$$

We shall denote  $\tilde{\mathbf{s}}_i = \hat{\mathbf{s}}_i - \bar{\mathbf{s}}$  and  $\tilde{\mathbf{c}}_i = \mathbf{c}_i - \bar{\mathbf{c}}$ . Putting (4.8) back to  $J$  gives

$$\begin{aligned}
J &= \sum_{i=1}^N w_i \|\tilde{\mathbf{s}}_i - \mathbf{R}\tilde{\mathbf{c}}_i\|^2 \\
&= -2 \sum_{i=1}^N w_i \tilde{\mathbf{s}}_i^T \mathbf{R} \tilde{\mathbf{c}}_i + \mathcal{K} \\
&= -2 \text{tr}(\mathbf{R} \sum_{i=1}^N w_i \tilde{\mathbf{c}}_i \tilde{\mathbf{s}}_i^T) + \mathcal{K}
\end{aligned} \tag{4.9}$$

where  $\mathcal{K} = \sum_{i=1}^N w_i (\|\tilde{\mathbf{s}}_i\|^2 + \|\tilde{\mathbf{c}}_i\|^2)$  is a constant independent of  $\mathbf{R}$ . Note that  $\mathbf{R}^T \mathbf{R} = \mathbf{I}$  has been used. Minimizing  $J$  is equivalent to maximizing  $\text{tr}(\mathbf{R} \sum_{i=1}^N w_i \tilde{\mathbf{c}}_i \tilde{\mathbf{s}}_i^T)$ . Let the SVD of  $\sum_{i=1}^N w_i \tilde{\mathbf{c}}_i \tilde{\mathbf{s}}_i^T$  be  $\mathbf{U}\mathbf{\Sigma}\mathbf{V}^T$ , then the optimal solution is [73]

$$\mathbf{R} = \mathbf{V} \text{diag}([\mathbf{1}^T, \det(\mathbf{V}\mathbf{U}^T)]^T) \mathbf{U}^T, \tag{4.10}$$

where the length of  $\mathbf{1}$  is  $K-1$ , and the value  $\det(\mathbf{V}\mathbf{U}^T)$  ensures the resulting rotation matrix fulfills  $\det(\mathbf{R}) = 1$ . Putting (4.10) back to (4.8) gives the solution for the translation vector. We shall denote the solution from step-1 as  $(\hat{\mathbf{R}}, \hat{\mathbf{t}})$ .

### 4.2.2 Step-2: Refinement

We square both sides of distance equation (4.3b), ignore the second order noise term and substitute (4.2) to obtain [53]

$$r_{mi}^2 = (\|\mathbf{a}_m - \mathbf{s}_i\| + n_{mi})^2 \tag{4.11a}$$

$$\approx \|\mathbf{a}_m\|^2 - 2\mathbf{a}_m^T \mathbf{s}_i + \|\mathbf{s}_i\|^2 + v_{mi} \tag{4.11b}$$

$$= \|\mathbf{a}_m\|^2 - 2\mathbf{a}_m^T (\mathbf{R}\mathbf{c}_i + \mathbf{t}) + \|\mathbf{c}_i\|^2 + 2\mathbf{t}^T \mathbf{R}\mathbf{c}_i + \|\mathbf{t}\|^2 + v_{mi} \tag{4.11c}$$

where  $v_{mi} = 2r_{mi}^o n_{mi}$ . The collection of  $v_{mi}$  gives the composite noise vector  $\mathbf{v}$  for the squared range values, which has a covariance matrix  $\mathbf{Q}_v = 4 \text{diag}(\mathbf{r}^o) \mathbf{Q}_n \text{diag}(\mathbf{r}^o)$  that is dependent on the true ranges. For implementation purpose, we replace the true range values by the measurements. Simulations show that the performance degradation is negligible, especially when the rigid body is far from the anchors.

Obtaining  $\mathbf{R}$  and  $\mathbf{t}$  directly from the squared measurements  $r_{mi}^2$  in (4.11c) is difficult because it contains the nonlinear terms  $\mathbf{t}^T \mathbf{R}$  and  $\|\mathbf{t}\|^2$ . We handle this challenge by expressing (4.11c) in terms of the correction to the step-1 solution  $(\hat{\mathbf{R}}, \hat{\mathbf{t}})$  and solving for the correction instead.

We can always decompose the translation vector as  $\mathbf{t} = \hat{\mathbf{t}} + \Delta \mathbf{t}$ . Under the assumption that the correction is not much such that  $\|\Delta \mathbf{t}\|/\|\hat{\mathbf{t}}\|$  is small enough to be neglected,

$$\|\mathbf{t}\|^2 \approx \|\hat{\mathbf{t}}\|^2 + 2\hat{\mathbf{t}}^T \Delta \mathbf{t}. \quad (4.12)$$

In addition,

$$\mathbf{t}^T \mathbf{R} \approx \hat{\mathbf{t}}^T \mathbf{R} + \Delta \mathbf{t}^T \hat{\mathbf{R}} \quad (4.13)$$

where  $\Delta \mathbf{t}^T \mathbf{R} \approx \Delta \mathbf{t}^T \hat{\mathbf{R}}$  has been used, which is valid when we ignore the second order correction between  $\mathbf{R}$  and  $\mathbf{t}$  to the step-1 solution.

Using linear approximations (4.12) and (4.13) in (4.11c) yields

$$\begin{aligned} & r_{mi}^2 - (\|\hat{\mathbf{t}} - \mathbf{a}_m\|^2 + \|\mathbf{c}_i\|^2) \\ &= 2(\hat{\mathbf{t}} - \mathbf{a}_m)^T \hat{\mathbf{R}} \mathbf{c}_i + 2(\hat{\mathbf{R}} \mathbf{c}_i + \hat{\mathbf{t}} - \mathbf{a}_m)^T \Delta \mathbf{t} + v_{mi}. \end{aligned} \quad (4.14)$$

The refinement will be based on this equation. We should emphasize that  $\mathbf{R}$  above needs to satisfy the  $SO(K)$  constraint.

It is tempted to use the same additive correction to decompose  $\mathbf{R}$  as for  $\mathbf{t}$ . Such a decomposition is unfavorable since it is  $\mathbf{R}$  that needs to satisfy the  $SO(K)$  constraint, rather than the additive correction. Here the rotation matrix  $\mathbf{R}$  is expressed in multiplicative form as

$$\mathbf{R} = \hat{\mathbf{R}}\mathbf{R}_\delta, \quad (4.15)$$

where  $\mathbf{R}_\delta$  is the corrective rotation matrix applied to  $\hat{\mathbf{R}}$ . The factorization is unique since  $\mathbf{R}_\delta$  is equal to  $\hat{\mathbf{R}}^T\mathbf{R}$  when premultiplying (4.15) by  $\hat{\mathbf{R}}^T$ .

$\mathbf{R}_\delta$  is represented by the Euler angles roll  $\phi$ , pitch  $\theta$ , and yaw  $\psi$  with sequence (1, 2, 3) [62]. Note that these Euler angles are close to zero when the preliminary solution is not far from the optimum. Using the approximation that  $\cos x \approx 1$  and  $\sin x \approx x$  for small  $x$ , we have for the 3D scenario [62]

$$\mathbf{R}_\delta = \begin{bmatrix} c_\theta c_\psi & c_\theta s_\psi & -s_\theta \\ s_\phi s_\theta c_\psi - c_\phi s_\psi & s_\phi s_\theta s_\psi + c_\phi c_\psi & c_\theta s_\phi \\ c_\phi s_\theta c_\psi + s_\phi s_\psi & c_\phi s_\theta s_\psi - s_\phi c_\psi & c_\theta c_\phi \end{bmatrix} \quad (4.16a)$$

$$\approx \begin{bmatrix} 1 & \psi & -\theta \\ -\psi & 1 & \phi \\ \theta & -\phi & 1 \end{bmatrix} \quad (4.16b)$$

where  $c_x = \cos x$  and  $s_x = \sin x$ .

In terms of the Euler angle vector  $\boldsymbol{\beta} = [\phi, \theta, \psi]^T$ , the vectorization of (4.16b) is

$$\text{vec}(\mathbf{R}_\delta) = \boldsymbol{\gamma} + \mathbf{L}\boldsymbol{\beta} \quad (4.17)$$

where  $\boldsymbol{\gamma}$  and  $\mathbf{L}$  are defined in Appendix B.3. For the 2D scenario,  $\mathbf{R}_\delta$  is a  $2 \times 2$  matrix given by (4.16a) after removing the middle column and the middle row. The vectorized form (4.17) remains valid with different definitions of  $\boldsymbol{\gamma}$ ,  $\mathbf{L}$  and  $\boldsymbol{\beta}$ .

Using multiplicative correction (4.15) and the vectorization formula, collecting refinement equation (4.14) for all the measurements in a column gives

$$\check{\mathbf{d}} - \mathbf{H}_1 \boldsymbol{\gamma} = \mathbf{H}_1 \mathbf{L} \boldsymbol{\beta} + \mathbf{F}_2 \Delta \mathbf{t} + \mathbf{v}, \quad (4.18)$$

where  $\check{\mathbf{d}}$  is a vector whose elements are the left hand side of (4.14). The rows of the matrix  $\mathbf{H}_1$  and  $\mathbf{F}_2$  are  $2[\mathbf{c}_i^T \otimes ((\hat{\mathbf{t}} - \mathbf{a}_m)^T \hat{\mathbf{R}})]$  and  $2(\hat{\mathbf{R}} \mathbf{c}_i + \hat{\mathbf{t}} - \mathbf{a}_m)^T$ , respectively. (4.18) is a linear equation in the unknowns  $\boldsymbol{\beta}$  and  $\Delta \mathbf{t}$ , whose WLS solution is

$$\begin{bmatrix} \hat{\boldsymbol{\beta}} \\ \Delta \hat{\mathbf{t}} \end{bmatrix} = (\mathbf{H}^T \mathbf{Q}_v^{-1} \mathbf{H})^{-1} \mathbf{H}^T \mathbf{Q}_v^{-1} (\check{\mathbf{d}} - \mathbf{H}_1 \boldsymbol{\gamma}), \quad (4.19)$$

where  $\mathbf{H} = [\mathbf{H}_1 \mathbf{L} \ \mathbf{F}_2]$  and  $\mathbf{Q}_v$  is defined below (4.11c).

After obtaining the Euler angles, we use them to construct the original  $\mathbf{R}_\delta$  as defined in (4.16a) without using the small angle approximation and obtain the final estimate of  $\mathbf{R}$  from (4.15). Since both  $\hat{\mathbf{R}}$  and the original  $\mathbf{R}_\delta$  are in  $SO(K)$ , the resulting solution for  $\mathbf{R}$  will satisfy the  $SO(K)$  constraint. Adding  $\Delta \hat{\mathbf{t}}$  to  $\hat{\mathbf{t}}$  yields the refined position vector.

The refinement solution developed here assumes the preliminary solution from step-1 is not far from the optimum. Simulations validate that the accuracy of the preliminary solution is sufficient to initiate the refinement procedure for producing a final solution approaching the CRLB accuracy. If the preliminary solution is less

accurate, the refinement step can be repeated one more time by updating  $\hat{\mathbf{R}}$  and  $\hat{\mathbf{t}}$ .

Note that the proposed step-2 refinement solution is not tied to the step-1 solution. Other initial solutions, such as the SCLS and CLS from [53] can be used instead. Nevertheless, the more accurate the initial solution, the better will be the refined solution.

### 4.3 2D Case

Here we discuss the special case where there is only one rotational degree of freedom for the rigid body. In such a case, the rotational axis is perpendicular to a certain plane. To facilitate the algorithm description, we consider the anchors and sensors are on the  $x$ - $y$  plane. Otherwise, we can augment the rotation matrix as block diagonal with blocks  $\mathbf{R}$  and 1 and add the third dimension into the translation vector  $\mathbf{t}$  to make the proposed method applicable.

We shall obtain the unknowns  $\mathbf{R}$  and  $\mathbf{t}$  directly from the measurements without first solving the intermediate variables  $\mathbf{s}_i$ . One advantage of not using the intermediate variables is that the algorithm can tolerate a larger noise level before the thresholding effect, due to the nature of the nonlinear estimation problem, occurs [74]. In addition, we only need a minimum of 2 distance measurements for each sensor as will be clear later.

When we represent  $\mathbf{R} \in \mathbb{R}^{2 \times 2}$  in four variables [53], there will be four constraints from  $SO(2)$  on the elements: three from  $\mathbf{R}^T \mathbf{R} = \mathbf{I}$  and one from  $\det(\mathbf{R}) = 1$ . Instead,

we express the rotation matrix as

$$\mathbf{R} = \begin{bmatrix} \cos \theta & -\sin \theta \\ \sin \theta & \cos \theta \end{bmatrix} \quad (4.20)$$

where  $\theta$  is the rotation angle of the local frame  $\mathcal{B}$  with respect to the inertial frame  $\mathcal{I}$  and it is counted in the counter-clockwise direction (see Fig. 4.1). This representation limits  $\mathbf{R}$  to be in  $SO(2)$  automatically. Through such representation, the step-1 and step-2 solutions can be obtained efficiently using the GTRS optimization technique.

#### 4.3.1 Step-1

We shall begin with the squared range equation (4.11b). Stacking (4.11b) over the available measurements for sensor  $i$  gives the vector form

$$\mathbf{d}_i = -2\mathbf{A}^T \mathbf{s}_i + \|\mathbf{s}_i\|^2 \mathbf{1} + \mathbf{v}_i \quad (4.21)$$

where  $\mathbf{d}_i$  is a vector with elements  $r_{mi}^2 - \|\mathbf{a}_m\|^2$  and  $\mathbf{A}$  is a matrix with columns  $\mathbf{a}_m$ . Let the covariance matrix of  $\mathbf{v}_i$  be  $\mathbf{Q}_i$ , which is the  $i$ -th diagonal block of  $\mathbf{Q}_v$  defined below (4.11c). We can express  $\|\mathbf{s}_i\|^2$  in terms of  $\mathbf{s}_i$  in a WLS manner using the weighting matrix  $\mathbf{Q}_i^{-1}$  as

$$\|\mathbf{s}_i\|^2 = (\mathbf{1}^T \mathbf{Q}_i^{-1} \mathbf{1})^{-1} \mathbf{1}^T \mathbf{Q}_i^{-1} (\mathbf{d}_i + 2\mathbf{A}^T \mathbf{s}_i) \quad (4.22)$$

Putting it back to (4.21) and substituting (4.2) as well give

$$\mathbf{T}_i \mathbf{d}_i = -2\mathbf{T}_i \mathbf{A}^T \mathbf{s}_i + \mathbf{v}_i \quad (4.23a)$$

$$= -2\mathbf{T}_i \mathbf{A}^T \mathbf{R} \mathbf{c}_i - 2\mathbf{T}_i \mathbf{A}^T \mathbf{t} + \mathbf{v}_i \quad (4.23b)$$

where  $\mathbf{T}_i = \mathbf{I} - \mathbf{1}\mathbf{1}^T \mathbf{Q}_i^{-1} / (\mathbf{1}^T \mathbf{Q}_i^{-1} \mathbf{1})$ . (4.23b) is valid as long as there are at least two measurements for each sensor so that  $\mathbf{T}_i$  is not zero.

Obtaining  $\theta$  directly from (4.23b) could be complicated since it appears as non-linear functions  $\cos \theta$  and  $\sin \theta$  inside  $\mathbf{R}$ . Note that optimizing over  $\theta$  is equivalent to optimizing over  $\mathbf{y} = [\cos \theta \ \sin \theta]^T$  with the constraint  $\|\mathbf{y}\|^2 = 1$ . Such an indirect approach will enable us to obtain a closed-form solution.

The vectorization of  $\mathbf{R}$  can be expressed in terms of  $\mathbf{y}$  as

$$\text{vec}(\mathbf{R}) = \mathbf{\Gamma} \mathbf{y} \quad (4.24)$$

where  $\mathbf{\Gamma}$  is a  $4 \times 2$  sparse matrix with the (1, 1), (2, 2) and (4, 1) elements equal to 1 and (3, 2) element  $-1$ . Using the vectorization formula (4.1) in the first term on the right of (4.23b) yields

$$\mathbf{T}_i \mathbf{d}_i = -2(\mathbf{c}_i^T \otimes \mathbf{T}_i \mathbf{A}^T) \mathbf{\Gamma} \mathbf{y} - 2\mathbf{T}_i \mathbf{A}^T \mathbf{t} + \mathbf{v}_i \quad (4.25)$$

which is linear in the unknowns  $\mathbf{y}$  and  $\mathbf{t}$ . Since they are common in all of the  $N$  sensors, stacking above equation over  $i$  forms the vector equation

$$\bar{\mathbf{d}} = \mathbf{E}_1 \mathbf{y} + \mathbf{E}_2 \mathbf{t} + \mathbf{v} \quad (4.26)$$



where  $\bar{\mathbf{d}}$  is the concatenation of the subvectors  $\mathbf{T}_i \mathbf{d}_i$ , and  $\mathbf{E}_1$  and  $\mathbf{E}_2$  are matrices formed by stacking the blocks  $-2(\mathbf{c}_i^T \otimes \mathbf{T}_i \mathbf{A}^T) \mathbf{\Gamma}$  and  $-2\mathbf{T}_i \mathbf{A}^T$ .

The translation parameter  $\mathbf{t}$  is unconstrained. The WLS solution for  $\mathbf{t}$  in terms of  $\mathbf{y}$  is

$$\mathbf{t} = (\mathbf{E}_2^T \mathbf{Q}_{\mathbf{v}}^{-1} \mathbf{E}_2)^{-1} \mathbf{E}_2^T \mathbf{Q}_{\mathbf{v}}^{-1} (\bar{\mathbf{d}} - \mathbf{E}_1 \mathbf{y}) \quad (4.27)$$

where the weighting matrix is  $\mathbf{Q}_{\mathbf{v}}^{-1}$  [20]. Let  $\mathbf{P} = \mathbf{I} - \mathbf{E}_2 (\mathbf{E}_2^T \mathbf{Q}_{\mathbf{v}}^{-1} \mathbf{E}_2)^{-1} \mathbf{E}_2^T \mathbf{Q}_{\mathbf{v}}^{-1}$ . Putting the estimated  $\mathbf{t}$  (4.27) back to (4.26) yields

$$\mathbf{P} \bar{\mathbf{d}} = \mathbf{P} \mathbf{E}_1 \mathbf{y} + \mathbf{v}. \quad (4.28)$$

We now need to solve the constrained optimization problem for  $\mathbf{y}$ :

$$\begin{aligned} \min_{\mathbf{y}} & (\mathbf{P} \bar{\mathbf{d}} - \mathbf{P} \mathbf{E}_1 \mathbf{y})^T \mathbf{Q}_{\mathbf{v}}^{-1} (\mathbf{P} \bar{\mathbf{d}} - \mathbf{P} \mathbf{E}_1 \mathbf{y}) \\ &= (\bar{\mathbf{d}} - \mathbf{E}_1 \mathbf{y})^T \mathbf{Q}_{\mathbf{v}}^{-1} \mathbf{P} (\bar{\mathbf{d}} - \mathbf{E}_1 \mathbf{y}) \\ \text{s.t. } & \|\mathbf{y}\|^2 = 1, \end{aligned} \quad (4.29)$$

where we have used  $\mathbf{P}^T \mathbf{Q}_{\mathbf{v}}^{-1} \mathbf{P} = \mathbf{Q}_{\mathbf{v}}^{-1} \mathbf{P}$ .

This quadratic optimization problem with a quadratic equality constraint can be solved by GTRS [17, 18] efficiently to obtain the global minimum solution. In particular, the solution is

$$\mathbf{y}(\lambda) = (\mathbf{E}_1^T \mathbf{Q}_{\mathbf{v}}^{-1} \mathbf{P} \mathbf{E}_1 + \lambda \mathbf{I}_2)^{-1} \mathbf{E}_1^T \mathbf{Q}_{\mathbf{v}}^{-1} \mathbf{P} \bar{\mathbf{d}} \quad (4.30)$$

and  $\lambda$  is the largest real root of

$$\begin{aligned}\varphi(\lambda) &= \|\mathbf{y}(\lambda)\|^2 - 1 \\ \lambda &\in (-\lambda_{\min}(\mathbf{E}_1^T \mathbf{Q}_v^{-1} \mathbf{P} \mathbf{E}_1), \infty)\end{aligned}\tag{4.31}$$

where  $\lambda_{\min}(\cdot)$  is the smallest eigenvalue of  $(\cdot)$ . The smallest eigenvalue is straightforward to obtain since the matrix  $\mathbf{E}_1^T \mathbf{Q}_v^{-1} \mathbf{P} \mathbf{E}_1$  has a size of 2 only.

The numerator of  $\varphi(\lambda)$  is quartic in  $\lambda$  and the root finding is straightforward to implement. Once we obtain the solution  $\mathbf{y}$  (and hence  $\theta$ ),  $\mathbf{t}$  is immediately available from (4.27).

Rather than using the above procedure of expressing  $\mathbf{t}$  in terms of  $\mathbf{y}$  and solving  $\mathbf{y}$  through (4.29), an alternative is to obtain them together by considering  $\boldsymbol{\xi} = [\mathbf{y}^T, \mathbf{t}^T]^T$  as a single unknown in (4.26) through the minimization of  $(\bar{\mathbf{d}} - \mathbf{E}\boldsymbol{\xi})^T \mathbf{Q}_v^{-1} (\bar{\mathbf{d}} - \mathbf{E}\boldsymbol{\xi})$  s.t.  $\boldsymbol{\xi}^T \mathbf{P} \boldsymbol{\xi} = 1$  using GTRS, where  $\mathbf{E} = [\mathbf{E}_1, \mathbf{E}_2]$  and  $\mathbf{P} = \text{diag}(\mathbf{I}_2, \mathbf{O}_2)$ . Solving them together can reduce computation if  $M$  and  $N$  are large. It can be shown analytically that both procedures will give the same solution of  $\mathbf{y}$  and  $\mathbf{t}$ .

### 4.3.2 Step-2

With the solution  $\hat{\mathbf{R}}$  and  $\hat{\mathbf{t}}$  from step-1, applying the vectorization formula (4.1) and  $\text{vec}(\mathbf{R})$  in (4.24) to the first term on the right of the refinement equation (4.14) gives

$$r_{mi}^2 - (\|\hat{\mathbf{t}} - \mathbf{a}_m\|^2 + \|\hat{\mathbf{t}}\|^2) \approx \mathbf{f}_{mi,1}^T \mathbf{y} + \mathbf{f}_{mi,2}^T \Delta \mathbf{t} + v_{mi}\tag{4.32}$$

where

$$\begin{aligned}\mathbf{f}_{mi,1}^T &= 2[\mathbf{c}_i^T \otimes (\hat{\mathbf{t}} - \mathbf{a}_m)^T] \mathbf{\Gamma} \\ \mathbf{f}_{mi,2}^T &= 2(\hat{\mathbf{R}}\mathbf{c}_i + \hat{\mathbf{t}} - \mathbf{a}_m)^T.\end{aligned}\tag{4.33}$$

Collecting the equations for all distance measurements into a single column forms

$$\check{\mathbf{d}} = \mathbf{F}_1 \mathbf{y} + \mathbf{F}_2 \Delta \mathbf{t} + \mathbf{v}\tag{4.34}$$

where  $\check{\mathbf{d}}$ ,  $\mathbf{F}_1$  and  $\mathbf{F}_2$  are the vector and matrices by collecting the elements on the left side and the rows  $\mathbf{f}_{mi,1}^T$  and  $\mathbf{f}_{mi,2}^T$ . (4.34) has the same structure as (4.26) in step-1 and the same procedure by using GTRS applies to the refinement as well to obtain the final estimates of  $\mathbf{y}$  and  $\Delta \mathbf{t}$ . Adding the estimate  $\Delta \mathbf{t}$  to  $\hat{\mathbf{t}}$  yields the improved solution for  $\mathbf{t}$ .

## 4.4 Moving Rigid Body Localization

We have so far considered the rigid body is stationary. There are many occasions in practice that the rigid body has motion, for example, a vehicle moving on the ground or an aircraft flying in the air. Simply pretending a moving rigid body is stationary will lead to poor localization performance. Assuming the angular and translational velocities are known may not be reasonable. We shall extend the study to localize a moving rigid body by estimating  $\mathbf{R}$ ,  $\mathbf{t}$ ,  $\boldsymbol{\omega}$  and  $\dot{\mathbf{t}}$  using both the distance and Doppler measurements.

In the sensor velocity model (4.4), the matrix  $[\boldsymbol{\omega}]^\times$  is [62]

$$[\boldsymbol{\omega}]^\times = \begin{bmatrix} 0 & -\omega_3 & \omega_2 \\ \omega_3 & 0 & -\omega_1 \\ -\omega_2 & \omega_1 & 0 \end{bmatrix} \quad (4.35)$$

for the 3D case and

$$[\omega]^\times = \begin{bmatrix} 0 & -\omega \\ \omega & 0 \end{bmatrix} \quad (4.36)$$

for the 2D case. The vectorized form of  $[\boldsymbol{\omega}]^\times$  that packs the angular velocity components in a vector is

$$\text{vec}([\boldsymbol{\omega}]^\times) = \boldsymbol{\Phi} \boldsymbol{\omega} \quad (4.37)$$

where

$$\begin{aligned} \boldsymbol{\Phi} &= \begin{bmatrix} 0 & 0 & 0 & 0 & 0 & 1 & 0 & -1 & 0 \\ 0 & 0 & -1 & 0 & 0 & 0 & 1 & 0 & 0 \\ 0 & 1 & 0 & -1 & 0 & 0 & 0 & 0 & 0 \end{bmatrix}^T, \\ \boldsymbol{\omega} &= [\omega_1, \omega_2, \omega_3]^T \end{aligned} \quad (4.38)$$

in the 3D case and

$$\boldsymbol{\Phi} = [0, 1, -1, 0]^T, \quad \boldsymbol{\omega} = \omega \quad (4.39)$$

in the 2D case.

Rather than using Doppler equation (4.5) directly, we multiply it and the distance

equation (4.3a) to obtain

$$r_{mi}\dot{r}_{mi} = \mathbf{s}_i^T \dot{\mathbf{s}}_i - \mathbf{a}_m^T \dot{\mathbf{s}}_i + \dot{r}_{mi}n_{mi} + r_{mi}\dot{n}_{mi} \quad (4.40)$$

where the second order noise term  $n_{mi}\dot{n}_{mi}$  is neglected.

It is straightforward to verify  $\mathbf{c}_i^T \mathbf{R}^T [\boldsymbol{\omega}]^\times \mathbf{R} \mathbf{c}_i = 0$  since  $[\boldsymbol{\omega}]^\times$  is skew-symmetric. Substituting  $\mathbf{s}_i$  in (4.2) and  $\dot{\mathbf{s}}_i$  in (4.4) relates (4.40) to the unknowns to be found:

$$r_{mi}\dot{r}_{mi} = (\mathbf{t} - \mathbf{a}_m)^T [\boldsymbol{\omega}]^\times \mathbf{R} \mathbf{c}_i + (\mathbf{R} \mathbf{c}_i + \mathbf{t} - \mathbf{a}_m)^T \dot{\mathbf{t}} + \dot{r}_{mi}n_{mi} + r_{mi}\dot{n}_{mi}. \quad (4.41)$$

The unknowns appear coupled with each other. The first term on the right contains the products of three unknowns and the second two. We shall follow the two steps approach to obtain a solution, where the first step provides a coarse preliminary solution and the second uses the preliminary solution to yield the final solution.

#### 4.4.1 Step-1

Using the processing described in Section 4.2 or 4.3, we are able to obtain an estimate of the rotation matrix and translation vector, which is denoted as  $(\hat{\mathbf{R}}, \hat{\mathbf{t}})$ . Approximating  $\mathbf{R}$  and  $\mathbf{t}$  by the estimates  $(\hat{\mathbf{R}}, \hat{\mathbf{t}})$  gives a linear equation in  $\boldsymbol{\omega}$  and  $\dot{\mathbf{t}}$  from (4.41),

$$r_{mi}\dot{r}_{mi} = [(\hat{\mathbf{R}} \mathbf{c}_i)^T \otimes (\hat{\mathbf{t}} - \mathbf{a}_m)^T] \boldsymbol{\Phi} \boldsymbol{\omega} + (\hat{\mathbf{R}} \mathbf{c}_i + \hat{\mathbf{t}} - \mathbf{a}_m)^T \dot{\mathbf{t}} + \dot{r}_{mi}n_{mi} + r_{mi}\dot{n}_{mi}, \quad (4.42)$$

where  $[\boldsymbol{\omega}]^\times$  is expressed in the vectorized form (4.37) after applying the vectorization formula. (4.42) is linear in  $\boldsymbol{\omega}$  and  $\dot{\mathbf{t}}$ . Applying the WLS minimization over the

available measurements yields their estimates  $\hat{\boldsymbol{\omega}}$  and  $\hat{\dot{\mathbf{t}}}$ , where the weighting matrix is [20]

$$([\text{diag}(\dot{\mathbf{r}})^T, \text{diag}(\mathbf{r})^T]^T \mathbf{Q} [\text{diag}(\dot{\mathbf{r}}), \text{diag}(\mathbf{r})])^{-1}. \quad (4.43)$$

Using both the distance and Doppler measurements will give more accurate sensor position estimates than using distances only as in Section 4.2.1 and hence better  $(\hat{\mathbf{R}}, \hat{\mathbf{t}})$ . The closed-form estimator from [71] that was developed for joint position and velocity estimation using TDOAs and FDOAs can be modified for this purpose. We summarize the major steps in Appendix B.4. The readers are referred to [71] for additional details.

#### 4.4.2 Step-2

The solution from step-1,  $(\hat{\mathbf{R}}, \hat{\mathbf{t}}, \hat{\boldsymbol{\omega}}, \hat{\dot{\mathbf{t}}})$ , will not reach the optimum performance since we do not consider  $\mathbf{R}$  and  $\mathbf{t}$  as unknowns when solving  $\boldsymbol{\omega}$  and  $\dot{\mathbf{t}}$ . We shall determine the amount of correction for the step-1 preliminary solution to obtain the final solution.

Putting rotation matrix multiplicative correction (4.15),  $\mathbf{t} = \hat{\mathbf{t}} + \Delta\mathbf{t}$ ,  $\boldsymbol{\omega} = \hat{\boldsymbol{\omega}} + \Delta\boldsymbol{\omega}$ , and  $\dot{\mathbf{t}} = \hat{\dot{\mathbf{t}}} + \Delta\dot{\mathbf{t}}$ , (4.41) becomes

$$\begin{aligned} & r_{mi}\dot{r}_{mi} - \hat{\mathbf{t}}^T \hat{\dot{\mathbf{t}}} + \mathbf{a}_m^T \hat{\dot{\mathbf{t}}} \\ &= (\hat{\mathbf{t}}^T [\hat{\boldsymbol{\omega}}]^\times - \mathbf{a}_m^T [\hat{\boldsymbol{\omega}}]^\times + \hat{\mathbf{t}}^T) \hat{\mathbf{R}} \mathbf{R}_\delta \mathbf{c}_i + ([\hat{\boldsymbol{\omega}}]^\times \hat{\mathbf{R}} \mathbf{c}_i + \hat{\mathbf{t}})^T \Delta\mathbf{t} \\ &+ [(\hat{\mathbf{R}} \mathbf{c}_i)^T \otimes (\hat{\mathbf{t}} - \mathbf{a}_m)^T] \boldsymbol{\Phi} \Delta\boldsymbol{\omega} + (\hat{\mathbf{R}} \mathbf{c}_i + \hat{\mathbf{t}} - \mathbf{a}_m)^T \Delta\dot{\mathbf{t}} + \dot{r}_{mi} n_{mi} + r_{mi} \dot{n}_{mi} \end{aligned} \quad (4.44)$$

where the second and third order correction terms have been ignored. Note that

this corresponds to setting  $\mathbf{R}_\delta$  to identity when multiplied with the other correction terms. Using the vectorization formula (4.1) and  $\text{vec}(\mathbf{R}_\delta)$  in (4.17), the first term on the right of (4.44) becomes

$$\begin{aligned} & (\hat{\mathbf{t}}^T[\hat{\boldsymbol{\omega}}]^\times - \mathbf{a}_m^T[\hat{\boldsymbol{\omega}}]^\times + \hat{\mathbf{t}}^T)\hat{\mathbf{R}}\mathbf{R}_\delta\mathbf{c}_i \\ &= [\mathbf{c}_i^T \otimes (\hat{\mathbf{t}}^T[\hat{\boldsymbol{\omega}}]^\times - \mathbf{a}_m^T[\hat{\boldsymbol{\omega}}]^\times + \hat{\mathbf{t}}^T)\hat{\mathbf{R}}](\boldsymbol{\gamma} + \mathbf{L}\boldsymbol{\beta}). \end{aligned} \quad (4.45)$$

Now (4.44) is linear in the amount of corrections  $\boldsymbol{\beta}$ ,  $\Delta\mathbf{t}$ ,  $\Delta\boldsymbol{\omega}$  and  $\Delta\hat{\mathbf{t}}$ .

Eq. (4.18) provides the distance equations in terms of the amounts of corrections for  $\mathbf{R}$  and  $\mathbf{t}$ . To make use of both distance and Doppler measurements, we stack (4.18) and (4.44) together to form a matrix equation. Applying the WLS minimization with the weighting [20]

$$(\mathbf{K}\mathbf{R}\mathbf{K}^T)^{-1}, \mathbf{K} = \begin{bmatrix} 2\text{diag}(\mathbf{r}) & \mathbf{O} \\ \text{diag}(\dot{\mathbf{r}}) & \text{diag}(\mathbf{r}) \end{bmatrix} \quad (4.46)$$

yields the solution of the correction terms. Adding them to the step-1 preliminary solution gives the final estimate of the unknowns.

In the specific case of 2D, we can use the vectorized representation (4.24) instead and the first term on the right of (4.44) is expressed as

$$\begin{aligned} & (\hat{\mathbf{t}}^T[\hat{\boldsymbol{\omega}}]^\times - \mathbf{a}_m^T[\hat{\boldsymbol{\omega}}]^\times + \hat{\mathbf{t}}^T)\mathbf{R}\mathbf{c}_i \\ &= [\mathbf{c}_i^T \otimes (\hat{\mathbf{t}}^T[\hat{\boldsymbol{\omega}}]^\times - \mathbf{a}_m^T[\hat{\boldsymbol{\omega}}]^\times + \hat{\mathbf{t}}^T)]\boldsymbol{\Gamma}\mathbf{y}. \end{aligned} \quad (4.47)$$

Applying GTRS with the constraint  $\|\mathbf{y}\|^2 = 1$  will solve the WLS optimization problem from the distance refinement equation (4.34) and the Doppler refinement equation (4.44) for  $\theta$  and the corrections.

## 4.5 Performance

### 4.5.1 Accuracy

The estimation performance is limited by the CRLB over the small error region where the estimation bias is negligible compared to the variance. Strictly speaking the CRLB is for an unbiased estimator only. Localization is a nonlinear estimation problem that often leads to a biased estimator. However, the CRLB has been used extensively in the literature as a reference for the localization performance, due to its simplicity of computation and good prediction on the performance limit over the small error region [20]. Under the distance measurement model (4.3a) and the  $SO(K)$  constraint on  $\mathbf{R}$ , the CRLBs for  $\mathbf{R}$  and  $\mathbf{t}$  of a stationary rigid body have been evaluated in [53]. The CRLBs for  $\theta$  and  $\mathbf{t}$  in the 2D case is provided in Appendix B.1. For a moving rigid body, the CRLBs for the unknown parameters are derived in Appendix B.2. In the simulation study of Section 4.6, we shall use the CRLB as a reference for performance evaluations of the proposed solutions. To supplement and support the simulations presented in the next section, we illustrate below some rationale and insight about the performance of the proposed methods.

Let us begin with the stationary rigid body localization algorithm in Section 4.2. The first step uses DAC to obtain a preliminary solution and the second estimates the correction to the step-1 solution. The DAC approach solves first the sensor positions and then the rotation and translation variables. Without considering the position relationship (4.2) among different sensors, many localization algorithms from the literature [21, 39, 75] can provide sensor position estimates that attain the CRLB accuracy. It can be shown directly through the theory of DAC [67] that when the



measurements corresponding to different sensors are independent, setting the weighting factor  $\mathbf{W}_i$  in optimization (4.6) to the Fisher information matrix (inverse of the CRLB matrix) for  $\mathbf{s}_i$  will yield a solution of the rotation and translation parameters reaching the CRLB. Unfortunately such a setting does not lead to a simple closed-form solution (except for the 2D case). We therefore set  $\mathbf{W}_i$  to a scalar weighting. Such setting results in suboptimum performance but enables a simple and reasonably accurate solution. This is in contrast to the approach in [53] by eliminating the  $\|\mathbf{s}_i\|^2$  terms of (4.11b), which seems to be more significant in contributing to the loss in accuracy.

In the step-2 refinement, we reformulate the squared range equation (4.11c) in terms of the corrections to the unknowns with respect to the step-1 solution. It has been demonstrated in Chapter 2 that with inverse range weighting, the squared range equation approximates to the original range equation when the measurement noise is small. The resulting refinement equation (4.18) embeds the  $SO(K)$  constraint through the multiplicative correction representation (4.15). It follows a linear model and the corresponding WLS solution (4.19), which is the same as the minimum variance unbiased (MVU) estimator, can reach the CRLB accuracy [20]. Consequently, we would expect the step-2 solution would be able to approach the CRLB performance over the small error region, provided that the amounts of correction relative to the actual values are not large so that (4.18) is reasonably accurate although ignoring the second order corrections.

We next turn to the solution for the specific case of 2D presented in Section 4.3. This solution remains to use the two steps approach but the solution in each step uses the GTRS optimization. The solution here is expected to tolerate larger amount

of noise before the thresholding effect occurs since the step-1 solution is obtained directly from the measurement equations without using the intermediate variables  $\mathbf{s}_i$ . Another interesting property is that it solves the rotation matrix directly in step-2 and does not require the correction angle formulation for the rotation matrix. As a result, the step-2 processing can accommodate larger amount of rotation correction.

For the moving rigid body localization elaborated in Section 4.4, the solution framework is similar to what we did before in using two steps. The Doppler measurement from (4.5) is exploited using the transformed equation (4.40). Previous studies [71] showed that such a transformed equation provides nearly the same information as the original under small noise condition. The transformed equation is used in estimating the initial estimates of the angular and translational velocities in step-1 and their correction amounts in step-2. The refinement equations (4.18) and (4.44) for step-2 both follow linear models with respect to the correction terms. The resulting WLS solution (equivalent to the MVU estimator) will provide the CRLB accuracy [20] under the models. Consequently, it is expected the performance of the final solution will not deviate too much from the CRLB over small error region when the amount of corrections relative to the true values are not significant so that the second and higher order correction terms can be neglected in (4.18) and (4.44).

### 4.5.2 Computational Complexity

We shall examine the computational complexity of the proposed methods for stationary rigid body case and compare it with SCLS and CLS. The complexity is shown in big  $O$  expressions in terms of the number of anchors  $M$ , the number of sensors  $N$  and the localization dimension  $K$  (2 or 3), with the diagonal structure of  $\mathbf{Q}_v$  exploited.

Note that the expressions illustrate the asymptotic complexity that is valid when  $M$  and  $N$  are sufficiently large.

For the proposed method in Section 4.2, step-1 requires  $O(K^2MN)$  flops to estimate the sensor positions and  $O(K^3)$  flops for an SVD to obtain the preliminary solution. Step-2 takes  $O(MN)$  flops to form the refinement equations and apply the WLS processing to generate the final solution.

For the algorithm of 2D localization in Section 4.3, in each step, forming the equations for optimization or GTRS computation when jointly estimating  $\mathbf{y}$  and  $\mathbf{t}$  takes about  $O(MN)$  flops.

For reference purpose, we estimate that the complexity of SCLS is  $O(MN \max(M, N))$  flops +  $O(K^3)$  flops, where  $O(K^3)$  is for SVD. It is  $O(M^3N^3)$  flops +  $O(K^2MN)L$  flops for CLS, where  $L$  is the number of iterations. It is clear when  $M$  and  $N$  are sufficiently large, the proposed algorithms have lower complexity. If  $M$  and  $N$  are not large, the proposed algorithms have similar complexity with SCLS and CLS, as illustrated in the simulations.

## 4.6 Simulations

We shall evaluate the performance of the proposed solutions for localization in 3D and 2D, using a number of geometries with randomly generated anchor positions. The CRLB is served here as a performance reference. We also include the results using the closed-form SCLS and the iterative CLS solution from [53] for comparison (please refer to Appendix B.5 for some details of our implementations of SCLS and CLS).

There are  $M = 6$  anchors and they are placed at uniformly distributed i.i.d. coordinates in a cube (3D case) or a square (2D case) having a length of 100 units centered at the origin in the inertial reference frame  $\mathcal{I}$ . To avoid degenerate geometry that yields poor performance, the separation between two anchors is at least 15 units. We generate  $G = 200$  realizations of anchor configurations and the results reported are the averages over them. The number of ensemble runs is  $L = 1000$  for a given anchor geometry. Each sensor is able to acquire the measurements from all anchors. The rigid body settings and sensor configurations will be specified later. The true distance and Doppler values in the weighting matrices of the proposed algorithms are replaced by the noisy measurements throughout the simulations.

The root mean squared error (RMSE) of a parameter estimate  $(*)$  is computed using

$$\text{RMSE}(*) = \sqrt{\frac{1}{LG} \sum_{g=1}^G \sum_{l=1}^L \|(\hat{*})^{(g,l)} - (*)\|^2} \quad (4.48)$$

where  $(\hat{*})^{(g,l)}$  is the estimation for  $(*)$  at the  $l$ -th ensemble run for the  $g$ -th anchor configuration. The norm is Euclidean when  $(*)$  is a vector and Frobenius when  $(*)$  is a matrix. Similarly, the estimation bias of  $(*)$  is calculated by

$$\text{bias}(*) = \sqrt{\frac{1}{G} \sum_{g=1}^G \left\| \frac{1}{L} \sum_{l=1}^L (\hat{*})^{(g,l)} - (*) \right\|^2}. \quad (4.49)$$

### 4.6.1 Stationary Rigid Body

The distance measurement noise is uncorrelated. Often the sensor array is small and far away from the anchors. We therefore set the noise powers of distances from a given anchor to all the sensors to be the same, but different for different anchors to exercise better the algorithm performance. The noise standard deviations  $\sigma_{mi}, m = 1, 2, \dots, 6$ , for the six anchors are  $\frac{\sigma}{6}[1, 2, 3, 4, 5, 6]$ .

#### 3D Case

We first evaluate the performance of the solution presented in Section 4.2 using a 3D localization scenario. The performance of the method for the 2D scenario is similar. The positions of the rigid body sensors are

$$\mathbf{C} = 3 \begin{bmatrix} 0.5 & 1.5 & 1.5 & 0.5 & 1 \\ 0 & 0 & 1.5 & 1.5 & 1 \\ 0 & 0 & 0 & 0 & 1 \end{bmatrix}$$

in  $\mathcal{B}$ , where each column is the sensor position  $\mathbf{c}_i$ . It is the rectangle based pyramid used in [53]. The orientation of the rigid body is set as follows: the two reference frames coincide at the beginning, then the rigid body rotates 20 deg,  $-25$  deg, and 10 deg with respect to  $x$ ,  $y$ ,  $z$  axes of  $\mathcal{I}$  in sequence. The translation vector is  $\mathbf{t} = [100 \ 100 \ 50]^T$ . In the proposed method, the two-stage estimator [39] is used to obtain  $\hat{\mathbf{s}}_i$  estimates in step-1 and the scalar weighting factors  $w_i$  is set to unity.

Fig. 4.2 shows the RMSE of the rotation matrix  $\mathbf{R}$  estimate, where the solid line is the root CRLB. The proposed step-1 preliminary solution (shown by cross-symbol), is suboptimum as expected. However, the step-2 solution (circle-symbol) is

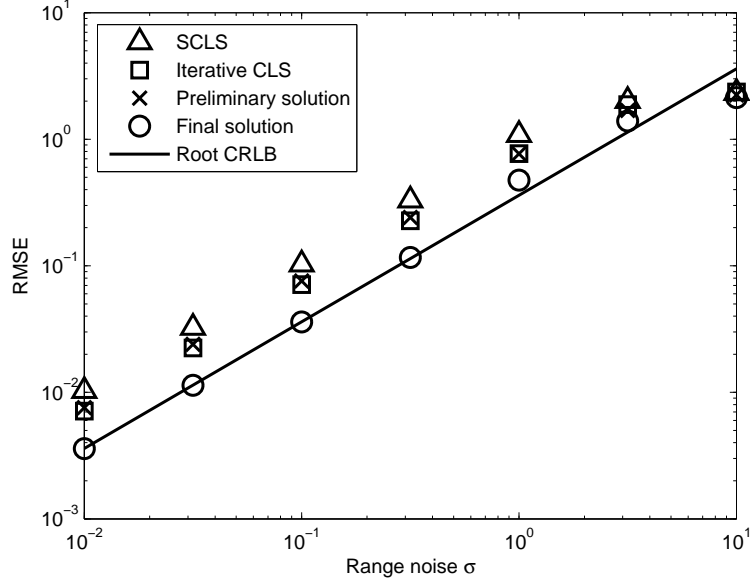


Figure 4.2: Performance for rotation matrix  $\mathbf{R}$  estimation in the 3D case, averaged over 200 realizations of anchor positions.

able to reach the CRLB performance when the measurement noise deviation  $\sigma$  is not larger than  $10^{-0.5}$  (0.32). Compared to SCLS (triangle-symbol), the step-1 solution is better. The iterative CLS (rectangle-symbol) can only achieve similar performance as the proposed step-1 solution, even though it requires more computation. The proposed step-2 solution provides about 3 dB reduction in RMSE over the iterative CLS solution in the small error region.

Fig. 4.3 gives the RMSE performance of the translation vector  $\mathbf{t}$  estimate. The observations are similar to those in Fig. 4.2. It is interesting to see that the step-1 solution gives better accuracy than CLS. The step-2 solution has about 3.3 dB improvement over CLS.

Figs. 4.4–4.5 are the results for estimation bias. We observe consistent behaviors in both rotation and translation that the proposed step-2 solution yields the smallest

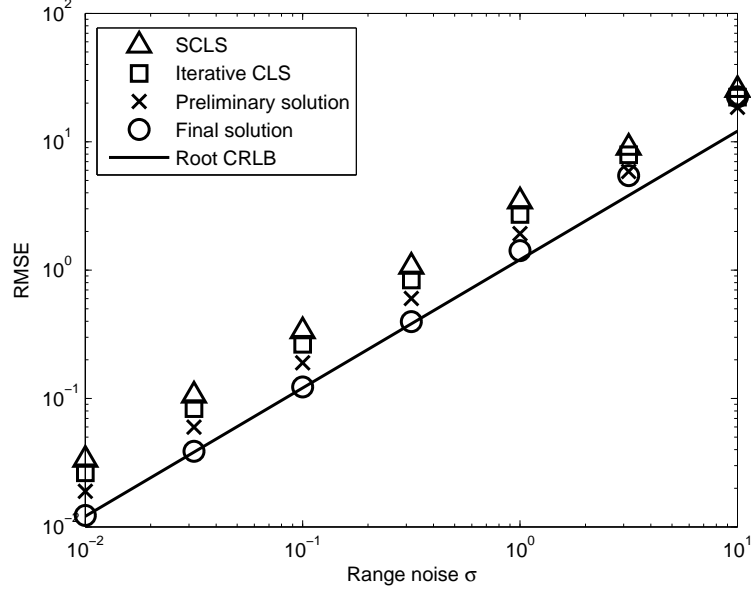


Figure 4.3: Performance for position  $\mathbf{t}$  estimation in the 3D case, averaged over 200 realizations of anchor positions.

bias and the SCLS has the largest, while the proposed step-1 and the iterative CLS solution have comparable results.

Fig. 4.6 illustrates the computation times (millisecond) for the different solutions obtained from MATLAB implementations. The step-1 solution takes slightly larger computation than the SCLS method. The proposed step-2 solution requires the largest computation. It is the price we pay for achieving better results approaching the CRLB. The complexity of CLS rises quickly if the noise deviation  $\sigma$  is larger than  $10^{-0.5}$  (0.32), due to larger number of iterations needed.

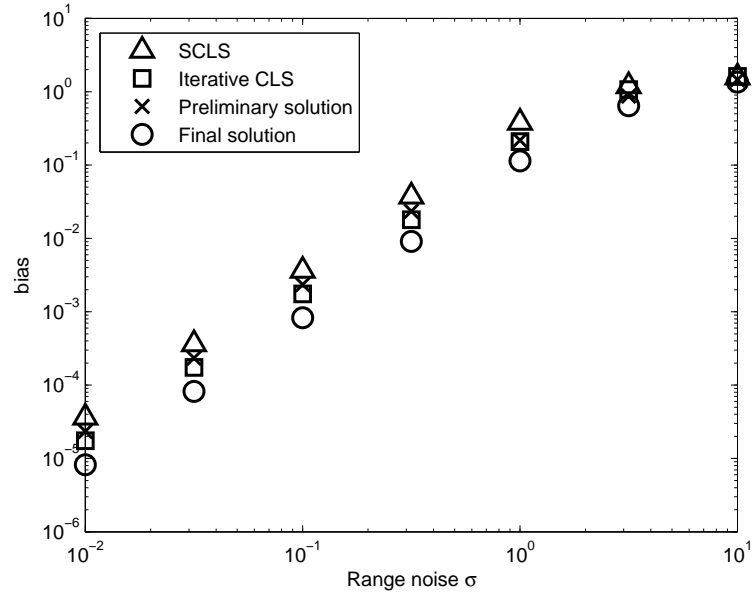


Figure 4.4: Bias for rotation matrix  $\mathbf{R}$  estimation in the 3D case, averaged over 200 realizations of anchor positions.

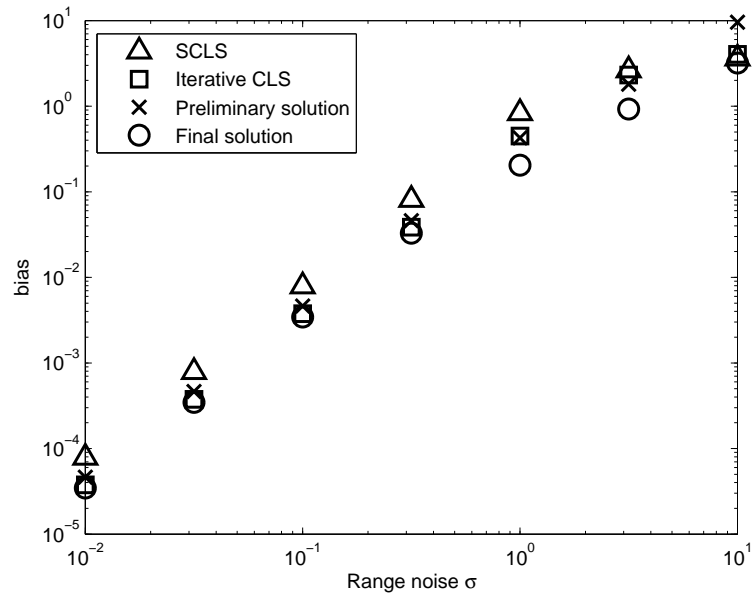


Figure 4.5: Bias for position  $\mathbf{t}$  estimation in the 3D case, averaged over 200 realizations of anchor positions.



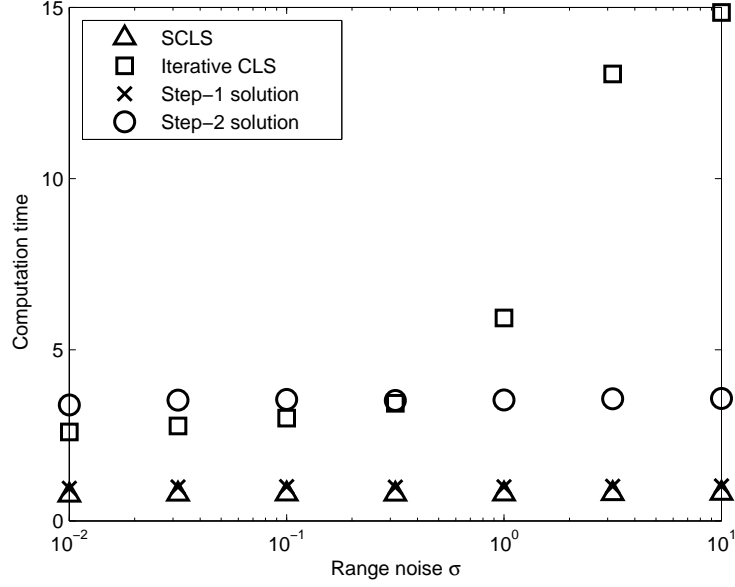


Figure 4.6: Computation time (millisecond) in each Monte-Carlo run in the 3D case, averaged over 200 realizations of anchor positions.

## 2D Case

We next examine the proposed algorithm in Section 4.3, which is for the special situation where the localization is in 2D. The sensor geometry is a square given by

$$\mathbf{C} = 5 \begin{bmatrix} 0 & 1 & 1 & 0 \\ 0 & 0 & 1 & 1 \end{bmatrix}$$

in the local reference frame  $\mathcal{B}$ . The rigid body has orientation  $\theta = 20$  deg and translation  $\mathbf{t} = [100 \ 100]^T$  with respect to  $\mathcal{I}$ .

Fig. 4.7 gives the RMSE for the orientation angle  $\theta$  and Fig. 4.8 for the translation  $\mathbf{t}$ . The behaviors of the different methods are similar for both parameters. The proposed step-1 solution provides 1.8 dB RMSE improvement in  $\theta$  and 1.2 dB in  $\mathbf{t}$

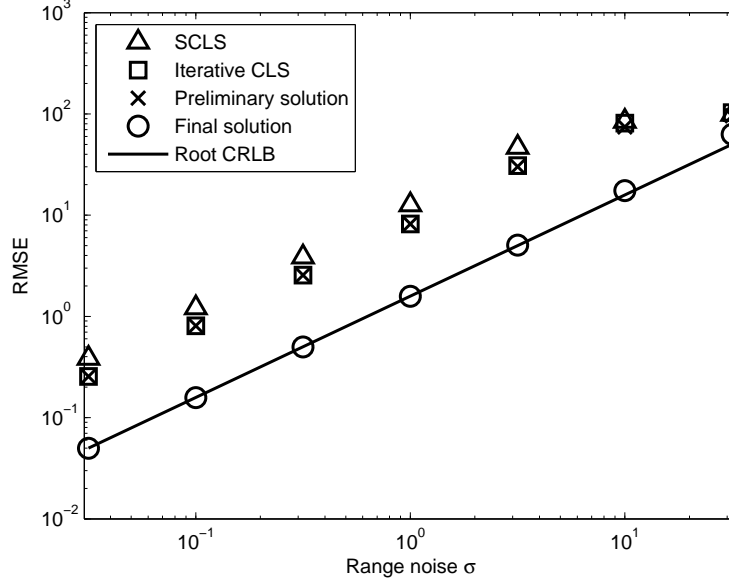


Figure 4.7: Performance for orientation  $\theta$  (deg) estimation in the 2D case, averaged over 200 realizations of anchor positions.

over the SCLS solution. The CLS method can only give comparable performance with the step-1 solution. The step-2 solution has 7.1 dB and 2.6 dB improvements for  $\theta$  and  $\mathbf{t}$  compared to the CLS solution, and it approaches the CRLB performance until the noise deviation  $\sigma$  is larger than 10.

The estimation bias results are shown in Figs. 4.9–4.10. It appears the method with less RMSE also has less bias. The proposed step-2 solution outperforms the others.

Fig. 4.11 illustrates the computation times for the estimation methods. The step-1 preliminary solution has similar computation time as SCLS. Unlike the method in Section 4.3, the step-2 final solution only takes slightly larger complexity. The complexity of the proposed solutions is relatively stable irrespective of the noise deviations. This is not the case for the iterative CLS method due to its iterative nature.

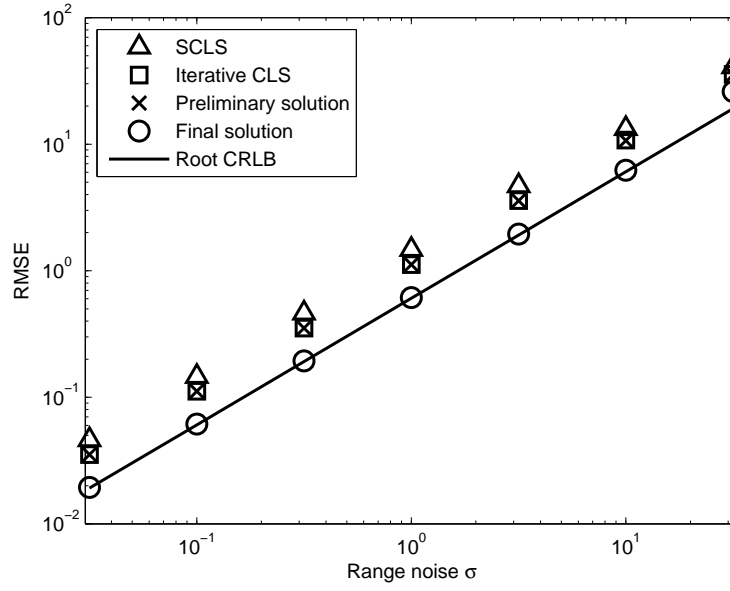


Figure 4.8: Performance for position  $\mathbf{t}$  estimation in the 2D case, averaged over 200 realizations of anchor positions.

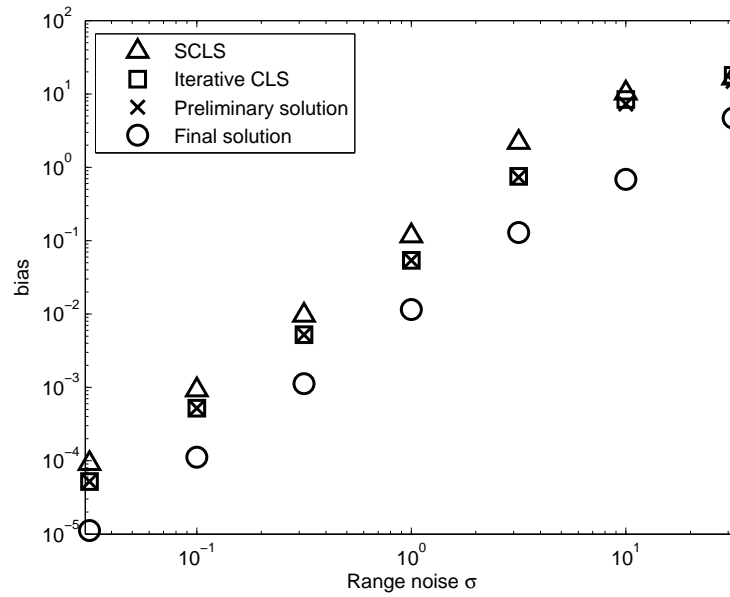


Figure 4.9: Bias for orientation  $\theta$  (deg) estimation in the 2D case, averaged over 200 realizations of anchor positions.

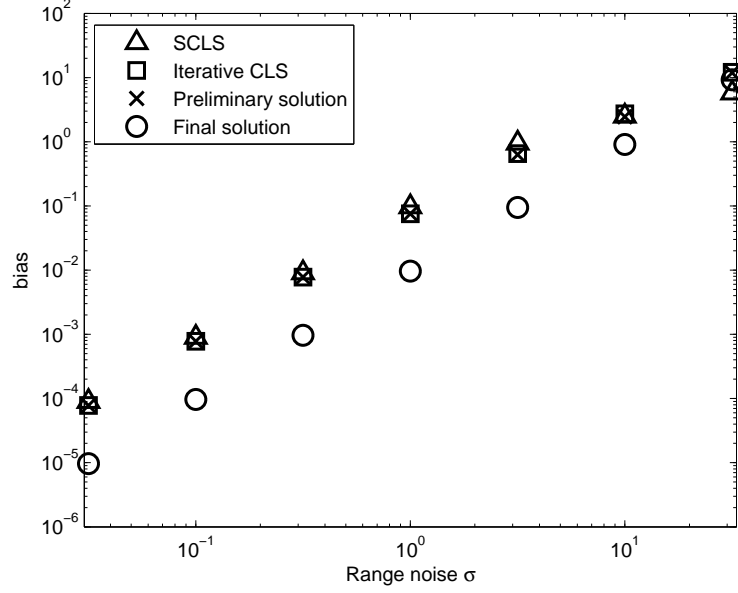


Figure 4.10: Bias for position  $\mathbf{t}$  estimation in the 2D case, averaged over 200 realizations of anchor positions.

The complexity of CLS is about double of the proposed solutions and this ratio rises to more than 5 times at noise deviation  $\sigma = 10$ .

#### 4.6.2 Moving Rigid Body

We use the same geometry settings as in the 3D stationary rigid body localization. The angular velocity is  $\boldsymbol{\omega} = [0.1, 0.2, 0.3]^T$  rad/s and translational velocity is  $\dot{\mathbf{t}} = [1, 1, 1]^T$ . The Doppler measurement noise is uncorrelated with the distance measurement noise and its covariance is  $\mathbf{Q}_{\dot{\mathbf{n}}} = 0.1\mathbf{Q}_{\mathbf{n}} = 0.1\sigma^2\mathbf{I}$ .

The results are generated using the algorithm given in Section 4.4. The initial solution  $(\hat{\mathbf{R}}, \hat{\mathbf{t}})$  needed in step-1 is obtained using both the distance and Doppler measurements. In particular, we apply the method in Appendix B.4 to obtain the

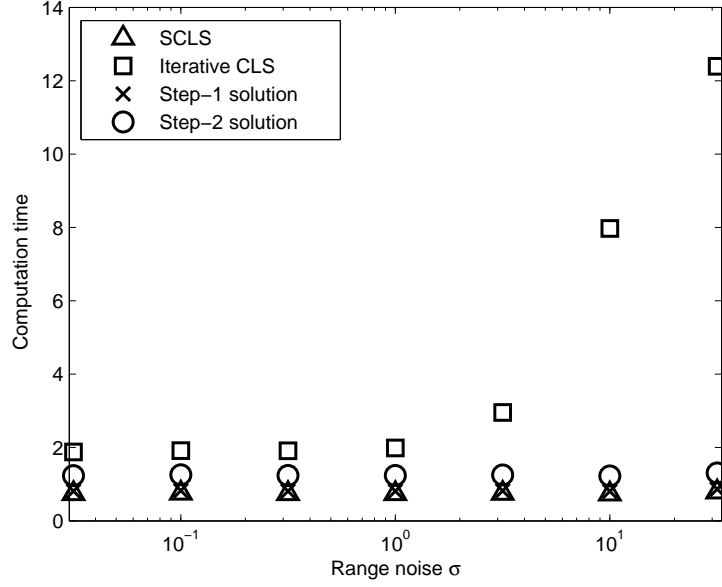


Figure 4.11: Computation time (millisecond) in each Monte-Carlo run in the 2D case, averaged over 200 realizations of anchor positions.

sensor position estimates and then (4.8) and (4.10) to form  $(\hat{\mathbf{R}}, \hat{\mathbf{t}})$ .

Figs. 4.12–4.15 illustrate the estimation performance of RMSE and bias for  $\mathbf{R}$ ,  $\mathbf{t}$ ,  $\boldsymbol{\omega}$  and  $\dot{\mathbf{t}}$ . The step-1 solutions are far from the CRLBs, especially for  $\mathbf{R}$ . The proposed step-2 solutions are able to reach the optimum performance before the noise deviation  $\sigma$  is larger than 0.1. The bias is relatively small compared to RMSE when the noise level is small.

For the 2D case, the step-2 refinement solution also provides performance close to the CRLB over the small noise region.

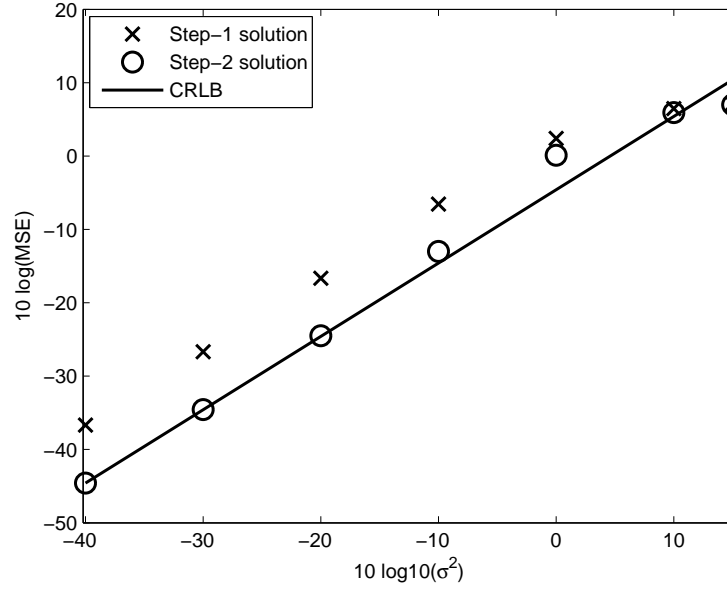


Figure 4.12: RMSE and bias performance of the rotation matrix  $\mathbf{R}$  estimation for a moving rigid body in the 3D case, averaged over 200 realizations of anchor positions.

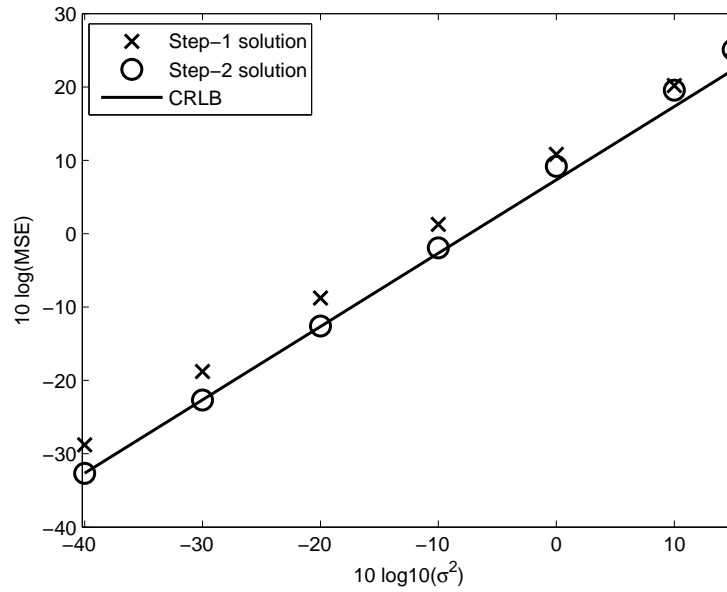


Figure 4.13: RMSE and bias performance of the position  $\mathbf{t}$  estimation for a moving rigid body in the 3D case, averaged over 200 realizations of anchor positions.

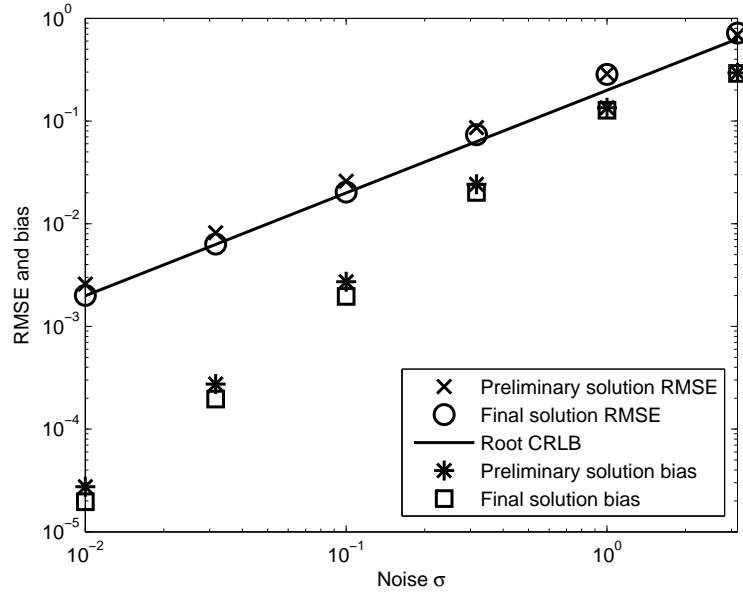


Figure 4.14: RMSE and bias performance of angular velocity  $\omega$  estimation for a moving rigid body in the 3D case, averaged over 200 realizations of anchor positions.

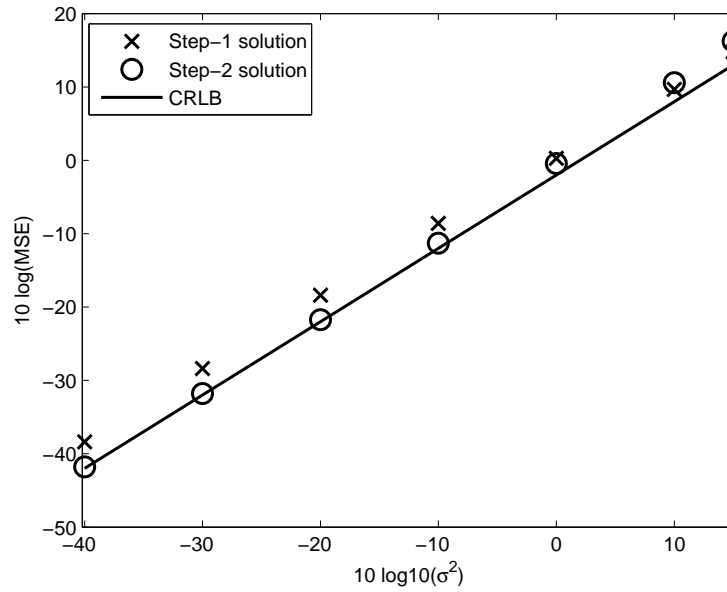


Figure 4.15: RMSE and bias performance of translational velocity  $\dot{\mathbf{t}}$  estimation for a moving rigid body in the 3D case, averaged over 200 realizations of anchor positions.

## 4.7 Alternative Method for Moving Rigid Body in 2D Case

For moving rigid body, the solution from Section 4.4 uses sequential estimation and refinement technique and is computationally demanding when the number of sensors is large. In this section, we try to directly obtain all the unknowns through estimated sensor positions and velocities for special 2D case.

### 4.7.1 New Method

Obtaining the unknown parameters directly from the measurements by putting (4.2) and (4.4) into (4.3) and (4.5) is difficult due to the highly nonlinear relationships and the coupling of the unknowns. We shall resort to the DAC approach by first obtaining  $(\mathbf{s}_i, \dot{\mathbf{s}}_i)$  from the measurements and next estimating the unknowns using them. Here we focus on the latter step here.

#### Utilizing Initial Estimate

Let  $(\hat{\mathbf{s}}_i, \hat{\dot{\mathbf{s}}}_i)$  be the solution from the first step with  $(\mathbf{n}_{\mathbf{s}_i}, \mathbf{n}_{\dot{\mathbf{s}}_i})$  the estimation noise. From (4.2) we have [70]

$$\hat{\mathbf{s}}_i = \mathbf{R}\mathbf{c}_i + \mathbf{t} + \mathbf{n}_{\mathbf{s}_i} = (\mathbf{c}_i^T \otimes \mathbf{I})\mathbf{\Gamma} \begin{bmatrix} \cos \theta \\ \sin \theta \end{bmatrix} + \mathbf{t} + \mathbf{n}_{\mathbf{s}_i} \quad (4.50)$$



Similarly, from (4.4)

$$\hat{\mathbf{s}}_i = [\omega]^\times \mathbf{R} \mathbf{c}_i + \dot{\mathbf{t}} + \mathbf{n}_{\hat{\mathbf{s}}_i} = (\mathbf{c}_i^T \otimes \begin{bmatrix} 0 & -1 \\ 1 & 0 \end{bmatrix}) \mathbf{\Gamma} \begin{bmatrix} \omega \cos \theta \\ \omega \sin \theta \end{bmatrix} + \dot{\mathbf{t}} + \mathbf{n}_{\hat{\mathbf{s}}_i}. \quad (4.51)$$

Stacking (4.50) and (4.51) over  $i$  from 1 to  $N$  yields

$$\mathbf{d} = \mathbf{E}_1 \begin{bmatrix} \cos \theta \\ \sin \theta \\ \omega \cos \theta \\ \omega \sin \theta \end{bmatrix} + \mathbf{E}_2 \begin{bmatrix} \mathbf{t} \\ \dot{\mathbf{t}} \end{bmatrix} + \mathbf{n}_s \quad (4.52)$$

where

$$\mathbf{E}_1 = \begin{bmatrix} (\mathbf{c}_1^T \otimes \mathbf{I}) \mathbf{\Gamma} & \mathbf{O} \\ \mathbf{O} & (\mathbf{c}_1^T \otimes \begin{bmatrix} 0 & -1 \\ 1 & 0 \end{bmatrix}) \mathbf{\Gamma} \\ \vdots & \vdots \\ (\mathbf{c}_N^T \otimes \mathbf{I}) \mathbf{\Gamma} & \mathbf{O} \\ \mathbf{O} & (\mathbf{c}_N^T \otimes \begin{bmatrix} 0 & -1 \\ 1 & 0 \end{bmatrix}) \mathbf{\Gamma} \end{bmatrix}, \mathbf{E}_2 = \mathbf{1} \otimes \mathbf{I} \quad (4.53)$$

and in  $\mathbf{E}_2$  the sizes of  $\mathbf{1}$  and  $\mathbf{I}$  are  $N$  and 4 respectively.  $\mathbf{n}_s$  is resulted from the estimation error of the first step and it can well be approximated as zero-mean Gaussian noise over the small error region. The covariance matrix is denoted by  $\mathbf{Q}_{\mathbf{n}_s}$ , which is block diagonal with individual block for each sensor since the measurements from different sensors are independent.

Although  $\theta$  and  $\omega$  are unconstrained, they are embedded in  $\cos \theta, \sin \theta, \omega \cos \theta$  and

$\omega \sin \theta$ . We propose to solve  $\mathbf{x} = [\cos \theta, \sin \theta, \omega \cos \theta, \omega \sin \theta]^T$  instead by imposing two quadratic constraints

$$x_1^2 + x_2^2 = 1 \quad (4.54)$$

$$x_1 x_4 = x_2 x_3. \quad (4.55)$$

It can be shown that the weighted linear least squares [20] solution to (4.52) with the two quadratic constraints will yield the optimum accuracy as solving  $(\theta, \omega)$  directly from (4.52). This constrained optimization problem remains challenging to solve. We shall propose a computationally attractive closed-form solution to the problem.

### Closed-form Solution

There are two sets of variables to be solved,  $\mathbf{x}$  and  $[\mathbf{t}^T, \dot{\mathbf{t}}^T]^T$ , both appear linear in (4.52) with constraints on the former only. In term of  $\mathbf{x}$ , the weighted least squares (WLS) solution for  $[\mathbf{t}^T, \dot{\mathbf{t}}^T]^T$  with weighting  $\mathbf{Q}_{\mathbf{n}_s}^{-1}$  is [20]

$$\begin{bmatrix} \hat{\mathbf{t}} \\ \hat{\dot{\mathbf{t}}} \end{bmatrix} = (\mathbf{E}_2^T \mathbf{Q}_{\mathbf{n}_s}^{-1} \mathbf{E}_2)^{-1} \mathbf{E}_2^T \mathbf{Q}_{\mathbf{n}_s}^{-1} (\mathbf{d} - \mathbf{E}_1 \mathbf{x}). \quad (4.56)$$

Putting it into (4.52) results in a linear equation with unknown  $\mathbf{x}$  only,

$$\mathbf{h}_1 = \mathbf{G}_1 \mathbf{x} + \mathbf{n}_s \quad (4.57)$$

where  $\mathbf{P} = \mathbf{I} - \mathbf{E}_2 (\mathbf{E}_2^T \mathbf{Q}_{\mathbf{n}_s}^{-1} \mathbf{E}_2)^{-1} \mathbf{E}_2^T \mathbf{Q}_{\mathbf{n}_s}^{-1}$ ,  $\mathbf{h}_1 = \mathbf{P} \mathbf{d}$  and  $\mathbf{G}_1 = \mathbf{P} \mathbf{E}_1$ .

We shall use the two-stage approach to solve for  $\mathbf{x}$  from (4.57) under constraints

(4.54) and (4.55). The first stage ignores the constraints to obtain  $\mathbf{x}$ . The second stage utilizes the constraints to construct another minimization process to improve the estimate. Once it is found,  $[\mathbf{t}^T, \dot{\mathbf{t}}^T]^T$  is immediately available from (4.56).

1) Stage-1

We omit the constraints and the resulting unconstrained WLS solution is

$$\hat{\mathbf{x}} = (\mathbf{G}_1^T \mathbf{W}_1 \mathbf{G}_1)^{-1} \mathbf{G}_1^T \mathbf{W}_1 \mathbf{h}_1 \quad (4.58)$$

where  $\mathbf{W}_1 = \mathbf{Q}_{\mathbf{n}_s}^{-1}$ . Let us denote the estimation error as  $\Delta \mathbf{x}$ . The covariance matrix of the estimate is  $\text{cov}(\hat{\mathbf{x}}) = (\mathbf{G}_1^T \mathbf{W}_1 \mathbf{G}_1)^{-1}$ .

2) Stage-2

We shall correct the stage-1 solution by taking the two constraints into account. Different from the traditional two-stage method for TDOA or TOA positioning that involves the quadratic constraint from squared variables [2, 39, 71], we will need to consider the cross-variable constraint (4.55).

It is more convenient to express these two constraints into different forms. Multiplying both sides of (4.55) by  $x_2$  and substituting (4.54) for  $x_2^2$  give

$$x_3 = (x_1 x_3 + x_2 x_4) x_1. \quad (4.59)$$

Similarly, multiplying both sides of (4.55) by  $x_1$  and using (4.54) yield

$$x_4 = (x_1 x_3 + x_2 x_4) x_2. \quad (4.60)$$

We shall choose the parameter vector as  $\boldsymbol{\zeta} = [\omega \cos \theta, \omega \sin \theta]^T$ . The two elements

have straightforward mapping with the two unknowns  $\theta$  and  $\omega$ , and they are simply the last two elements of  $\mathbf{x}$ , i.e.  $\boldsymbol{\zeta} = [x_3, x_4]^T$ .

To utilize the constraint (4.59), we express the right side in terms of the elements of  $\hat{\mathbf{x}}$  and obtain, after ignoring the second and third order errors,

$$\begin{aligned} x_3 = & (\hat{x}_1\hat{x}_3 + \hat{x}_2\hat{x}_4)\hat{x}_1 - (2\hat{x}_1\hat{x}_3 + \hat{x}_2\hat{x}_4)\Delta x_1 \\ & - \hat{x}_1\hat{x}_4\Delta x_2 - \hat{x}_1^2\Delta x_3 - \hat{x}_1\hat{x}_2\Delta x_4. \end{aligned} \quad (4.61)$$

Applying the same process gives the corresponding expression for (4.60).

We can now construct the matrix equation for stage-2 as

$$\mathbf{B}_2\Delta\mathbf{x} = \mathbf{h}_2 - \mathbf{G}_2\boldsymbol{\zeta} \quad (4.62)$$

where

$$\begin{aligned} \mathbf{B}_2 = & \begin{bmatrix} 0 & 0 & 1 & 0 \\ 2\hat{x}_1\hat{x}_3 + \hat{x}_2\hat{x}_4 & \hat{x}_1\hat{x}_4 & \hat{x}_1^2 & \hat{x}_1\hat{x}_2 \\ 0 & 0 & 0 & 1 \\ \hat{x}_2\hat{x}_3 & 2\hat{x}_2\hat{x}_4 + \hat{x}_1\hat{x}_3 & \hat{x}_1\hat{x}_2 & \hat{x}_2^2 \end{bmatrix}, \\ \mathbf{h}_2 = & \begin{bmatrix} \hat{x}_3 \\ (\hat{x}_1\hat{x}_3 + \hat{x}_2\hat{x}_4)\hat{x}_1 \\ \hat{x}_4 \\ (\hat{x}_1\hat{x}_3 + \hat{x}_2\hat{x}_4)\hat{x}_2 \end{bmatrix}, \quad \mathbf{G}_2 = \begin{bmatrix} 1 & 0 \\ 1 & 0 \\ 0 & 1 \\ 0 & 1 \end{bmatrix}. \end{aligned} \quad (4.63)$$

The WLS solution for  $\boldsymbol{\zeta}$  is

$$\hat{\boldsymbol{\zeta}} = (\mathbf{G}_2^T \mathbf{W}_2 \mathbf{G}_2)^{-1} \mathbf{G}_2^T \mathbf{W}_2 \mathbf{h}_2 \quad (4.64)$$

where the weighting matrix is from the covariance of  $\hat{\mathbf{x}}$ :

$$\begin{aligned}\mathbf{W}_2 &= [\mathbf{B}_2(\mathbf{G}_1^T \mathbf{W}_1 \mathbf{G}_1)^{-1} \mathbf{B}_2^T]^{-1} \\ &= \mathbf{B}_2^{-T} (\mathbf{G}_1^T \mathbf{W}_1 \mathbf{G}_1) \mathbf{B}_2^{-1}.\end{aligned}\tag{4.65}$$

Finally, we can recover the estimates for  $\theta$  and  $\omega$  by

$$\hat{\omega} = \|\hat{\boldsymbol{\zeta}}\| \text{sgn}(\hat{x}_1 \hat{x}_3 + \hat{x}_2 \hat{x}_4)\tag{4.66}$$

$$\hat{\theta} = \arctan2(\hat{\zeta}_2/\hat{\omega}, \hat{\zeta}_1/\hat{\omega})\tag{4.67}$$

where  $\arctan2$  is the four-quadrant inverse tangent function. Updating  $\mathbf{x}$  and putting it into (4.56) give the estimates for the position  $\mathbf{t}$  and translational velocity  $\dot{\mathbf{t}}$ . The final estimates of the sensor positions and velocities can now be obtained using (4.2) and (4.4).

### 4.7.2 Simulations

There are  $M = 6$  anchors placed uniformly on the circle with  $\mathbf{a}_m = 25[\cos \frac{2\pi}{M}(m - 1), \sin \frac{2\pi}{M}(m - 1)]^T$ . Each sensor is able to acquire the measurements from all anchors. Other setting is the quite similar to that in Section 4.6. The sensor geometry is a square given by

$$\mathbf{C} = 5 \begin{bmatrix} 0 & 1 & 1 & 0 \\ 0 & 0 & 1 & 1 \end{bmatrix}$$

in the local reference frame, where  $\mathbf{C}$  consists of  $\mathbf{c}_i$ 's. The rigid network has orientation  $\theta = 20 \text{ deg}$  and position  $\mathbf{t} = [100 \ 100]^T$  with respect to the global coordinate

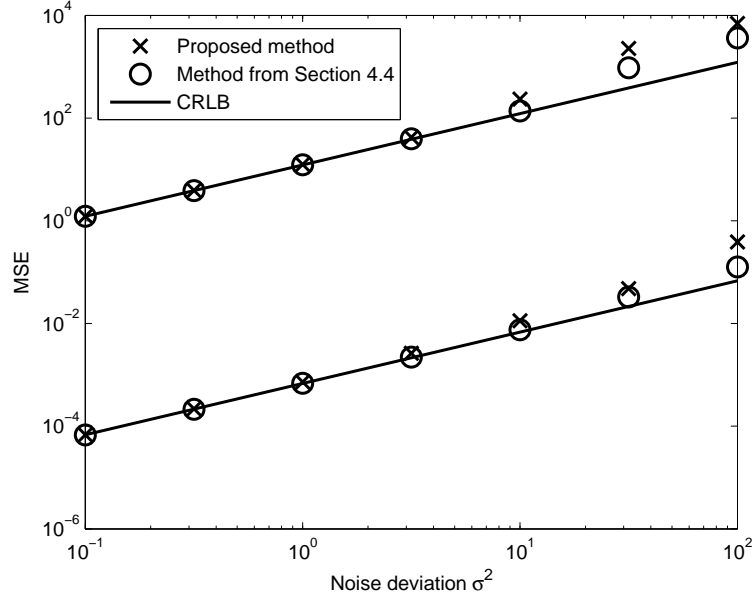


Figure 4.16: Performance for orientation  $\theta$  (deg, upper curves) and angular velocity  $\omega$  (lower curves) estimations.

frame. The angular velocity is  $\omega = 0.3$  rad/s and translational velocity is  $\dot{\mathbf{t}} = [1, 1]^T$ . The covariance matrix of the distance measurement is  $\mathbf{Q}_n = \sigma^2 \mathbf{I}$ . The range rate measurement noise is uncorrelated with the distance measurement noise and its covariance matrix is  $\mathbf{Q}_{\dot{n}} = 0.1 \mathbf{Q}_n$ . The number of ensemble runs is  $L = 2000$ .

### Accuracy Comparison

Fig. 4.16 shows the results of the orientation angle (upper curves) and angular velocity (lower curves) using the proposed method and the previous method from Section 4.4. The proposed method reaches the CRLB performance over small error region as in the previous method, and it deviates from the bound a bit earlier as the noise level increases. We have similar observations for the position and translational velocity estimates as shown in Fig. 4.17.

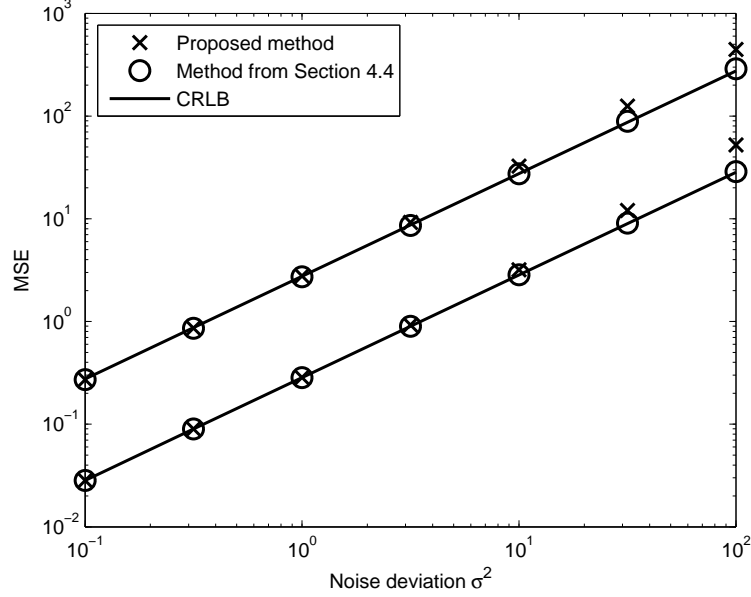


Figure 4.17: Performance for position  $\mathbf{t}$  (upper curves) and translational velocity  $\dot{\mathbf{t}}$  (lower curves) estimations.

Fig. 4.18 illustrates the performance in terms of the sensor position and velocity estimates. When we exploit the known relative sensor locations, the accuracy is much better than without (the initial estimate) in both positions and velocities. We generated the CRLB for comparison using the CRLB of the four parameters through the relationships (4.2) and (4.4) [20]. The proposed algorithm achieves the optimum performance when the noise level is not significant and it is only worse than previous method if the noise level is high.

### Computational Time Comparison

Although the accuracy of the proposed method is not as good as that of Section 4.4 at large noise level, it has the benefit of lower computational complexity. Fig. 4.19 illustrates the computational times (millisecond) of each ensemble run obtained from

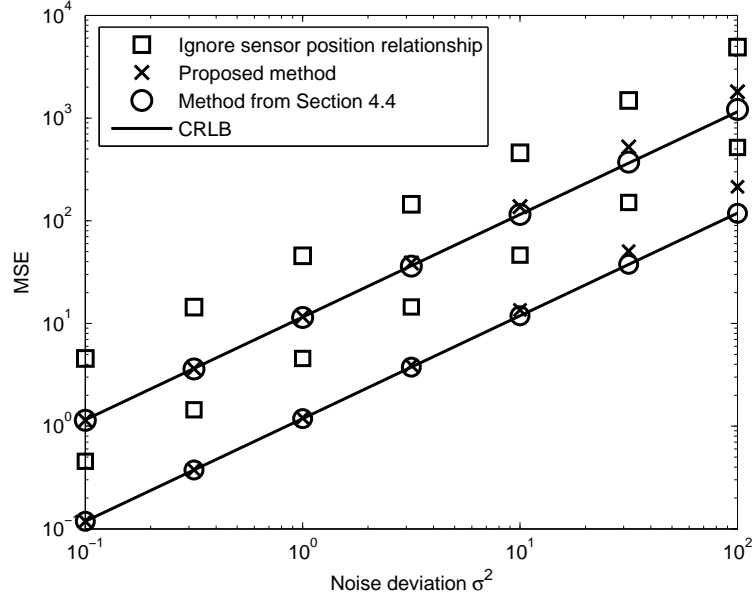


Figure 4.18: Performance for sensor positions (upper curves) and velocities (lower curves) estimations.

MATLAB implementation of two methods, when the number of anchors  $M$  varies from 3 to 18 with a step of 3. The computational advantage of proposed method is obvious when the number of anchors is large. The proposed method is a good alternative when the noise power is not significant.

## 4.8 Conclusion

This chapter develops methods to locate a rigid body using a number of on-board sensors through the distance measurements with respect to a number of anchors if it is stationary, and the Doppler as well if it is moving. The proposed method consists of an initial step and a refinement step. The initial step provides a suboptimum preliminary solution using the DAC approach and the refinement step estimates the



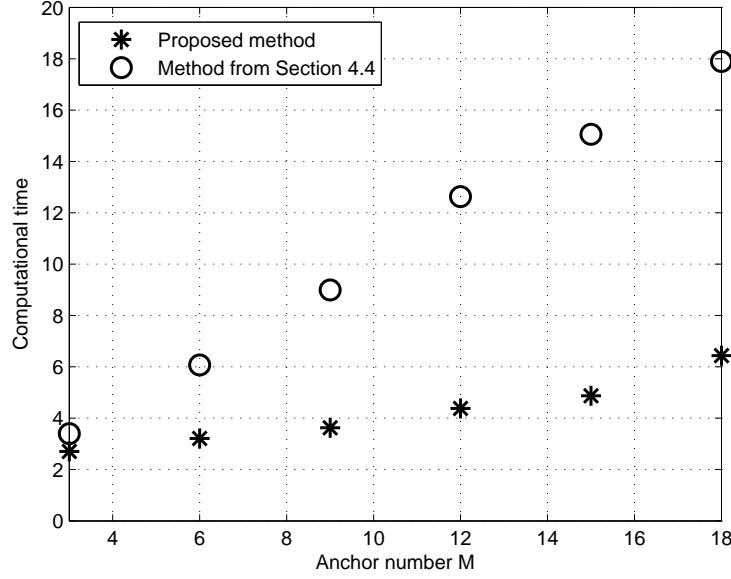


Figure 4.19: Computational times vs anchor number  $M$ .

corrections to the preliminary solution using the Euler angles formulation to achieve better estimation accuracy. Both steps involve only closed-form solution evaluations and are not iterative. We have also shown that the problem can be solved using 2 GTRS optimizations for the special case of 2D localization. For the stationary rigid body localization, we are able to advance the previous works and provide more accurate solutions with comparable complexity.

For the moving rigid body localization, we have developed closed-form solutions for obtaining not only the rotation matrix and translation vector but also the angular and translational velocities. In addition, a new estimator for locating a moving rigid sensor network in 2D is presented. The proposed estimator uses the DAC approach where initial sensor positions and velocities are estimated from the measurements first and the unknowns are obtained next using them by utilizing the relative positions of

the sensors. We have developed a computationally attractive closed-form solution for the second step that involves two quadratic constraints. It requires less computation than the previous solution, with the tradeoff that the performance deviates from the optimum at a lower noise level.

## Chapter 5

# Estimation of Position and Orientation Using AOA Measurements

We continue to study the pose estimation using AOA measurements with respect to landmarks instead of distance measurements discussed in Chapter 4. We solve the 3D scenario that is seldom considered before, and extend the study to the scenario where there is more than one AOA sensor on-board, which either increases the robustness and accuracy or decreases the minimum requirement on number of landmarks.

This chapter is organized as follows. Section 5.1 provides the scenario for pose estimation using AOA measurements. Section 5.2 proposes the method for single sensor case in 3D. Section 5.3 extends the study to multiple sensors on-board and provides solutions for 3D and 2D respectively. Section 5.4 supports the performance of the proposed solutions by simulations. Section 5.5 concludes the chapter.

## 5.1 Scenario

The object would self-determine its position and orientation in the surrounding environment based on the AOA measurements with respect to known landmarks. Viewed in local reference frame  $\mathcal{B}$ , the position of  $m$ -th landmark is

$$\mathbf{a}_m^{\mathcal{B}} = \mathbf{R}\mathbf{a}_m + \mathbf{t} \quad (5.1)$$

where  $\mathbf{R}$  and  $\mathbf{t}$  are the rotation matrix and translation for the coordinate transform between  $\mathcal{B}$  and global frame  $\mathcal{I}$  (notice that the definition of  $\mathbf{R}$  and  $\mathbf{t}$  here is different from that in Chapter 4 for convenience). Then we can model the azimuth angle measurement

$$\theta_{mi} = \text{atan2}(a_{my}^{\mathcal{B}} - c_{iy}, a_{mx}^{\mathcal{B}} - c_{ix}) + n_{\theta_{mi}} \quad (5.2)$$

and, if in 3D, the elevation angle measurement

$$\phi_{mi} = \arcsin\left(\frac{a_{mz}^{\mathcal{B}} - c_{iz}}{r_{mi}^o}\right) + n_{\phi_{mi}} \quad (5.3)$$

where subscripts  $x, y, z$  represent corresponding coordinate component, and  $n_{\theta_{mi}}$  and  $n_{\phi_{mi}}$  are the additive noise.  $\mathbf{n} = [n_{\theta_{11}} \ n_{\phi_{11}} \ \cdots \ n_{\theta_{M1}} \ n_{\phi_{M1}} \ \cdots \ n_{\theta_{1N}} \ n_{\phi_{1N}} \ \cdots \ n_{\theta_{MN}} \ n_{\phi_{MN}}]^T$  is the noise vector that follows zero-mean Gaussian distribution with covariance matrix  $\mathbf{Q}_n$ . And the subscript "i" will be dropped when there is only one sensor on board.

The self-localization aims at determining  $\mathbf{R}$  and  $\mathbf{t}$  using the AOA measurements. Once they are obtained, it is straightforward to obtain the position and orientation observed in  $\mathcal{I}$ :  $\mathbf{R}^T$  and  $-\mathbf{R}^T\mathbf{t}$ . The CRLB for this problem is straightforward to

derive following [53] and Appendix B.1.

To facilitate the algorithm development, we transform (5.2) and (5.3) without noise to obtain the linear equation of  $\mathbf{a}_m^{\mathcal{B}}$  (i.e.  $\mathbf{R}$  and  $\mathbf{t}$ )

$$[\sin \theta_{mi}^o, -\cos \theta_{mi}^o](\mathbf{a}_m^{\mathcal{B}} - \mathbf{c}_i) = 0 \quad (5.4)$$

in 2D and

$$[\sin \theta_{mi}^o, -\cos \theta_{mi}^o, 0](\mathbf{a}_m^{\mathcal{B}} - \mathbf{c}_i) = 0 \quad (5.5a)$$

$$[\sin \phi_{mi}^o \cos \theta_{mi}^o, \sin \phi_{mi}^o \sin \theta_{mi}^o, -\cos \phi_{mi}^o](\mathbf{a}_m^{\mathcal{B}} - \mathbf{c}_i) = 0 \quad (5.5b)$$

in 3D [88]. Notice that when there is only one sensor, even the term  $\mathbf{a}_m^{\mathcal{B}} - \mathbf{c}_i$  above becomes  $-(\mathbf{a}_m^{\mathcal{B}} - \mathbf{c}_i)$ , the equation still holds. In other word, if  $\mathbf{a}_m^{\mathcal{B}}$  is the solution, so is  $2\mathbf{c}_1 - \mathbf{a}_m^{\mathcal{B}}$ . This is because we treat the four-quadrant atan2 function as two-quadrant arctan function to obtain above linear equations, creating the ambiguous reflection of original landmarks across the sensor. Obviously, the ambiguity of  $\mathbf{a}_m^{\mathcal{B}}$  implies the ambiguity of  $(\mathbf{R}, \mathbf{t})$ . We will handle this ambiguity later.

Once initial solutions  $(\hat{\mathbf{R}}, \hat{\mathbf{t}})$  are obtained, we can perform the corrections for them using the weighted least squares (WLS) based on (5.4), or (5.5a) and (5.5b) and achieve CRLB performance.

## 5.2 Single Sensor in 3D

According to Section 4.2, we can obtain the anchor position  $\mathbf{a}_m^{\mathcal{B}}$  in  $\mathcal{B}$ , and then compare it with  $\mathbf{a}_m$  in  $\mathcal{I}$  to obtain the position and orientation of object. However,

directly solving  $\mathbf{a}_m^{\mathcal{B}}$  from (5.5a) and (5.5b) is very difficult due to the presence of two solutions. For example, we can perform the minimization

$$\begin{aligned}
\min \sum_m & \quad |[\sin \theta_m, -\cos \theta_m, 0](\mathbf{a}_m^{\mathcal{B}} - \mathbf{c}_1)| \\
& \quad + |[\sin \phi_m \cos \theta_m, \sin \phi_m \sin \theta_m, -\cos \phi_m](\mathbf{a}_m^{\mathcal{B}} - \mathbf{c}_1)| \\
\text{s.t.} \quad & \quad \|\mathbf{a}_i^{\mathcal{B}} - \mathbf{a}_j^{\mathcal{B}}\|^2 = \|\mathbf{a}_i - \mathbf{a}_j\|^2,
\end{aligned} \tag{5.6}$$

and use semidefinite relaxation technique to handle the quadratic distance constraint [57]. But convex optimization toolbox CVX using default setting always returns the solution close to  $\mathbf{c}_1$  that is the analytic center of two optimal solutions  $\mathbf{a}_m^{\mathcal{B}}$  and  $2\mathbf{c}_1 - \mathbf{a}_m^{\mathcal{B}}$ . And similar problem still happens if we add the constraint on the sign of  $a_{my}^{\mathcal{B}} - c_{1y}$  according to the measurement  $\theta_{mi}$ . Furthermore, even we can obtain two optimal solutions simultaneously, we still need to pick up the better solution according to the original AOA measurements, e.g. through the residual comparison.

Alternatively, we propose to obtain the anchor position  $\mathbf{a}_m^{\mathcal{B}}$  in indirect way. The idea is to obtain the distance  $r_m$  between the sensor and the  $m$ -th anchor and then combine it with the measured unit vector  $\boldsymbol{\rho}_m = [\cos \phi_m \cos \theta_m, \cos \phi_m \sin \theta_m, \sin \phi_m]^T$  pointing from the sensor to the  $m$ -th anchor, then  $\hat{\mathbf{a}}_m^{\mathcal{B}} = r_m \boldsymbol{\rho}_m + \mathbf{c}_1$ .

To solve  $r_m$ , we can exploit the relationship between  $r_m$ 's utilizing the law of cosine for the triangle consisting of  $i$ -th anchor,  $j$ -th anchor and sensor

$$r_i^{o2} + r_j^{o2} - 2r_i^o r_j^o \cos \alpha_{ij}^o = d_{ij}^2 \tag{5.7}$$

where  $\cos \alpha_{ij}^o = \boldsymbol{\rho}_i^{oT} \boldsymbol{\rho}_j^o / \|\boldsymbol{\rho}_i^o\| \|\boldsymbol{\rho}_j^o\| = \boldsymbol{\rho}_i^{oT} \boldsymbol{\rho}_j^o$  and  $d_{ij} = \|\mathbf{a}_i^{\mathcal{B}} - \mathbf{a}_j^{\mathcal{B}}\| = \|\mathbf{a}_i - \mathbf{a}_j\|$ . Denote

$(i, j)$  the pair of anchors used in this triangle. Since utilizing all  $\binom{M}{2}$  triangles causes redundancy, we only use part of the pairs. We first choose four anchors that are not coplanar, and therefore have  $\binom{4}{2} = 6$  related triangles; each remaining anchor can form 4 triangles with previously chosen four anchors. So in total, we only use  $6 + 4(M - 4) = 4M - 10$  triangles. Denote the set of all the anchor pairs chosen as  $\mathcal{N}$ .

Therefore, we propose the following minimization problem

$$\begin{aligned} \min_{r'_i s} \quad & \sum_{(i,j) \in \mathcal{N}} |r_i^2 + r_j^2 - 2r_i r_j \cos \alpha_{ij} - d_{ij}^2| \\ \text{s.t. } & r_i > 0, r_i + r_j > d_{ij}, -d_{ij} < r_i - r_j < d_{ij}, \end{aligned} \quad (5.8)$$

where we utilize triangle inequality. By denoting  $\mathbf{r} = [r_1 r_2 \cdots r_M]^T$  and expressing quadratic term of  $r_i$  by element of  $\mathbf{X} = \mathbf{r}\mathbf{r}^T$ , this optimization can be solved through relaxing  $\mathbf{X} = \mathbf{r}\mathbf{r}^T$  to convex constraint  $\mathbf{X} \succeq \mathbf{r}\mathbf{r}^T$  [57]. Then we can construct anchor position  $\hat{\mathbf{a}}_n^{\mathcal{B}}$  and finally obtain the position and orientation of object.

### 5.3 Multiple Sensors

When there is only one sensor, some landmarks may be unobservable due to blockage, while more sensors mean more opportunities to observe enough landmarks. In addition, putting more sensors also relaxes the minimum requirement on the number of landmarks: specifically, in 3D case it requires at least 4 landmarks under one sensor but at least 3 landmarks under multiple sensors; in 2D case it requires at least 3 landmarks under one sensor but at least 2 landmarks under multiple sensors.

Without loss of generality, we assume all the sensors have the same orientation; otherwise, if the relative orientation between sensors is known *a priori*, our method can be easily modified. In addition, we consider very general scenario and do not require: every sensor can observe more than one landmark or obtain both azimuth angle and elevation angle, or every landmark can be observed by more than two sensors.

### 5.3.1 3D Case

Unlike single sensor case, directly solving anchor position  $\mathbf{a}_m^{\mathcal{B}}$  by the optimization similar to (5.6) using semidefinite relaxation is feasible, however, the resultant number of unknowns is  $3M + M(M + 1)/2 = O(M^2)$ . The method with constant number of unknowns is much more preferred, which can be achieved by directly solving  $\mathbf{R}$  and  $\mathbf{t}$ .

Proper parameterization of  $\mathbf{R}$  is needed. Due to the complexity in solving the optimization problem, we prefer the order for  $\mathbf{R}$  representation or the constraint is not more than 2 in terms of parameterization variables, i.e., either in linear or quadratic form. After excluding the parameterizations by Euler angle, axis-angle representation, Gibbs vector (also called Rodrigues parameters) or modified Rodrigues parameters (MRP), we choose unit quaternion representation [62]. The unit quaternion uses unit vector  $\mathbf{q} = [q_0 \ q_1 \ q_2 \ q_3]^T = [q_0 \ \mathbf{q}_v^T]^T$  to represent the rotation matrix

$$\mathbf{R} = (q_0^2 - \|\mathbf{q}_v\|^2)\mathbf{I} + 2\mathbf{q}_v\mathbf{q}_v^T + 2q_0[\mathbf{q}_v]^\times \quad (5.9)$$

where  $[\mathbf{q}_v]^\times$  is a skew-symmetric matrix formed by  $\mathbf{q}_v$ . Obviously,  $\mathbf{R}$  is quadratic in



$\mathbf{q}$  and unit vector constraint  $\|\mathbf{q}\|^2 = 1$  is also quadratic.

**Remark:**  $\mathbf{q}$  and  $-\mathbf{q}$  result in the same rotation matrix  $\mathbf{R}$ , but we can set  $0 \leq q_0$  to avoid the ambiguity.

Denote  $\mathbf{Y} = \mathbf{q}\mathbf{q}^T$ ,  $\mathbf{R}$  can be expressed linearly by the element of  $\mathbf{Y}$  (denote  $\mathbf{R} = \mathbf{f}(\mathbf{Y})$ ), and  $\|\mathbf{q}\|^2 = 1$  becomes  $\text{tr}(\mathbf{Y}) = 1$ . Based on (5.5a) and (5.5b), we solve following convex optimization

$$\begin{aligned} \min_{\mathbf{q}, \mathbf{Y}, \mathbf{t}} \sum_{m,i} & |[\sin \theta_{mi}, -\cos \theta_{mi}, 0](\mathbf{f}(\mathbf{Y})\mathbf{a}_m + \mathbf{t} - \mathbf{c}_i)| \\ & + |[\sin \phi_{mi} \cos \theta_{mi}, \sin \phi_{mi} \sin \theta_{mi}, -\cos \phi_{mi}](\mathbf{f}(\mathbf{Y})\mathbf{a}_m + \mathbf{t} - \mathbf{c}_i)| \\ \text{s.t. } & 0 \leq q_0 \leq 1, -1 \leq q_1, q_2, q_3 \leq 1, \mathbf{Y} \succeq \mathbf{q}\mathbf{q}^T, \text{tr}(\mathbf{Y}) = 1. \end{aligned} \quad (5.10)$$

**Remark:** Since  $\mathbf{R}$  does not contain any linear term of  $\mathbf{q}$ , putting  $\mathbf{q}$  into optimization can not improve the accuracy. Alternatively, we can handle the optimization without  $\mathbf{q}$  under  $\mathbf{Y} \succeq \mathbf{O}$ . And for  $i \neq j$ ,  $|q_i q_j| \leq \frac{1}{2}(q_i^2 + q_j^2) \leq \frac{1}{2}\|\mathbf{q}\|^2 = \frac{1}{2}$ , we have  $-\frac{1}{2} \leq Y_{i,j} \leq \frac{1}{2}$ .

Once we obtain the estimation of  $\mathbf{Y}$ ,  $\hat{\mathbf{R}}$  can be easily constructed by (5.9). Notice due to omission of nonconvex constraint  $\text{rank } \mathbf{Y} = 1$ ,  $\hat{\mathbf{R}}$  from  $\mathbf{Y}$  may not exactly satisfy the rotation matrix requirement. Therefore we can choose the nearest rotation matrix to  $\hat{\mathbf{R}}$  by

$$\min_{\mathbf{R} \in SO(3)} \|\mathbf{R} - \hat{\mathbf{R}}\|_F^2 \quad (5.11)$$

which can be solved by orthogonal Procrustes problem technique in closed-form [73]: let the SVD of  $\hat{\mathbf{R}}$  be  $\mathbf{U}\Sigma\mathbf{V}^T$ , the optimal solution is  $\mathbf{U}\text{diag}([1, 1, \det(\mathbf{U}\mathbf{V}^T)]^T)\mathbf{V}^T$ .

### 5.3.2 2D Case

Using orientation  $\theta$  to parameterize rotation matrix and vectorizing it as in (4.24), (5.4) becomes

$$[\sin \theta_{mi}^o, -\cos \theta_{mi}^o][(\mathbf{a}_m^T \otimes \mathbf{I})\Gamma \mathbf{y} + \mathbf{t} - \mathbf{c}_i] = 0. \quad (5.12)$$

Stacking above equation but with noisy measurement  $\theta_{mi}$  results in

$$\mathbf{d} = \mathbf{E}_1 \mathbf{y} + \mathbf{E}_2 \mathbf{t} + \text{residual}. \quad (5.13)$$

The following constrained least squares

$$\begin{aligned} \min_{\mathbf{y}, \mathbf{t}} \quad & \|\mathbf{W}^{-\frac{1}{2}}(\mathbf{E}_1 \mathbf{y} + \mathbf{E}_2 \mathbf{t} - \mathbf{d})\|^2 \\ \text{s.t.} \quad & \|\mathbf{y}\|^2 = 1, \end{aligned} \quad (5.14)$$

where  $\mathbf{W}$  is the covariance matrix of the residual in (5.13), belongs to quadratic optimization problem with a quadratic equality constraint, and therefore can be solved by GTRS [17, 18] efficiently to obtain the global minimum solution. Since  $\mathbf{W}$  depends on unknown  $\mathbf{y}$  and  $\mathbf{t}$ , we can first perform the minimization without weighting, and then construct  $\mathbf{W}$  utilizing the obtained  $\mathbf{y}$  and  $\mathbf{t}$ , and finally perform again the minimization with the weighting.

## 5.4 Simulations

We shall evaluate the performance of the proposed solutions.  $M$  landmarks are placed uniformly on the same plane as  $\mathbf{a}_m = 100[\cos \frac{m-1}{M}2\pi, \sin \frac{m-1}{M}2\pi, 0]^T$ . To facilitate the

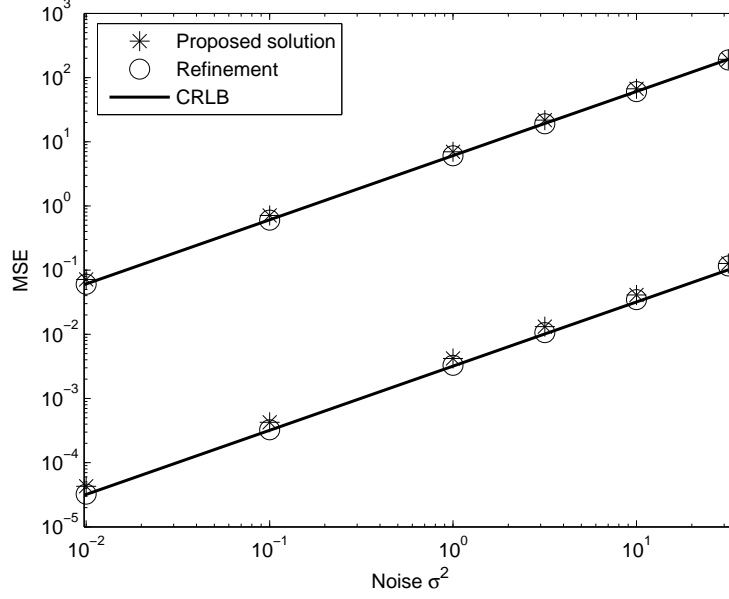


Figure 5.1: 3D single sensor case, performance for position (upper curves) and orientation (lower curves) estimations.

demonstration, we set the same orientation for  $\mathcal{B}$  and  $\mathcal{I}$ . The translation and sensor positions will be specified later. The number of ensemble runs is  $L = 1000$ . The AOA measurement noise is Gaussian i.i.d. with power  $\sigma^2$  ( $\text{deg}^2$ ). The definition of MSE is the same as in Chapter 4 Simulations.

#### 5.4.1 3D Single Sensor

We choose  $M = 4$  anchors forming a square, the sensor is at the origin of  $\mathcal{B}$  and the translation  $\mathbf{t} = [0, 0, -100]^T$ . Fig. 5.1 shows the result for estimating position  $\mathbf{t}$  (upper curves) and orientation  $\mathbf{R}$  (lower curves). The proposed solution has less than 1.5 dB deviation from the CRLB and the further refinement achieves the CRLB performance.

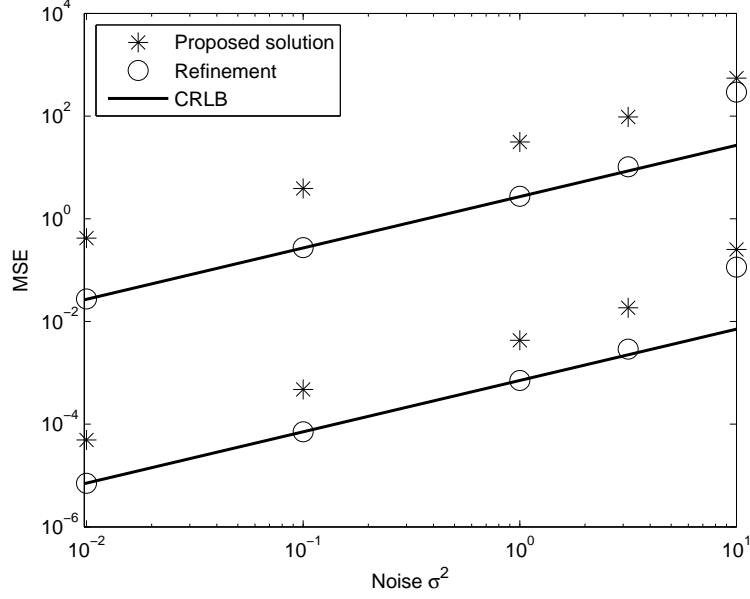


Figure 5.2: 3D multiple sensors case, performance for position (upper curves) and orientation (lower curves) estimations.

## 5.4.2 Multiple Sensors

### 3D Case

We choose  $M = 3$  anchors forming an equilateral triangle, two sensors are at the origin and  $[0, 0, 20]^T$  in  $\mathcal{B}$ , and the translation is  $\mathbf{t} = [0, 0, -30]^T$ .

In Fig. 5.2, the proposed solution has significant deviation from the CRLB, but the refinement gives CRLB performance over small error region. Maybe the semidefinite relaxation  $\mathbf{Y} \succeq \mathbf{q}\mathbf{q}^T$  is not tight enough here and some technique taking into account  $\text{rank } \mathbf{Y} = 1$  is needed for better performance.

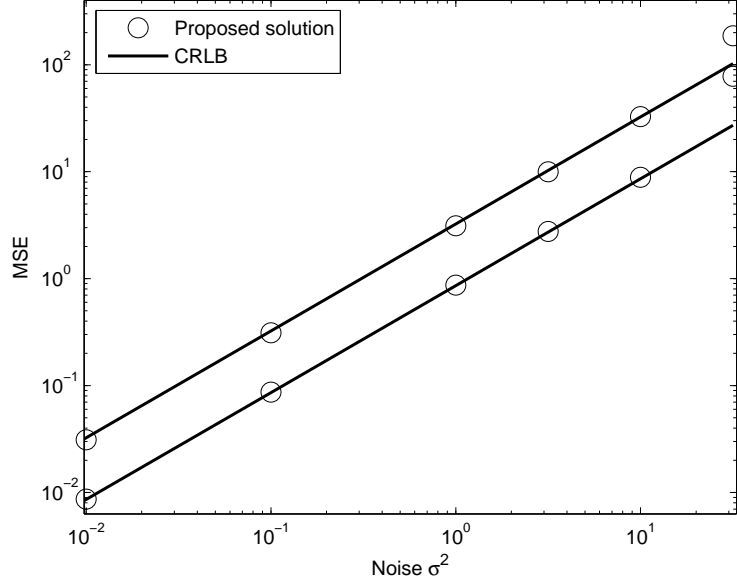


Figure 5.3: 2D multiple sensors case, performance for position (upper curves) and orientation (lower curves, in deg) estimations.

## 2D Case

We choose  $M = 2$  anchors, two sensors are at the origin and  $[0, 20]^T$  in  $\mathcal{B}$  and the translation  $\mathbf{t} = [0, -50]^T$ . As shown in Fig. 5.3, the proposed closed-form solution achieves the CRLB performance over small error region, which confirms its advantages in accuracy and computation.

## 5.5 Conclusion

Based on AOA measurements with respect to landmarks, a general scenario for object self-localization was considered, where the localization can be in 3D or 2D, and the number of sensors on-board can be one or more. Different methods were proposed

respectively and the refinement was conducted. The simulations demonstrate the effectiveness of algorithms.

# Chapter 6

## Future Work

Compared to the point source localization in Chapters 2–3, the rigid body localization, position and orientation estimation studied in Chapters 4–5, is much more complex and challenging, and fewer research has been conducted. We will discuss some possible extensions of this work mainly focusing on algorithm development.

For stationary rigid body localization in Chapter 4, both [53] and our proposed method in Section 4.2 require that each sensor can connect to multiple anchors, such requirement may not be satisfied when blockage occurs. It is necessary to develop the algorithm that does not impose additional restriction once the measurements are sufficient to recover the pose of rigid body, which would lower the requirement on the number of available measurements and enhance the localization system applicability.

Another issue is that distance measurement requires clock synchronization between anchor and sensor, which needs complex clock synchronization protocol and repeated synchronization query. Therefore it is practical to consider the localization under TDOA measurements that does not require clock synchronization. Although

our proposed method in Section 4.2 can be directly applied to this scenario, it is necessary to develop the method that imposes less restriction on the number of available measurements at each sensor, and to propose specific method for much simpler 2D case.

For the pose estimation using AOA measurements in Section 5, due to the use of semidefinite relaxation in 3D case, it is important to investigate the algorithm performance loss with respect to CRLB over different geometric configurations of anchors and sensors, and study when the algorithm performs well. In addition, we shall explore much more computationally efficient or even closed-form solution for 3D single sensor case and improve the accuracy for 3D multiple sensors case.



# Appendix A

## Appendix for Chapter 2

In this Appendix, we will provide the bias analysis formulas for SR-LS and SR-WLS, and for SRD-LS and SRD-WLS.

### A.1 Bias of SR-LS

When the noise is small, we have from (2.25) using the Neumann expansion [25]

$$\begin{aligned}\mathbf{F}_{\text{SR-LS}}^{\prime\prime-1} &= \left\{ 8\mathbf{K}\mathbf{B}\mathbf{\Gamma}^T \left[ \mathbf{I} - (\mathbf{K}\mathbf{B}\mathbf{\Gamma}^T)^{-1} (\mathbf{n}^T \mathbf{B}\mathbf{Q}^{-1} \mathbf{1}) \right] + o(\|\mathbf{n}\|)\mathbf{I} \right\}^{-1} \\ &= \frac{1}{8} (\mathbf{K}\mathbf{B}\mathbf{\Gamma}^T)^{-1} \left[ \mathbf{I} + (\mathbf{K}\mathbf{B}\mathbf{\Gamma}^T)^{-1} (\mathbf{n}^T \mathbf{B}\mathbf{Q}^{-1} \mathbf{1}) \right] + o(\|\mathbf{n}\|)\mathbf{1}\mathbf{1}^T.\end{aligned}\quad (\text{A.1})$$

Using (2.21) and maintaining up to second order noise term,

$$E[\mathbf{F}_{\text{SR-LS}}^{\prime\prime-1} \mathbf{f}'_{\text{SR-LS}}] = -\frac{1}{2} (\mathbf{K}\mathbf{B}\mathbf{\Gamma}^T)^{-1} \left[ \mathbf{K}\mathbf{q} + 2 (\mathbf{K}\mathbf{B}\mathbf{\Gamma}^T)^{-1} \mathbf{K}\mathbf{B}\mathbf{Q}\mathbf{B}\mathbf{Q}^{-1} \mathbf{1} \right] \quad (\text{A.2})$$

where  $\mathbf{q} = [Q_{11} \ Q_{22} \ \cdots \ Q_{MM}]^T$ .

In the second bias component,  $\bar{\mathbf{F}}''_{\text{SR-LS}}$  and  $E[\mathbf{M}] = \mathbf{Q}_{\text{SR-LS}}$  are given in (2.26) and (2.27). From (2.24),

$$\mathbf{F}'''_{l,\text{SR-LS}} = 8 [\mathbf{e}_l \mathbf{1}^T \mathbf{K}^T + \mathbf{K} \mathbf{1} \mathbf{e}_l^T + (\mathbf{e}_l^T \mathbf{K} \mathbf{1}) \mathbf{I}] \quad (\text{A.3})$$

where column vector  $\mathbf{e}_l$  has 1 in  $l$ -th row and 0 in other rows. Notice that (A.3) doesn't contain noise and  $\bar{\mathbf{F}}'''_{l,\text{SR-LS}} = \mathbf{F}'''_{l,\text{SR-LS}}$ .

Putting (2.26), (2.27), (A.2) and (A.3) into (2.19) gives the bias of SR-LS.

## A.2 Bias of SR-WLS

Starting from (2.33),

$$\begin{aligned} \mathbf{F}''^{-1}_{\text{SR-WLS}} = & \frac{1}{8} (\Gamma \mathbf{Q}^{-1} \Gamma^T)^{-1} \left\{ \mathbf{I} + [(\mathbf{n}^T \mathbf{Q}^{-1} \mathbf{B}^{-1} \mathbf{1}) \mathbf{I} + \Gamma \mathbf{B}^{-1} \text{diag}(\mathbf{n}) \mathbf{Q}^{-1} \Gamma^T \right. \\ & \left. + \Gamma \mathbf{Q}^{-1} \text{diag}(\mathbf{n}) \mathbf{B}^{-1} \Gamma^T] (\Gamma \mathbf{Q}^{-1} \Gamma^T)^{-1} \right\} + o(\|\mathbf{n}\|) \mathbf{1} \mathbf{1}^T. \end{aligned} \quad (\text{A.4})$$

$\mathbf{f}'_{\text{SR-WLS}}$  is given in (2.30). Hence up to second order noise terms

$$\begin{aligned} E[\mathbf{F}''^{-1}_{\text{SR-WLS}} \mathbf{f}'_{\text{SR-WLS}}] = & - (\Gamma \mathbf{Q}^{-1} \Gamma^T)^{-1} \times \\ & \left[ -\frac{1}{2} \Gamma \mathbf{Q}^{-1} \mathbf{B}^{-1} \mathbf{q} - \Gamma \mathbf{B}^{-1} \mathbf{1} + (\Gamma \mathbf{Q}^{-1} \Gamma^T)^{-1} \Gamma \mathbf{Q}^{-1} \mathbf{B}^{-1} \mathbf{1} + \Gamma \mathbf{B}^{-1} \mathbf{a} + \Gamma \mathbf{Q}^{-1} \mathbf{b} \right] \end{aligned} \quad (\text{A.5})$$

where the column vector  $\mathbf{a} = [a_i]$ ,  $i = 1, 2, \dots, M$ , and  $a_i = \mathbf{e}_i^T \mathbf{Q}^{-1} \Gamma^T (\Gamma \mathbf{Q}^{-1} \Gamma^T)^{-1} \Gamma \mathbf{e}_i$ ; similarly, the column vector  $\mathbf{b} = [b_i]$ ,  $i = 1, 2, \dots, M$ , and  $b_i = \mathbf{e}_i^T \mathbf{B}^{-1} \Gamma^T (\Gamma \mathbf{Q}^{-1} \Gamma^T)^{-1} \Gamma \mathbf{e}_i$ .

$\bar{\mathbf{F}}''_{\text{SR-WLS}}$  and  $\mathbf{Q}_{\text{SR-WLS}}$  are in (2.34) and (2.35). From (2.32),

$$\bar{\mathbf{F}}'''_{l,\text{SR-WLS}} = 8 [\mathbf{e}_l(\mathbf{\Gamma}\mathbf{Q}^{-1}\mathbf{B}^{-1}\mathbf{1})^T + \mathbf{\Gamma}\mathbf{Q}^{-1}\mathbf{B}^{-1}\mathbf{1}\mathbf{e}_l^T + (\mathbf{e}_l^T\mathbf{\Gamma}\mathbf{Q}^{-1}\mathbf{B}^{-1}\mathbf{1})\mathbf{I}] . \quad (\text{A.6})$$

As a result, we can obtain the bias of SR-WLS from (2.19).

### A.3 Bias of SRD-LS

According to (2.45),

$$\begin{aligned} \mathbf{F}_{\text{SRD-LS}}''^{-1} &= \frac{1}{8} (\mathbf{K}_d\mathbf{B}_d\mathbf{\Gamma}_d^T)^{-1} \times \\ &\left\{ \mathbf{I} + [\mathbf{K}_d\mathbf{n}_d\boldsymbol{\rho}_1^T + \boldsymbol{\rho}_1(\mathbf{K}_d\mathbf{n}_d)^T - (\mathbf{n}_d^T\mathbf{B}_d\mathbf{Q}_d^{-1}\mathbf{r}_d^o)\mathbf{X}^o] (\mathbf{K}_d\mathbf{B}_d\mathbf{\Gamma}_d^T)^{-1} \right\} + o(\|\mathbf{n}_d\|)\mathbf{1}\mathbf{1}^T. \end{aligned} \quad (\text{A.7})$$

Using  $\mathbf{f}'_{\text{SRD-LS}}$  in (2.41) and keeping up to second noise terms

$$\begin{aligned} &E[\mathbf{F}_{\text{SRD-LS}}''^{-1}\mathbf{f}'_{\text{SRD-LS}}] \\ &= \frac{1}{2} (\mathbf{K}_d\mathbf{B}_d\mathbf{\Gamma}_d^T)^{-1} \left[ 2\boldsymbol{\rho}_1\mathbf{1}^T\mathbf{B}_d\mathbf{1} - \mathbf{K}_d\mathbf{q}_d - 2\mathbf{\Gamma}_d\mathbf{B}_d^2\mathbf{K}_d^T (\mathbf{K}_d\mathbf{B}_d\mathbf{\Gamma}_d^T)^{-1} \boldsymbol{\rho}_1 \right. \\ &\quad \left. - 2\boldsymbol{\rho}_1\text{tr}(\mathbf{B}_d\mathbf{\Gamma}_d^T (\mathbf{K}_d\mathbf{B}_d\mathbf{\Gamma}_d^T)^{-1} \mathbf{K}_d\mathbf{B}_d) + 2\mathbf{X}^o (\mathbf{K}_d\mathbf{B}_d\mathbf{\Gamma}_d^T)^{-1} \mathbf{K}_d\mathbf{B}_d\mathbf{Q}_d\mathbf{B}_d\mathbf{Q}_d^{-1}\mathbf{r}_d^o \right] \end{aligned} \quad (\text{A.8})$$

where  $\mathbf{q}_d = [Q_{d22} \ Q_{d33} \ \cdots \ Q_{dMM}]^T$ .

$\bar{\mathbf{F}}''_{\text{SRD-LS}}$  and  $\mathbf{Q}_{\text{SRD-LS}}$  are in (2.46) and (2.47). From (2.44),

$$\bar{\mathbf{F}}'''_{l,\text{SRD-LS}} = -8 [\mathbf{c}_l(\mathbf{K}_d\mathbf{r}_d^o)^T + (\mathbf{K}_d\mathbf{r}_d^o)\mathbf{c}_l^T + (\mathbf{e}_l^T\mathbf{K}_d\mathbf{r}_d^o)\mathbf{X}^o] \quad (\text{A.9})$$

where  $\mathbf{c}_l = \frac{\partial}{\partial u_l} \frac{\mathbf{u} - \mathbf{s}_1}{\|\mathbf{u} - \mathbf{s}_1\|} \Big|_{\mathbf{u}=\mathbf{u}^o} = \mathbf{X}^o \mathbf{e}_l$ . The bias for SRD-LS as shown in (2.19) can be evaluated.

## A.4 Bias of SRD-WLS

From (2.52) and under small noise assumption,

$$\begin{aligned} & \mathbf{F}_{\text{SRD-WLS}}^{\prime\prime-1} \\ &= \frac{1}{8} (\Gamma_d \mathbf{Q}_d^{-1} \Gamma_d^T)^{-1} \left\{ \mathbf{I} + [\Gamma_d \mathbf{Q}_d^{-1} \mathbf{B}_d^{-1} \text{diag}(\mathbf{n}_d) (\Gamma_d + \boldsymbol{\rho}_1 \mathbf{1}^T)^T \right. \\ & \quad + (\Gamma_d + \boldsymbol{\rho}_1 \mathbf{1}^T) \mathbf{B}_d^{-1} \text{diag}(\mathbf{n}_d) \mathbf{Q}_d^{-1} \Gamma_d^T - (\mathbf{n}_d^T \mathbf{Q}_d^{-1} \mathbf{B}_d^{-1} \mathbf{r}_d^o) \mathbf{X}^o \\ & \quad \left. + (\Gamma_d \mathbf{Q}_d^{-1} (\Gamma_d \mathbf{B}_d^{-1})^T + \Gamma_d \mathbf{B}_d^{-1} \mathbf{Q}_d^{-1} \Gamma_d^T) \boldsymbol{\alpha}^T \mathbf{n}_d] (\Gamma_d \mathbf{Q}_d^{-1} \Gamma_d^T)^{-1} \right\} + o(\|\mathbf{n}_d\|) \mathbf{1} \mathbf{1}^T. \end{aligned} \quad (\text{A.10})$$

Using  $\mathbf{f}'_{\text{SRD-WLS}}$  given in (2.49) and keeping up to second order noise terms

$$\begin{aligned} E[\mathbf{F}_{\text{SRD-WLS}}^{\prime\prime-1} \mathbf{f}'_{\text{SRD-WLS}}] &= \frac{1}{2} (\Gamma_d \mathbf{Q}_d^{-1} \Gamma_d^T)^{-1} \times \\ & \left\{ \Gamma_d \mathbf{Q}_d^{-1} \mathbf{B}_d^{-1} \mathbf{q}_d + 2(\Gamma_d + \boldsymbol{\rho}_1 \mathbf{1}^T) \mathbf{B}_d^{-1} \mathbf{1} + 2\Gamma_d (\mathbf{Q}_d^{-1} \mathbf{B}_d^{-1} + \mathbf{B}_d^{-1} \mathbf{Q}_d^{-1}) \mathbf{Q}_d \boldsymbol{\alpha} \right. \\ & \quad - 2\Gamma_d \mathbf{Q}_d^{-1} \mathbf{B}_d^{-1} \mathbf{g} - 2(\Gamma_d + \boldsymbol{\rho}_1 \mathbf{1}^T) \mathbf{B}_d^{-1} \mathbf{h} + 2\mathbf{X}^o (\Gamma_d \mathbf{Q}_d^{-1} \Gamma_d^T)^{-1} \Gamma_d \mathbf{Q}_d^{-1} \mathbf{B}_d^{-1} \mathbf{r}_d^o \\ & \quad \left. - 2 [\Gamma_d \mathbf{Q}_d^{-1} (\Gamma_d \mathbf{B}_d^{-1})^T + \Gamma_d \mathbf{B}_d^{-1} \mathbf{Q}_d^{-1} \Gamma_d^T] (\Gamma_d \mathbf{Q}_d^{-1} \Gamma_d^T)^{-1} \Gamma_d \boldsymbol{\alpha} \right\} \end{aligned} \quad (\text{A.11})$$

where column vector  $\mathbf{g} = [g_i], i = 1, \dots, M-1$ , and  $g_i = \mathbf{e}_i^T (\Gamma_d + \boldsymbol{\rho}_1 \mathbf{1}^T)^T (\Gamma_d \mathbf{Q}_d^{-1} \Gamma_d^T)^{-1} \Gamma_d \mathbf{e}_i$ ; similarly, column vector  $\mathbf{h} = [h_i], i = 1, \dots, M-1$ , and  $h_i = \mathbf{e}_i^T \mathbf{Q}_d^{-1} \Gamma_d^T (\Gamma_d \mathbf{Q}_d^{-1} \Gamma_d^T)^{-1} \Gamma_d \mathbf{e}_i$ .

$\bar{\mathbf{F}}''_{\text{SRD-WLS}}$  and  $\mathbf{Q}_{\text{SRD-WLS}}$  are in (2.53) and (2.54). Using (2.51),

$$\bar{\mathbf{F}}'''_{l,\text{SRD-WLS}} = -8 \left[ \mathbf{c}_l (\boldsymbol{\Gamma}_d \mathbf{Q}_d^{-1} \mathbf{B}_d^{-1} \mathbf{r}_d^o)^T + (\boldsymbol{\Gamma}_d \mathbf{Q}_d^{-1} \mathbf{B}_d^{-1} \mathbf{r}_d^o) \mathbf{c}_l^T + (\mathbf{e}_l^T \boldsymbol{\Gamma}_d \mathbf{Q}_d^{-1} \mathbf{B}_d^{-1} \mathbf{r}_d^o) \mathbf{X}^o \right]. \quad (\text{A.12})$$

The bias of SRD-WLS can now be found from (2.19).

# Appendix B

## Appendix for Chapter 4

### B.1 CRLB for 2D Stationary Rigid Body Localization: Parameterization of Rotation Matrix $\mathbf{R}$ by Rotation Angle $\theta$

In the 2D stationary rigid body localization algorithm presented in Section 4.3, the unknown vector is  $[\theta, \mathbf{t}^T]^T$  since we use  $\theta$  to parameterize the rotation matrix  $\mathbf{R}$ . The derivatives are

$$\frac{\partial r_{mi}^o}{\partial \theta} = \frac{1}{r_{mi}^o} (\mathbf{a}_m - \mathbf{t})^T \begin{bmatrix} \sin \theta & \cos \theta \\ -\cos \theta & \sin \theta \end{bmatrix} \mathbf{c}_i \quad (\text{B.1})$$

and

$$\frac{\partial r_{mi}^o}{\partial \mathbf{t}} = \frac{\mathbf{R} \mathbf{c}_i + \mathbf{t} - \mathbf{a}_m}{r_{mi}^o}. \quad (\text{B.2})$$

Stacking the rows  $\frac{\partial r_{mi}^o}{\partial[\theta, \mathbf{t}^T]}$  from different measurements gives the matrix  $\mathbf{J}$ . The Fisher information matrix (FIM) is

$$\mathbf{FIM} = \mathbf{J}^T \mathbf{Q}_n^{-1} \mathbf{J} \quad (\text{B.3})$$

whose inverse is the CRLB [20], where  $\mathbf{Q}_n$  is the covariance matrix of the distance measurement noise.

## B.2 CRLB for Moving Rigid Body Localization

### B.2.1 2D Case

The unknown parameter vector is  $[\theta, \mathbf{t}^T, \omega, \dot{\mathbf{t}}^T]^T$ . Since the distance equation does not contain  $\omega$  and  $\dot{\mathbf{t}}$ , we have

$$\frac{\partial r_{mi}^o}{\partial \omega} = 0, \quad \frac{\partial r_{mi}^o}{\partial \dot{\mathbf{t}}} = \mathbf{0}.$$

Using the derivatives  $\frac{\partial r_{mi}^o}{\partial \theta}$  and  $\frac{\partial r_{mi}^o}{\partial \mathbf{t}}$  derived in Appendix B.1, we can stack the rows  $\frac{\partial r_{mi}^o}{\partial[\theta, \mathbf{t}^T, \omega, \dot{\mathbf{t}}^T]}$  to form the gradient matrix  $\mathbf{J}_{r^o}$  for the distance measurements.

For the Doppler measurements, we have from (4.5),

$$\begin{aligned}
\frac{\partial \dot{r}_{mi}^o}{\partial \theta} &= -\frac{1}{r_{mi}^o} (\mathbf{t}^T [\omega]^\times - \mathbf{a}_m^T [\omega]^\times + \dot{\mathbf{t}}^T) \begin{bmatrix} \sin \theta & \cos \theta \\ -\cos \theta & \sin \theta \end{bmatrix} \mathbf{c}_i - \frac{\dot{r}_{mi}^o}{r_{mi}^o} \frac{\partial r_{mi}^o}{\partial \theta}, \\
\frac{\partial \dot{r}_{mi}^o}{\partial \mathbf{t}} &= \frac{1}{r_{mi}^o} ([\omega]^\times \mathbf{R} \mathbf{c}_i + \dot{\mathbf{t}}) - \frac{\dot{r}_{mi}^o}{r_{mi}^o} \frac{\partial r_{mi}^o}{\partial \mathbf{t}}, \\
\frac{\partial \dot{r}_{mi}^o}{\partial \omega} &= \frac{1}{r_{mi}^o} \Phi^T [(\mathbf{R} \mathbf{c}_i) \otimes (\mathbf{t} - \mathbf{a}_m)], \\
\frac{\partial \dot{r}_{mi}^o}{\partial \dot{\mathbf{t}}} &= \frac{1}{r_{mi}^o} (\mathbf{R} \mathbf{c}_i + \mathbf{t} - \mathbf{a}_m),
\end{aligned} \tag{B.4}$$

where  $\frac{\partial r_{mi}^o}{\partial \theta}$  and  $\frac{\partial r_{mi}^o}{\partial \mathbf{t}}$  are given in Appendix B.1 and  $\Phi$  is defined in (4.39). Stacking the derivatives  $\frac{\partial \dot{r}_{mi}^o}{\partial [\theta, \mathbf{t}^T, \omega, \dot{\mathbf{t}}^T]}$  forms the gradient matrix  $\mathbf{J}_{\mathbf{r}^o}$ . The resulting FIM is

$$\mathbf{FIM} = \begin{bmatrix} \mathbf{J}_{\mathbf{r}^o} \\ \mathbf{J}_{\dot{\mathbf{r}}^o} \end{bmatrix}^T \mathbf{Q}^{-1} \begin{bmatrix} \mathbf{J}_{\mathbf{r}^o} \\ \mathbf{J}_{\dot{\mathbf{r}}^o} \end{bmatrix}, \tag{B.5}$$

whose inverse is the CRLB.

### B.2.2 3D Case

We shall first evaluate the FIM of the unknown parameter vector  $\boldsymbol{\zeta} = [\mathbf{q}^T, \mathbf{t}^T, \omega^T, \dot{\mathbf{t}}^T]^T$  without having the  $SO(3)$  constraint, where  $\mathbf{q} = \text{vec}(\mathbf{R})$ . The gradients  $\frac{\partial \dot{r}_{mi}^o}{\partial \mathbf{t}}$ ,  $\frac{\partial \dot{r}_{mi}^o}{\partial \omega}$  and  $\frac{\partial \dot{r}_{mi}^o}{\partial \dot{\mathbf{t}}}$  are the same as those in the 2D case, where  $\Phi$  is given in (4.38). From (4.5),

$$\frac{\partial \dot{r}_{mi}^o}{\partial \mathbf{q}} = \frac{1}{r_{mi}^o} [\mathbf{c}_i \otimes ([\omega]^\times \mathbf{a}_m - [\omega]^\times \mathbf{t} + \dot{\mathbf{t}})] - \frac{\dot{r}_{mi}^o}{r_{mi}^o} \frac{\partial r_{mi}^o}{\partial \mathbf{q}} \tag{B.6}$$



where  $\frac{\partial r_{mi}^o}{\partial \mathbf{q}} = \frac{1}{r_{mi}^o} \mathbf{c}_i \otimes (\mathbf{R}\mathbf{c}_i + \mathbf{t} - \mathbf{a}_m)$ . We can now form  $\mathbf{J}_{\mathbf{r}^o}$  and  $\mathbf{J}_{\dot{\mathbf{r}}^o}$ , and obtain the FIM using (B.5).

The constrained CRLB by imposing  $\mathbf{R}$  to  $SO(3)$  is obtained by the FIM together with the gradient matrix of the constraints with respect to  $\boldsymbol{\zeta}$ , the readers are referred to [53] for details (note that [53] omits the constraint  $\det(\mathbf{R}) = 1$  on the rotation matrix which could result in a bound that is higher than the actual. Imposing the constraint  $\mathbf{R}^T \mathbf{R} = \mathbf{I}$  is not sufficient since it implies not only  $\det(\mathbf{R}) = 1$  representing rotation but also  $\det(\mathbf{R}) = -1$  representing reflection).

### B.3 Definition of $\boldsymbol{\gamma}$ and $\mathbf{L}$ for Multiplicative Corrective Rotation Matrix

In general 3D case,  $\boldsymbol{\gamma}$  is a  $9 \times 1$  sparse vector with value 1 for the 1st, 5th and 9th elements and 0 otherwise, and  $\mathbf{L}$  is a  $9 \times 3$  sparse matrix with the (3, 2), (4, 3) and (8, 1) elements equal to 1, (2, 3), (6, 1) and (7, 2) elements equal to  $-1$  and 0 otherwise.

We would like to point out that we cannot choose the Euler angle sequence (3, 1, 3) (rotates with respect to  $z, x, z$  axes in sequence) to represent  $\mathbf{R}_\delta$ . Such a choice will cause the matrix  $\mathbf{H}^T \mathbf{Q}_v^{-1} \mathbf{H}$  to be singular and cannot be inverted.

In 2D case,  $\boldsymbol{\beta} = \theta$ ,  $\boldsymbol{\gamma} = [1, 0, 0, 1]^T$  and  $\mathbf{L} = [0, 1, -1, 0]^T$ .

## B.4 The Two-Stage Method for Localization Using TOA and Doppler Measurements

We shall obtain the position and velocity of each sensor individually. Following [71], the nonlinearly transformed measurement equations for  $i$ -th sensor are

$$\epsilon_{t,m} = r_{mi}^2 - \|\mathbf{a}_m\|^2 - (-2\mathbf{a}_m^T \mathbf{s}_i + \|\mathbf{s}_i\|^2) \approx 2r_{mi}^o n_{mi} \quad (\text{B.7})$$

$$\epsilon_{f,m} = r_{mi} \dot{r}_{mi} - (\mathbf{s}_i^T \dot{\mathbf{s}}_i - \mathbf{a}_m^T \dot{\mathbf{s}}_i) \approx \dot{r}_{mi}^o n_{mi} + r_{mi}^o \dot{n}_{mi} \quad (\text{B.8})$$

for  $m = 1, 2, \dots, M$ . We solve for the unknowns  $\boldsymbol{\theta}_1 = [\mathbf{s}_i^T, \|\mathbf{s}_i\|^2, \dot{\mathbf{s}}_i^T, \mathbf{s}_i^T \dot{\mathbf{s}}_i]^T$  from the matrix equation constructed from (B.7) and (B.8),

$$\boldsymbol{\epsilon}_1 = \begin{bmatrix} \epsilon_t \\ \epsilon_f \end{bmatrix} = \mathbf{h}_1 - \mathbf{G}_1 \boldsymbol{\theta}_1 \quad (\text{B.9})$$

where

$$\mathbf{h}_1 = \begin{bmatrix} r_{1i}^2 - \|\mathbf{a}_1\|^2 \\ \vdots \\ r_{Mi}^2 - \|\mathbf{a}_M\|^2 \\ r_{1i} \dot{r}_{1i} \\ \vdots \\ r_{Mi} \dot{r}_{Mi} \end{bmatrix}, \quad \mathbf{G}_1 = \begin{bmatrix} -2\mathbf{a}_1^T & 1 & \mathbf{0}^T & 0 \\ \vdots & & & \\ -2\mathbf{a}_M^T & 1 & \mathbf{0}^T & 0 \\ \mathbf{0}^T & 0 & -\mathbf{a}_1^T & 1 \\ & & \vdots & \\ \mathbf{0}^T & 0 & -\mathbf{a}_M^T & 1 \end{bmatrix}. \quad (\text{B.10})$$

In  $\mathbf{G}_1$ ,  $\mathbf{0}$  is a  $3 \times 1$  vector of zeros. The solution is

$$\hat{\boldsymbol{\theta}}_1 = (\mathbf{G}_1^T \mathbf{W}_1 \mathbf{G}_1)^{-1} \mathbf{G}_1^T \mathbf{W}_1 \mathbf{h}_1 \quad (\text{B.11})$$

where  $\mathbf{W}_1 = (E[\boldsymbol{\epsilon}_1 \boldsymbol{\epsilon}_1^T])^{-1}$ .  $E[\boldsymbol{\epsilon}_1 \boldsymbol{\epsilon}_1^T]$  are defined by the correlations  $E[\epsilon_{t,k} \epsilon_{t,l}] = 4r_{ki}^o r_{li}^o \times E[n_{ki} n_{li}]$ ,  $E[\epsilon_{f,k} \epsilon_{f,l}] = \dot{r}_{ki}^o \dot{r}_{li}^o E[n_{ki} n_{li}] + r_{ki}^o r_{li}^o E[\dot{n}_{ki} \dot{n}_{li}] + \dot{r}_{ki}^o r_{li}^o E[n_{ki} \dot{n}_{li}] + r_{ki}^o \dot{r}_{li}^o E[\dot{n}_{ki} n_{li}]$  and  $E[\epsilon_{t,k} \epsilon_{f,l}] = 2r_{ki}^o \dot{r}_{li}^o E[n_{ki} n_{li}] + 2r_{ki}^o r_{li}^o E[n_{ki} \dot{n}_{li}]$ , where the noise correlation values can be obtained from the elements of  $\mathbf{Q}$ .

From the elements of  $\hat{\boldsymbol{\theta}}_1$  and their ideal relations, we can construct the matrix equation

$$\boldsymbol{\epsilon}_2 = \mathbf{h}_2 - \mathbf{G}_2 \boldsymbol{\theta}_2 \quad (\text{B.12})$$

where

$$\mathbf{h}_2 = \begin{bmatrix} \hat{\boldsymbol{\theta}}_1(1:3) \odot \hat{\boldsymbol{\theta}}_1(1:3) \\ \hat{\theta}_1(4) \\ \hat{\boldsymbol{\theta}}_1(1:3) \odot \hat{\boldsymbol{\theta}}_1(5:7) \\ \hat{\theta}_1(8) \end{bmatrix}, \quad \mathbf{G}_2 = \begin{bmatrix} \mathbf{I} & \mathbf{O} \\ \mathbf{1}^T & \mathbf{0}^T \\ \mathbf{O} & \mathbf{I} \\ \mathbf{0}^T & \mathbf{1}^T \end{bmatrix},$$

$$\boldsymbol{\theta}_2 = \begin{bmatrix} \mathbf{s}_i \odot \mathbf{s}_i \\ \mathbf{s}_i \odot \dot{\mathbf{s}}_i \end{bmatrix} \quad (\text{B.13})$$

where  $\hat{\boldsymbol{\theta}}_1(k:l)$  denotes a subvector by collecting the  $k$ -th to the  $l$ -th elements of  $\hat{\boldsymbol{\theta}}_1$  and  $\hat{\theta}_1(k)$  is its  $k$ -th element. In  $\mathbf{G}_2$ ,  $\mathbf{I}$  and  $\mathbf{O}$  are size 3 identity and zero matrices, and  $\mathbf{1}$  and  $\mathbf{0}$  are length 3 vectors of unity and zero. The solution of  $\boldsymbol{\theta}_2$  is

$$\hat{\boldsymbol{\theta}}_2 = (\mathbf{G}_2^T \mathbf{W}_2 \mathbf{G}_2)^{-1} \mathbf{G}_2^T \mathbf{W}_2 \mathbf{h}_2 \quad (\text{B.14})$$

where

$$\mathbf{W}_2 = [\mathbf{X}(\mathbf{G}_1^T \mathbf{W}_1 \mathbf{G}_1)^{-1} \mathbf{X}^T]^{-1}. \quad (\text{B.15})$$

$\mathbf{X}$  is defined by the  $2 \times 2$  block form with the blocks  $\mathbf{X}_{11} = \text{diag}([2\mathbf{s}_i^T, 1]^T)$ ,  $\mathbf{X}_{12} = \mathbf{O}$ ,

$\mathbf{X}_{21} = \text{diag}([\hat{\mathbf{s}}_i^T, 0]^T)$ , and  $\mathbf{X}_{22} = \text{diag}([\mathbf{s}_i^T, 1]^T)$ .

The position and velocity estimate of  $i$ -th sensor is

$$\begin{aligned}\hat{\mathbf{s}}_i &= \text{diag}(\text{sgn}(\hat{\boldsymbol{\theta}}_1(1:3))) \left[ \sqrt{\hat{\theta}_2(1)}, \sqrt{\hat{\theta}_2(2)}, \sqrt{\hat{\theta}_2(3)} \right]^T \\ \hat{\dot{\mathbf{s}}}_i &= \hat{\boldsymbol{\theta}}_2(4:6) ./ \hat{\mathbf{s}}_i.\end{aligned}\tag{B.16}$$

where  $\text{sgn}(\cdot)$  is signum function and  $./$  is element-wise division.

## B.5 Implementation Details for SCLS and CLS

For the implementation of SCLS, we use the solution from (25) instead of (24) from [53]. The anchor positions are randomly assigned in our simulation. As a result, degenerate anchor topology may occur which leads to worse result using (24). We impose  $\det(\mathbf{R}) = 1$  when adopting orthogonal Procrustes problem technique.

For the implementation of CLS, we initialize it with the proposed step-1 solution instead of SCLS since the former gives better accuracy. The iteration of CLS stops when the relative gradient magnitude is less than  $10^{-10}$  [76] or when the maximum number of iterations, set to 50, is reached.

# Bibliography

- [1] J. O. Smith and J. S. Abel, “Closed-form least-squares source location estimation from range-difference measurements,” *IEEE Trans. Acoust., Speech, Signal Process.*, vol. ASSP-35, pp. 1661–1669, Dec. 1987.
- [2] Y. T. Chan and K. C. Ho, “A simple and efficient estimator for hyperbolic location,” *IEEE Trans. Signal Process.*, vol. 42, no. 8, pp. 1905–1915, Aug. 1994.
- [3] G. W. Pulford, “Analysis of a nonlinear least square procedure used in global positioning systems,” *IEEE Trans. Signal Process.*, vol. 58, no. 9, pp. 4526–4534, Sept. 2010.
- [4] S. Gogineni and A. Nehorai, “Target estimation using sparse modeling for distributed MIMO radar,” *IEEE Trans. Signal Process.*, vol. 59, no. 11, pp. 5315–5325, Nov. 2011.
- [5] M. Sun and K. C. Ho, “An asymptotically efficient estimator for TDOA and FDOA positioning of multiple disjoint sources in the presence of sensor location uncertainties,” *IEEE Trans. Signal Process.*, vol. 59, no. 7, pp. 3434–3440, Jul. 2011.

- [6] W.-Y. Chiu and B.-S. Chen, “Mobile positioning problem in manhattan-like urban areas: Uniqueness of solution, optimal deployment of BSs, and fuzzy implementation,” *IEEE Trans. Signal Process.*, vol. 57, no. 12, pp. 4918–4929, Dec. 2009.
- [7] G. Destino and G. Abreu, “On the maximum likelihood approach for source and network localization,” *IEEE Trans. Signal Process.*, vol. 59, no. 10, pp. 4954–4970, Oct. 2011.
- [8] A. J. Weiss, “Direct geolocation of wideband emitters based on delay and Doppler,” *IEEE Trans. Signal Process.*, vol. 59, no. 6, pp. 2513–2521, Jun. 2011.
- [9] C. Liu, Y. V. Zakharov, and T. Chen, “Broadband underwater localization of multiple sources using basis pursuit de-noising,” *IEEE Trans. Signal Process.*, vol. 60, no. 4, pp. 1708–1717, Apr. 2012.
- [10] S. Li and B. L. F. Daku, “Optimal amplitude weighting for near-field passive source localization,” *IEEE Trans. Signal Process.*, vol. 59, no. 12, pp. 6175–6185, Dec. 2011.
- [11] J. Caffery and G. Stuber, “Subscriber location in CDMA cellular networks,” *IEEE Trans. Veh. Technol.*, vol. 47, no. 2, pp. 406–416, May 1998.
- [12] J. Caffery, “A new approach to the geometry of TOA location,” in *Proc. IEEE VTC 2000-Fall*, Boston, MA, Sept. 2000, vol. 4, pp. 1943–1949.
- [13] D. Li and H. Hu, “Least square solutions of energy based acoustic source localization problems,” in *Proc. IEEE ICPP Workshops*, Montreal, Canada, Aug. 2004, pp. 443–446.

- [14] F. K. W. Chan, H. C. So, J. Zheng, and K. W. K. Lui, “Best linear unbiased estimator approach for time-of-arrival based localization,” *IET Signal Process.*, vol. 2, no. 2, pp. 156–162, Jun. 2008.
- [15] H. C. Schau and A. Z. Robinson, “Passive source localization employing intersecting spherical surfaces from time-of-arrival differences,” *IEEE Trans. Acoust., Speech, Signal Process.*, vol. ASSP-35, pp. 1223–1225, Aug. 1987.
- [16] S. Zhu and Z. Ding, “A simple approach of range-based positioning with low computational complexity,” *IEEE Trans. Wireless Commun.*, vol. 8, no. 12, pp. 5832–5836, Dec. 2009.
- [17] A. Beck, P. Stoica, and J. Li, “Exact and approximate solutions for source localization problems,” *IEEE Trans. Signal Process.*, vol. 56, no. 5, pp. 1770–1778, May 2008.
- [18] J. J. Moré, “Generalizations of the trust region problem,” *Optim. Methods Softw.*, vol. 2, pp. 189–209, 1993.
- [19] E. Larsson and D. Danev, “Accuracy comparison of LS and squared range LS for source localization,” *IEEE Trans. Signal Process.*, vol. 58, no. 2, pp. 916–923, Feb. 2010.
- [20] S. M. Kay, *Fundamentals of Statistical Signal Processing: Estimation Theory*. Englewood Cliffs, NJ: Prentice Hall, 1993.
- [21] K. W. Cheung, H. C. So, W. K. Ma, and Y. T. Chan, “Least squares algorithms for time-of-arrival-based mobile location,” *IEEE Trans. Signal Process.*, vol. 52, no. 4, pp. 1121–1228, Apr. 2004.

- [22] Y. Huang, J. Benesty, G. W. Elko, and R. M. Mersereau, “Real-time passive source localization: A practical linear correction least-squares approach,” *IEEE Trans. Speech Audio Process.*, vol. 9, no. 8, pp. 943–956, Nov. 2002.
- [23] L. Ljung, *System Identification: Theory for the User*. 2nd ed. Englewood Cliffs, NJ: Prentice Hall, 1998.
- [24] D.-H. Shin and T.-K. Sung, “Comparisons of error characteristics between TOA and TDOA positioning,” *IEEE Trans. Aerosp. Electron. Syst.*, vol. 38, no. 1, pp. 307–310, Jan. 2002.
- [25] T. K. Moon and W. C. Stirling, *Mathematical Methods and Algorithms for Signal Processing*. Englewood Cliffs, NJ: Prentice-Hall, 2000.
- [26] J. Bosse, A. Ferreol, and P. Larzabal, “A spatio-temporal array processing for passive localization of radio transmitters,” *IEEE Trans. Signal Process.*, vol. 61, no. 22, pp. 5485–5494, Nov. 2013.
- [27] H. Chenji and R. Stoleru, “Toward accurate mobile sensor network localization in noisy environments,” *IEEE Trans. Mobile Comput.*, vol. 12, no. 6, pp. 1094–1106, Jun. 2013.
- [28] S. Coraluppi, “Multistatic sonar localization,” *IEEE J. Ocean. Eng.*, vol. 31, no. 4, pp. 964–974, Oct. 2006.
- [29] S. S. Dias and M. G. S. Bruno, “Cooperative target tracking using decentralized particle filtering and RSS sensors,” *IEEE Trans. Signal Process.*, vol. 61, no. 14, pp. 3632–3646, Jul. 2013.



- [30] L. Dong, “Cooperative localization and tracking of mobile ad hoc networks,” *IEEE Trans. Signal Process.*, vol. 60, no. 7, pp. 3907–3913, Jul. 2012.
- [31] K. C. Ho, “Bias reduction for an explicit solution of source localization using TDOA,” *IEEE Trans. Signal Process.*, vol. 60, no. 5, pp. 2102–2114, May 2012.
- [32] H. Jamali-Rad and G. Leus, “Sparsity-aware multi-source TDOA localization,” *IEEE Trans. Signal Process.*, vol. 61, no. 19, pp. 4874–4887, Oct. 2013.
- [33] P. H. Leong, T. D. Abhayapala, and T. A. Lamahewa, “Multiple target localization using wideband echo chirp signals,” *IEEE Trans. Signal Process.*, vol. 61, no. 16, pp. 4077–4089, Aug. 2013.
- [34] N. Patwari, J. N. Ash, S. Kyperountas, A. O. Hero, R. L. Moses, and N. S. Correal, “Locating the nodes: cooperative localization in wireless sensor networks,” *IEEE Signal Process. Mag.*, vol. 22, no. 4, pp. 54–69, Jul. 2005.
- [35] H.-D. Qi, N. Xiu, and X. Yuan, “A Lagrangian dual approach to the single-source localization problem,” *IEEE Trans. Signal Process.*, vol. 61, no. 15, pp. 3815–3826, Aug. 2013.
- [36] E. Tsalolikhin, I. Bilik, and N. Blaunstein, “A single-base-station localization approach using a statistical model of the NLOS propagation conditions in urban terrain,” *IEEE Trans. Veh. Technol.*, vol. 60, no. 3, pp. 1124–1137, Mar. 2011.
- [37] R. M. Vaghefi, M. R. Gholami, R. M. Buehrer, and E. G. Strom, “Cooperative received signal strength-based sensor localization with unknown transmit powers,” *IEEE Trans. Signal Process.*, vol. 61, no. 6, pp. 1389–1403, Mar. 2013.

- [38] F. Yin, C. Fritsche, F. Gustafsson, and A. M. Zoubir, “TOA-based robust wireless geolocation and Cramer-Rao Lower Bound analysis in harsh LOS/NLOS environments,” *IEEE Trans. Signal Process.*, vol. 61, no. 9, pp. 2243–2255, May 2013.
- [39] Z. Ma and K. C. Ho, “TOA localization in the presence of random sensor position errors,” in *Proc. Acoust., Speech and Signal Process. (ICASSP)*, May 2011, pp. 2468–2471.
- [40] K. C. Ho, X. Lu, and L. Kovavisaruch, “Source localization using TDOA and FDOA measurements in the presence of receiver location errors: analysis and solution,” *IEEE Trans. Signal Process.*, vol. 55, no. 2, pp. 684–696, Feb. 2007.
- [41] L. Kovavisaruch and K. C. Ho, “Modified Taylor-series method for source and receiver localization using TDOA measurements with erroneous receiver position,” in *Proc. IEEE Int. Symp. Circuits Syst. (ISCAS)*, vol. 3, May 2005, pp. 2295–2298.
- [42] K. W. K. Lui, W.-K. Ma, H. C. So, and F. K. W. Chan, “Semi-definite programming algorithms for sensor network node localization with uncertainties in anchor positions and/or propagation speed,” *IEEE Trans. Signal Process.*, vol. 57, no. 2, pp. 752–763, Feb. 2009.
- [43] R. J. Kozick and B. M. Sadler, “Accuracy of source localization based on squared-range least squares (SR-LS) criterion,” *2009 3rd IEEE International Workshop on Computational Advances in Multi-Sensor Adaptive Processing*, 2009, pp. 37–40.

- [44] C. Knapp and G. C. Carter, “The generalized correlation method for estimation of time delay,” *IEEE Trans. Acoust., Speech, Signal Process.*, vol. 24, no. 4, pp. 320–327, Aug. 1976.
- [45] G. C. Carter, “Time delay estimation for passive sonar signal processing,” *IEEE Trans. Acoust., Speech, Signal Process.*, vol. 29, no. 3, pp. 463–470, Jun. 1981.
- [46] A. Quazi, “An overview on the time delay estimate in active and passive systems for target localization,” *IEEE Trans. Acoust., Speech, Signal Process.*, vol. 29, no. 3, pp. 527–533, Jun. 1981.
- [47] A. J. Weiss and E. Weinstein, “Fundamental limitations in passive time delay estimation—Part I: Narrow-band systems,” *IEEE Trans. Acoust., Speech, Signal Process.*, vol. 31, no. 2, pp. 472–486, Apr. 1983.
- [48] B. Barshan and H. F. Durrant-Whyte, “Inertial navigation systems for mobile robots,” *IEEE Trans. Robot. Autom.*, vol. 11, no. 3, pp. 328–342, Jun. 1995.
- [49] J. L. Crassidis, R. Alonso, and J. L. Junkins, “Optimal attitude and position determination from line-of-sight measurements,” *J. Astronautical Sciences*, vol. 48, no. 2, pp. 391–408, 2000.
- [50] A. I. Mourikis, N. Trawny, S. I. Roumeliotis, A. E. Johnson, A. Ansar, and L. Matthies, “Vision-aided inertial navigation for spacecraft entry, descent, and landing,” *IEEE Trans. Robot.*, vol. 25, no. 2, pp. 264–280, Apr. 2009.
- [51] Y. Shen and M. Z. Win, “On the accuracy of localization systems using wideband antenna arrays,” *IEEE Trans. Comm.*, vol. 58, no. 1, pp. 270–280, Jan. 2010.

- [52] F. Aghili and A. Salerno, “Driftless 3-D attitude determination and positioning of mobile robots by integration of IMU with two RTK GPSs,” *IEEE/ASME Trans. Mechatronics*, vol. 18, no. 1, pp.21–31, Feb. 2013.
- [53] S. P. Chepuri, G. Leus, and A.-J. van der Veen, “Rigid body localization using sensor networks,” *IEEE Trans. Signal Process.*, vol. 62, no. 18, pp. 4911–4924, Sept. 2014.
- [54] A. Alcocer, P. Oliveira, A. Pascoal, and J. Xavier, “Estimation of attitude and position from range-only measurements using geometric descent optimization on the special Euclidean group,” in *Proc. 9th Int. Conf. Inf. Fusion*, Jul. 2006, pp. 1–8.
- [55] A. Alcocer, P. Oliveira, A. Pascoal, R. Cunha, and C. Silvestre, “A dynamic estimator on  $SE(3)$  using range-only measurements,” in *Proc. 47th IEEE Conf. Decision & Control*, Dec. 2008, pp. 2302–2307.
- [56] K. Pahlavan, X. Li, and J.-P. Makela, “Indoor geolocation science and technology,” *IEEE Comm. Mag.*, vol. 40, no. 2, pp. 112–118, Feb. 2002.
- [57] P. Biswas, T.-C. Liang, K.-C. Toh, Y. Ye, and T.-C. Wang, “Semidefinite programming approaches for sensor network localization with noisy distance measurements,” *IEEE Trans. Autom. Sci. Eng.*, vol. 3, no. 4, pp. 360–371, Oct. 2006.
- [58] Y. Shen and M. Z. Win, “Fundamental limits of wideband localization—part I: a general framework,” *IEEE Trans. Inf. Theory*, vol. 56, no. 10, pp. 4956–4980, Oct. 2010.

- [59] Y. Shen and M. Z. Win, “Fundamental limits of wideband localization—part II: cooperative framework,” *IEEE Trans. Inf. Theory*, vol. 56, no. 10, pp. 4981–5000, Oct. 2010.
- [60] M. Z. Win, A. Conti, S. Mazuelas, Y. Shen, W. M. Gifford, D. Dardari, and M. Chiani, “Network localization and navigation via cooperation,” *IEEE Comm. Mag.*, vol. 49, no. 5, pp. 56–62, May 2011.
- [61] Y. Shen, S. Mazuelas, and M. Z. Win, “Network navigation: theory and interpretation,” *IEEE J. Sel. Areas Comm.*, vol. 30, no. 9, pp. 1823–1834, Oct. 2012.
- [62] J. Diebel, “Representing attitude: Euler angles, unit quaternions, and rotation vectors,” *Matrix*, vol. 58, pp. 15–16, 2006.
- [63] E. Foxlin, “Pedestrian tracking with shoe-mounted inertial sensors,” *IEEE Comput. Graph. Appl. Mag.*, vol. 25, no. 6, pp. 38–46, Nov.-Dec. 2005.
- [64] S. Mazuelas, Y. Shen and M. Z. Win, “Belief condensation filtering,” *IEEE Trans. Signal Process.*, vol. 61, no. 18, pp. 4403–4415, Sept. 15, 2013.
- [65] K. Plarre<sup>1</sup> and P. R. Kumar, “Tracking objects with networked scattered directional sensors,” *EURASIP J. on Advances in Signal Processing*, vol. 2008, pp. 1–10, 2008.
- [66] S. P. Chepuri, A. Simonetto, G. Leus and A. J. Van der Veen, “Tracking position and orientation of a mobile rigid body,” in *IEEE 5th International Workshop on Computational Advances in Multi-Sensor Adaptive Processing (CAMSAP)*, Dec. 2013, pp. 37–40.

- [67] J. S. Abel, “A divide and conquer approach to least-squares estimation,” *IEEE Trans. Aerosp. Electron. Syst.*, vol. 26, no. 2, pp. 423–427, Mar. 1990.
- [68] W. Gander, “Least squares with a quadratic constraint,” *Numerische Mathematik*, vol. 36, no. 3, pp. 291–307, 1980.
- [69] G. Golub and U. Matt, “Quadratically constrained least squares and quadratic problems,” *Numerische Mathematik*, vol. 59, no. 1, pp. 561–580, 1991.
- [70] R. A. Horn and C. R. Johnson, *Topics in Matrix Analysis*. Cambridge University Press, Cambridge, 1991.
- [71] K. C. Ho and W. Xu, “An accurate algebraic solution for moving source location using TDOA and FDOA measurements,” *IEEE Trans. Signal Process.*, vol. 52, no. 9, pp. 2453–2463, Sept. 2004.
- [72] S. Umeyama, “Least-squares estimation of transformation parameters between two point patterns,” *IEEE Trans. Pattern Anal. Mach. Intell.*, vol. 13, no. 4, pp. 376–380, Apr. 1991.
- [73] D. W. Eggert, A. Lorusso, and R. B. Fisher, “Estimating 3-D rigid body transformations: a comparison of four major algorithms,” *Machine Vision & Applications*, vol. 9, no. 5–6, pp. 272–290, Mar. 1997.
- [74] H. L. Van Trees, *Detection, Estimation, and Modulation Theory, Part I*. New York: Wiley, 1968.
- [75] H.-W. Wei, Q. Wan, Z.-X. Chen, and S.-F. Ye, “A novel weighted multidimensional scaling analysis for time-of-arrival-based mobile location,” *IEEE Trans. Signal Process.*, vol. 56, no. 7, pp. 3018–3022, Jul. 2008.

- [76] T. Viklands, “Algorithms for the weighted orthogonal Procrustes problem and other least squares problems,” Ph.D. dissertation, Umea Univ., Umea, Sweden, 2008.
- [77] C. Savarese, J. Rabaey, and J. Beutel, “Locationing in distributed ad-hoc wireless sensor networks,” in *Proc. Acoust., Speech and Signal Process. (ICASSP)*, Salt Lake City, USA, May 2001, pp. 2037–2040.
- [78] R. L. Moses, D. Krishnamurthy, and R. M. Patterson, “A self-localization method for wireless sensor networks,” *EURASIP J. Applied Signal Process.*, no. 4, pp. 348–358, 2003.
- [79] A. T. Ihler, J. W. Fisher, R. L. Moses, and A. S. Willsky, “Nonparametric belief propagation for self-localization of sensor networks,” *IEEE J. Sel. Areas Commun.*, vol. 23, no. 4, pp. 809–819, Apr. 2005.
- [80] M. Betke and L. Gurvits, “Mobile robot localization using landmarks,” *IEEE Trans. Robot. Autom.*, vol. 13, no. 2, pp. 251–263, Apr. 1997.
- [81] I. Shimshoni, “On mobile robot localization from landmark bearings,” *IEEE Trans. Robot. Autom.*, vol. 18, no. 6, pp. 971–976, Dec. 2002.
- [82] K. Dogancay, “Self-localization from landmark bearings using pseudolinear estimation techniques,” *IEEE Trans. Aerosp. Electron. Syst.*, vol. 50, no. 3, pp. 2361–2368, Jul. 2014.
- [83] H.-J. Shao, X.-P. Zhang, and Z. Wang, “Efficient closed-form algorithms for AOA based self-localization of sensor nodes using auxiliary variables,” *IEEE Trans. Signal Process.*, vol. 62, no. 10, pp. 2580–2594, May 2014.

- [84] J. Kim and H. Hmam, “3D self-Localization from angle of arrival measurements,” Electronic Warfare and Radar Division - Defence Science and Technology Organisation, DSTO-TR-2278, 2009.
- [85] H. Durrant-Whyte and T. Bailey, “Simultaneous localization and mapping: part I,” *IEEE Robot. Autom. Mag.*, vol. 13, no. 2, pp. 99–110, Jun. 2006.
- [86] K. E. Bekris, M. Click, and E. E. Kavraki, “Evaluation of algorithms for bearing-only SLAM,” in *Proc. IEEE Int. Conf. Robot. Autom. (ICRA)*, Orlando, Florida, May 2006, pp. 1937–1943.
- [87] P. Jensfelt, D. Kragic, J. Folkesson, and M. Bjorkman, “A framework for vision based bearing only 3D SLAM,” in *Proc. IEEE Int. Conf. Robot. Autom. (ICRA)*, Orlando, Florida, May 2006, pp. 1944–1950.
- [88] L. Badriasl, H. Kennedy, and A. Finn, “Effects of coordinate system rotation on two novel closed-form localization estimators using azimuth/elevation,” in *16th Int. Conf. Inf. Fusion (FUSION)*, Istanbul, Jul. 2013, pp. 1797–1804.
- [89] W. H. Foy, “Position-location solutions by Taylor-series estimation,” *IEEE Trans. Aerosp. Electron. Syst.*, vol. 12, no. 2, pp. 187–194, Mar. 1976.
- [90] G. Wahba, “A least squares estimate of satellite attitude,” *SIAM Review*, vol. 7, no. 3, pp. 409, 1965.
- [91] B. K. P. Horn, “Closed-form solution of absolute orientation using unit quaternions,” *J. Opt. Soc. Amer. A*, vol. 4, no. 4, pp. 629–642, 1987.



- [92] F. L. Markley, “Attitude determination using vector observations and the singular value decomposition,” *The Journal of the Astronautical Sciences*, vol. 36, no. 3, pp. 245-258, 1988.

## VITA

Shanjie Chen received the B.S. degree in electrical engineering from the Nanjing Agricultural University, Nanjing, China, in 2007, and M.S. degree in electrical engineering from the University of Science and Technology of China, Hefei, China, in 2010. He joined the Department of Electrical and Computer Engineering at the University of Missouri-Columbia in January 2011 as a Ph.D. student.